Long-Term Deformations and Prestress Losses in Precast, Prestressed Bridge Girders

by

Tyler Lee Neal

A thesis submitted to the Graduate Faculty of
Auburn University
in partial fulfillment of the
requirements for the Degree of
Master of Science

Auburn, Alabama
August 1, 2015

Keywords: self-consolidating concrete, prestressed concrete, prestress losses, camber

Approved by

Robert W. Barnes, Chair, Associate Professor of Civil Engineering
Anton K. Schindler, Professor of Civil Engineering
J. Michael Stallings, Professor of Civil Engineering

Abstract

Self-consolidating concrete (SCC) is widely becoming used to construct precast, prestressed bridge girders. In order to determine the acceptance of SCC for bridge girders in the state of Alabama, The Alabama Department of Transportation (ALDOT) sponsored an investigation to be performed by the Auburn University Highway Research Center. The objective of this report is to research the time-dependent deformation for the bridge girders included in this investigation.

Twenty-eight bulb tee girders were instrumented with strain gauges for the replacement bridge constructed on State Route 22 over Hillabee Creek in Tallapoosa County, Alabama. Half of the spans girders were constructed with SCC while the remaining half were constructed with conventional vibrated concrete (VC). Fresh concrete properties were determined while the girders were located at the plant, while internal strain and camber measurements were taken from the time of prestress transfer until the bridge was in service for one year. These internal strains were used to determine the prestress losses at various stages of the construction process.

The measured prestress losses for the girers were compared with predicted values determined using the provisions of the AASHTO LRFD 2012 Bridge Design Specification. Time-dependent deformation comparisons were also made between SCC and VC girders. The AASHTO 2012 prediction method over predicted the prestress losses for both types of concrete. There seemed to be no differences in the time-dependent deformations between the SCC and VC girders in this investigation.

Acknowledgments

I would first like to thank my committee chair, Dr. Robert Barnes, for his knowledge and expertise provided throughout the entirety of this investigation. It is only due to his outstanding oversight that this report is possible. Special thanks is also in order to my fellow graduate students who aided in the collection and processing of the data for this report including Sam Keske, Brandon Johnson, Eric Miller, Dave Mante, Zach Skinner, and Andric Hofrichter. This report would not have been possible without the support from the Auburn University Highway Research Center and the Alabama Department of Transportation. A special thank you is in order to my parents, Randy and Lynda Neal, for their unwavering support and sacrifice. I will be eternally indebted to them for all that they have done for me. I would also like to thank Mary Chandler Allen for the unconditional love and support necessary for me to complete this thesis. Lastly, I must give thanks to my Lord and Savior for all his blessings. It is through His power and glory that I attribute my successes.

Table of Contents

List of Tables

List of Figures

List of Abbreviations

AASHTO	American Association of State Highway and Transportation Officials
ACI	American Concrete Institute
ALDOT	Alabama Department of Transportation
BT-54	Bulb-tee girder 54 in. in height
BT-72	Bulb-tee girder 72 in. in height
VC	Conventionally vibrated concrete
SCC	Self-consolidating concrete
CTE	Coefficient of Thermal Expansion

Chapter 1 Introduction

1.1 Background

Precast, prestressed girders are commonly used in the state of Alabama for bridge construction. New types of concrete have been implemented in precast construction including high performance concrete and self-consolidating concrete (SCC). As these new types of concrete continue to be used in construction, questions regarding their performance in relation to conventionally vibrated concrete (VC) start to surface. It is important that these new materials exhibit a level of performance that parallels or exceeds that of VC. Another issue is the validity of current methods used to predict time-dependent deformations for these new materials. Time-dependent deformations must be properly predicted so that prestress losses and camber can be accurately predicted in precast, prestressed bridge girders.

Inaccurate predictions of prestress losses can cause a significant increase in the amount of prestressing placed in the girder, and in turn drive up the cost of that girder. Furthermore, notably over predicting camber may result in additional quantities of deck concrete or the bridge may experience excessive deflection induced by superimposed dead loads. In order to investigate the use of SCC and address the issue of predicting time-dependent deformations in precast, prestressed bridge girders in the state of Alabama, the Alabama Department of Transportation (ALDOT) sponsored an investigation to be performed by Auburn University researchers. This investigation was performed on twenty eight bulb-tee girders for use in a replacement bridge constructed on

State Route 22 over Hillabee Creek in Tallapoosa County, Alabama. Two spans of the bridge contain girders are constructed with SCC while the remaining two are constructed with VC. These girders were instrumented to collect internal strain, and camber measurements were taken for an extended period of time. Complete details of the entire research study have been reported by Keske et al. (2015a and 2015b).

In a past investigation by Schrantz (2012), the Auburn University Highway Research Center developed a time step prediction procedure to predict time-dependent deformations for the replacement bridge on State Route 22. This program was modified and used by Johnson (2012) to predict time-dependent deformations for the girders used in the replacement bridge on State Route 22. These predictions were compared with internal strain and camber measurements taken from the time of prestress transfer until the girders were transported from the precast plant.

It is important to understand the time-dependent deformations of precast, prestressed bridge girders throughout the service life of the girders. The *AASHTO LRFD Bridge Design Specifications* 2012 edition provides a model to predict prestress losses from time of prestress transfer through the service life of precast, prestressed bridge girders. This investigation uses the *AASHTO LRFD Bridge Design Specifications* 2012 creep and shrinkage models to predict prestress losses and compares these predictions with measured prestress losses through the service life of the precast, prestressed bridge girders used in the replacement bridge on State Route 22. Furthermore, this investigation will seek to compare measured time-dependent deformations of girders constructed with SCC to those with VC.

1.2 Research Objectives

Specific research objectives are stated below:

1. Compare measured time-dependent deformations of PCI bulb-tee girders constructed with CVC to those of PCI bulb-tee girders constructed with SCC.
2. Compare the time-dependent deformations measured in SCC and VC girders to predicted deformations developed from the *AASHTO LRFD Bridge Design Specifications* 2012 model.

1.3 Research Scope

Predicted prestress losses were found for girders manufactured for use in this project. These prestress losses were found by using the *AASHTO LRFD Bridge Design Specifications* 2012 model. Time-dependent deformations of the girders were tracked using vibrating-wire strain gauges to measure internal strains, and a surveyors level was used to measure camber. Due to lack of reliable data and equipment failure, only a few interior girders time-dependent deformations were tracked and compared with predicted values.

1.4 Organization of Thesis

Chapter 2 outlines the principles of predicting time-dependent deformations in precast, prestressed bridge girders. The AASHTO 2012 time-dependent deformation prediction model used in this investigation is explained. A review of previous studies regarding time-dependent deformations in bridge girders follows.

Chapter 3 discusses the design and fabrication of the bulb-tee girders used in this study. The dimensions of the girders along with the material properties for the concrete, prestressing steel and nonprestressed reinforcement are provided. Details regarding the design and material properties for the composite deck, web-walls, and barriers are also

included. The fabrication and construction processes of the girders and composite bridge components are also discussed in detail.

Chapter 4 presents the surveying method used to collect the camber measurements,

Chapter 5 discusses the process used to measure the internal strain in the girders and deck. Included in this section is the type of gauge used, the location of the gauges within the girders and deck, and the data acquisition system used to record the measurements.

Chapter 6 is a presentation of the results of this study. It starts with an explanation of how measured results were adjusted to account for thermal effects. Next, the inputs and assumptions associated with implementing the AASHTO 2012 time-dependent prediction model are presented. Finally, camber histories along with measured and predicted prestress losses are reported.

Chapter 7 presents a brief overview of the study along with final conclusions drawn from the results.

Chapter 2 Literature Review

2.1 Introduction

A major portion of this investigation involved the comparison of predicted time-dependent deformations to actual measured deformations in bulb-tee girders constructed with self-consolidating concrete (SCC) and conventionally vibrated concrete (VC). The predictions were developed from the *AASHTO LRFD Bridge Design Specifications* 2012 time-dependent deformation prediction model. In the investigation by Johnson (2012), it was determined that prediction models displayed a higher level of accuracy when measured material properties were used in lieu of predicted material properties. The time-dependent deformation predictions were used to compare the level effective prestress to measured prestress levels. Subsequent sections in this chapter explain the AASHTO LRFD 2012 time-dependent deformation prediction model. The end of this chapter discusses previous studies relating to time-dependent deformation of prestressed, precast concrete girders containing SCC.

2.2 AASHTO 2012 Total Loss of Prestress

The procedure outlined in the *AASHTO LRFD Bridge Design Specifications* 2012 time-dependent deformation prediction model is based on the principles of compatibility, linear-elastic stress-strain material behavior, equilibrium, and the assumption that plane sections remain plane. These fundamental properties provide the framework for which the AASHTO 2012 model computes complicated cross-sectional deformations at different stages in the girders life. As mentioned earlier, actual measured material

properties were used in the prediction model. AASHTO 2012 separates the estimation of total prestress loss into two different categories: instantaneous and time-dependent losses. Losses due to anchorage set, friction, and elastic shortening are instantaneous, whereas losses due to creep, shrinkage, and relaxation are time-dependent (AASHTO 2012). Values of prestress losses shall be applicable to normal weight concrete only and for specified concrete strengths up to 15.0 ksi, unless stated otherwise (AASHTO 2012). In lieu of more detailed analysis, total prestress losses in members constructed and prestressed in a single stage, relative to the stress immediately before transfer for pretensioned members, Δf_{pT} may be taken as follows in Equation 2-1.

$$\Delta f_{pT} = \Delta f_{pES} + \Delta f_{pLT} \qquad \text{Equation 2-1}$$

Where:

Δf_{pT} = the total prestress loss

Δf_{pES} = the sum of all losses or gains due to elastic shortening or extension at the time of application of prestress and/or external loads

Δf_{pLT} = the losses due to long-term shrinkage and creep of concrete, and relaxation of the steel (ksi)

As seen in Equation 2-1 anchorage and friction losses are not included. For pretensioned members designers are not required by AASTHO 2012 to determine these losses. It is typically the responsibility of the precaster to supply these losses in the contract documents and then they are verified during construction.

2.3 AASTHO Refined Estimates of Time-Dependent Losses

AASHTO 2012 offers two approaches in order to estimate time-dependent losses: an approximate or a refined approach. The approximate approach uses one expression to

estimate the long-term prestress loss, Δf_{pLT}, due to creep, shrinkage, and relaxation of steel. The approximate approach is not applicable for members of unusual dimensions, level of prestressing, construction staging, or concrete constituent materials (AASHTO 2012). It is stated in AASHTO 2012 that estimates utilizing the refined approach can lead to a better estimate of total losses compared with values obtained using the approximate approach. The expressions used in the AASHTO 2012 refined method for estimating prestress losses are based upon research in Tadros et al. (2003), which aimed at extending applicability of the provisions of these specifications to high-strength concrete. The refined method splits the estimation of long-term losses into two separate time periods: from time of transfer to the time of deck casting and from after deck is cast to final time. The refined approach to estimate the change in steel stress due to time-dependent loss, Δf_{pLT}, is defined by Equation 2-2 as follows.

$$\Delta f_{pLT} = \left(\Delta f_{pSR} + \Delta f_{pCR} + \Delta f_{pR1}\right)_{id} + \left(\Delta f_{pSD} + \Delta f_{pCD} + \Delta f_{pR2} - \Delta f_{pSS}\right)_{df} \quad \text{Equation 2-2}$$

Where

Δf_{pSR}= prestress loss due to shrinkage of girder concrete between transfer and deck placement (ksi)

Δf_{pCR} = prestress loss due to creep of girder concrete between transfer and deck placement (ksi)

Δf_{pR1} = prestress loss due to relaxation of prestressing strands between time of transfer and deck placement (ksi)

Δf_{pR2} = prestress loss due to relaxation of prestressing strands in composite section between time of deck placement and final time (ksi)

Δf_{pSD} = prestress loss due to shrinkage of girder concrete between time of deck placement and final time (ksi)

Δf_{pCD} = prestress loss due to creep of girder concrete between time of deck placement and final time (ksi)

Δf_{pSS} = prestress gain due to shrinkage of deck in composite section (ksi)

$\left(\Delta f_{pSR} + \Delta f_{pCR} + \Delta f_{pR1}\right)_{id}$ = sum of time-dependent prestress losses between transfer and deck placement (ksi)

$\left(\Delta f_{pSD} + \Delta f_{pCD} + \Delta f_{pR2} - \Delta f_{pSS}\right)_{df}$ = sum of time-dependent prestress losses after deck placement (ksi)

Creep is defined as "the time-dependent increase of strain in hardened concrete subjected to sustained stress" (ACI 209 1992). Many studies have been conducted to determine the creep characteristics of different types of concrete. Neville (1997) concluded that creep in concrete that underwent accelerated curing can be thirty to fifty percent lower than creep in concrete that underwent non-accelerated curing. When hard coarse aggregates are used in concrete mixtures, creep was found to be reduced when compared to mixtures using soft coarse aggregates (Mokhtarzadeh and French 2000). Studies have also shown that concrete with a higher compressive strength will exhibit less creep than concrete with a lower compressive strength (Hinkle 2006). In AASHTO 2012 Section 5.4.2.3 values associated in determining the losses due to shrinkage and creep are presented. AASHTO 2012 allows the user to determine the effects of creep and shrinkage by using the provisions of three different methods: Articles 5.4.2.3.2 and 5.4.2.3.3 in AASHTO 2012, the CEB-FIP model code, or ACI 209. In the investigation by Johnson (2012) all three of the provisions were used to compare predicted to measured

time-dependent deformations. This investigation focuses on using the provisions in AASHTO 2012 Sections 5.4.2.3.2 and 5.4.2.3.3. The methods of determining creep and shrinkage, as specified in AASHTO 2012 Sections 5.4.2.3.2 and Sections 5.4.2.3.3, are based on Huo et al. (2001), Al-Omaishi (2001), Tadros (2003), and Collins and Mitchell (1991) (AASHTO 2012). These methods are based on the recommendation of ACI Committee 209 as modified by additional recently published data (AASHTO 2012). In AASHTO Section 5.4.2.3.2 a creep coefficient is introduced in order to estimate time-dependent prestress losses. The creep coefficient is applied to the compressive strain caused by permanent loads in order to obtain the strain due to creep (AASHTO 2012). Creep is influenced by the same factors as shrinkage, and also by: magnitude and duration of the stress, maturity of the concrete at the time of loading, and the temperature of concrete (AASHTO 2012). The creep coefficient, $\Psi(t, t_i)$, at different time intervals is determined by the following equations:

$$\Psi(t, t_i) = 1.9 k_s k_{hc} k_f k_{td} t_i^{-0.118} \qquad \text{Equation 2-3}$$

in which:

$$k_s = 1.45 - 0.13(V/S) \geq 1.0 \qquad \text{Equation 2-4}$$

$$k_{hc} = 1.56 - 0.008H \qquad \text{Equation 2-5}$$

$$k_f = \frac{5}{1 + f'_{ci}} \qquad \text{Equation 2-6}$$

$$k_{td} = \left(\frac{t}{61 - 4f'_{ci} + t} \right) \qquad \text{Equation 2-7}$$

where

k_s = factor for the effect of the volume-to-surface ratio of the component

V/S = volume to surface ratio (in.)

k_{hc} = humidity factor for creep

H = relative humidity (%)

k_f = factor for the effect of the concrete strength

f'_{ci} = specified compressive strength of concrete at time of prestressing for pretensioned members and at time of initial loading for nonprestressed members. If concrete age at time of initial loading is unkown at design time, f'_{ci} may be taken as $0.80f'_c$ (ksi)

k_{td} = time development factor

t = maturity of concrete (day), defined as age of concrete between time of loading for creep calculations, or end of curing for shrinkage calculations, and time being considered for analysis of creep or shrinkage effects

t_i = age of concrete at time of load application (day)

AASHTO 2012 states that the surface area used in determining the volume-to-surface ratio should include only the area that is exposed to atmospheric drying, and for precast members with cast-in-place topping, the total precast surface should be used.

Shrinkage is defined as the time-dependent strain measured from an unloaded and unrestrained concrete specimen. The two major types of shrinkage accounted for in prediction models are drying shrinkage and autogenous shrinkage. Drying shrinkage occurs primarily because of moisture loss during the drying or curing process. Autogenous shrinkage results from self-densification occurring in the concrete as a result of hydration.

Shrinkage, like creep, causes a shortening in the overall length of the member, and in the case of a prestressed member, this would cause a loss of prestress force. Therefore, it is important to identify the shrinkage properties of a concrete mixture so that an accurate shrinkage strain prediction can be made

AASHTO 2012 states that shrinkage of concrete can vary over a wide range from nearly nil if continually immersed in water to in excess of 0.0008 for thin sections made with high shrinkage aggregates and sections that are not properly cured. Shrinkage is affected by: aggregate characteristics and proportions, average humidity at the bridge site, water to cement ratio (*W/C*), type of cure, volume to surface area ratio of member, and duration of drying period (AASHTO 2012). Shrinkage prediction for this method is based on aggregate characteristics, concrete strength, curing method, average humidity, volume-to-surface area ratio, duration of drying, and the age at the start of drying. The expression found in AASHTO 2012 Section 5.4.2.3.3 may be used to determine the strain due to shrinkage, ε_{sh}, for concretes not utilizing shrinkage-prone aggregates, at any time, *t*, which can be seen in Equation 2-8.

$$\varepsilon_{sh} = k_s k_{hs} k_f k_{td} 0.48 \times 10^{-3} \qquad \text{Equation 2-8}$$

in which:

$$k_{hs} = (2.00 - 0.014H) \qquad \text{Equation 2-9}$$

where

k_{hs} = humidity factor for shrinkage

AASHTO 2012 states that if the concrete is exposed to drying before 5 days of curing have elapsed, the shrinkage as determined in Equation 2-8 should be increased by 20 percent.

2.3.1 Losses: Time of Transfer to Time of Deck Placement

In AASHTO 2012 Section 5.9.5.4.2 contains the expressions derived in Tadros et al. (2003) to determine the losses due to shrinkage, creep, and relaxation of steel from time of initial transfer to time of deck placement. The prestress loss due to the shrinkage of girder concrete between time of initial transfer and deck placement, Δf_{pSR}, is determined by Equation 2-10.

$$\Delta f_{pSR} = \varepsilon_{bid} E_p K_{id} \qquad \text{Equation 2-10}$$

in which

$$K_{id} = \frac{1}{1 + \frac{E_p}{E_{ci}} \frac{A_{ps}}{A_g} \left(1 + \frac{A_g e_{pg}^2}{I_g}\right) \left[1 + 0.7\Psi_b(t_f, t_i)\right]} \qquad \text{Equation 2-11}$$

where

ε_{bid} = concrete shrinkage strain of girder between the time of transfer and deck placement per Equation 2-8

K_{id} = transformed section coefficient that accounts for time-dependent interaction between concrete and bonded steel in the section being considered for time period between transfer and deck placement

e_{pg} = eccentricity of prestressing force with respect to centroid of girder (in); positive in common construction where it is below girder centroid

$\Psi_b(t_f, t_i)$ = girder creep coefficient at final time due to loading introduced at transfer per Equation 2-3

t_f = final age (days)

t_i = age at transfer (days)

The prestress loss due to creep of girder concrete between time of initial transfer and deck placement, Δf_{pCR}, is determined by Equation 2-12.

$$\Delta f_{pCR} = \frac{E_p}{E_{ci}} f_{cgp} \Psi_b(t_d, t_i) K_{id} \qquad \text{Equation 2-12}$$

where

$\Psi_b(t_d, t_i)$ = girder creep coefficient at time of deck placement due to loading introduced at transfer per Equation 2-3

t_d = age at deck placement (days)

AASTHO 2012 provides a few different ways to estimate the prestress loss due to relaxation of prestressing strands between time of transfer and deck placement. One of which AASHTO 2012 states that the relaxation loss between time of transfer and deck placement, Δf_{pR1}, may be assumed equal to 1.2 ksi for low-relaxation strands. Furthermore AASHTO provides two expressions in which, Δf_{pR1}, may be estimated, one of which can be found in Equation 2-13.

$$\Delta f_{pR1} = \frac{f_{pt}}{K_L}\left(\frac{f_{pt}}{f_{py}} - 0.55\right) \qquad \text{Equation 2-13}$$

where

f_{pt}= stress in prestressing strands immediately after transfer, taken not less than $0.55 f_{py}$ in Equation 2-13

K_L = 30 for low relaxation strands and 7 for other prestressing steel, unless more accurate manufacturer's data are available

2.3.2 Losses: Time of Deck Placement to Final Time

In AASHTO LRFD Section 5.9.5.4.3 contains the expressions derived in Tadros et al. (2003) to determine the losses due to shrinkage, creep, and relaxation of steel from

time of deck placement to final time. The prestress loss due to shrinkage of girder concrete between time of deck placement and final time, Δf_{pSD}, was determined by Equation 2-14.

$$\Delta f_{pSD} = \varepsilon_{bdf} E_p K_{df} \qquad \text{Equation 2-14}$$

in which

$$K_{df} = \frac{1}{1 + \frac{E_p}{E_{ci}} \frac{A_{ps}}{A_c} \left(1 + \frac{A_c e_{pc}^2}{I_c}\right) \left[1 + 0.7 \Psi_b (t_f, t_i)\right]} \qquad \text{Equation 2-15}$$

where

ε_{bdf} = shrinkage strain of girder between time of deck placement and final time per Equation 2-8

K_{df} = transformed section coefficient that accounts for time-dependent interaction between concrete and bonded steel in the section being considered for time period between deck placement and final time

e_{pc} = Eccentricity of prestressing force with respect to centroid of composite section (in.), positive in typical construction where prestressing force is below centroid of section

A_c = area of section calculated using the gross composite concrete section properties of the girder and the deck and the deck-to-girder modular ratio (in.^{2})

I_c = moment of inertia of section calculated using the gross composite concrete section properties of the girder and the deck and the deck-to-girder modular ratio at service (in.^{4})

The prestress loss or gain due to the creep of girder concrete between time of deck placement and final time, Δf_{pCD}, where a loss is positive and gain is negative can be estimated by Equation 2-16.

$$\Delta f_{pCD} = \frac{E_p}{E_{ci}} f_{cgp}\left[\Psi_b(t_f, t_i) - \Psi_b(t_d, t_i)\right] K_{df} + \frac{E_p}{E_c} \Delta f_{cd} \Psi_b(t_f, t_d) K_{df} \quad \text{Equation 2-16}$$

where

Δf_{cd} = change in concrete stress at centroid of prestressing strands due to long-term losses between transfer and deck placement, combined with deck weight and superimposed loads (ksi)

$\Psi_b(t_f, t_d)$ = girder creep coefficient at final time due to loading at deck placement per Equation 2-3

AASHTO 2012 states about one-half of the losses due to relaxation occur before deck placement; therefore, the losses after deck placement are equal to the prior losses. The prestress loss due to relaxation of prestressing strands in composite section between time of deck placement and final time, Δf_{pR2}, can be determined by Equation 2-17.

$$\Delta f_{pR2} = \Delta f_{pR1} \quad \text{Equation 2-17}$$

After composite action is achieved, the deck concrete shrinks, and this shrinkage is restricted by the top of the girder. This restriction exerts a compressive force on the top of the girder, and thusly an equal tensile force into the deck. This action causes a downward deflection, and also causes tension to develop in the bottom of the girder. For girders with prestressing located in the bottom of the girder, the shrinkage of the deck concrete causes the strands to experience an increase in tension. The expression used in

AASHTO 2012 to determine the prestress gain due to shrinkage of deck composite section, Δf_{pSS}, shall be determined by Equation 2-18.

$$\Delta f_{pSS} = \frac{E_p}{E_c} \Delta f_{cdf} K_{df} \left[1 + 0.7\Psi_b\left(t_f, t_d\right)\right] \quad \text{Equation 2-18}$$

in which

$$\Delta f_{cdf} = \frac{\varepsilon_{ddf} A_d E_{cd}}{\left[1 + 0.7\Psi_d\left(t_f, t_d\right)\right]} \left(\frac{1}{A_c} - \frac{e_{pc} e_d}{I_c}\right) \quad \text{Equation 2-19}$$

where

Δf_{cdf} = change in concrete stress at centroid of prestressing strands due to shrinkage of deck concrete (ksi)

ε_{ddf} = shrinkage strain of deck concrete between placement and final time per Equation 2-8

A_d = area of deck concrete (in.^{2})

E_{cd} = modulus of elasticity of deck concrete (ksi)

e_d = eccentricity of deck with respect to the gross composite section, positive in typical construction where deck is above girder (in.)

$\Psi_d\left(t_f, t_d\right)$ = creep coefficient of deck concrete at final time due to loading introduced shortly after deck placement (i.e. overlays, barriers, etc.) per Equation 2-3

2.4 Previous Research on Time-Dependent Deformations of SCC

One of the questions regarding implementing SCC for use in precast, prestressed bridge girders is how time-dependent deformations differ from girders constructed with VC. Several research projects have been conducted in North America to investigate the time-dependent deformations of precast, prestressed bridge girders constructed with SCC

to those constructed with VC. Labonte et al. (2005) in conjunction with the Florida Department of Transportation investigated AASHTO Type II precast, prestressed bridge girders constructed with both SCC and VC. No notable differences were found in prestress transfer length, mean camber growth, flexural capacity, shear capacity, or observed web cracking (during load testing) between the SCC and VC beams (Labonte et al. 2005). Trent (2007) monitored prestress losses in girders constructed with SCC and VC. The investigation revealed that girders constructed with VC experienced slightly larger prestress losses than girders constructed with SCC. Schrantz (2012) found no significance differences in camber or camber growth between girders constructed with SCC and VC. Johnson (2012) performed an investigation of the time-dependent deformations of the same bulb-tee girders explored in this investigation. Johnson (2012) performed an analysis of the girders from time of prestress transfer until just before the girders were erected. He concluded that based on time-dependent behavior; there is no reason to deter the implementation of SCC for precast, prestressed girders when produced as specified for the Hillabee Creek Bridge project.

Accurately predicting time-dependent deformations is essential in the design of prestressed bridge girder applications. As SCC begins to be implemented into prestressed bridge girder construction, questions regarding how accurate current methods predict time-dependent deformations of SCC prestressed bridge girders begin to arise. Schrantz (2012) analyzed various types of girders using different SCC and VC mixtures. Schrantz compared predictions using design concrete material properties to actual measured properties. The girders analyzed by Schrantz included AASHTO Type-I girders. However, Johnson (2012) found that predictions developed for the BT-54

girders were incorrect because of an error in the program used to develop the predictions. The ½ in. diameter strands were neglected in the analysis, and this is discussed further in Johnson (2012).

Johnson (2012) compared measured time-dependent deformations of actual bridge girders constructed with both SCC and VC to various creep and shrinkage prediction methods. The girders analyzed by Johnson included PCI BT-54 and PCI BT-74 girders, and actual measured material properties were used in the prediction models. The creep and shrinkage prediction methods implemented by Johnson include: ACI 209, AASHTO 2004, AASHTO 2010, CEB-FIB Model Code 1990 (MC 90), and MC 90-KAV. Where, MC 90-KAV is a variation of the MC 90 method yielded from research conducted by Kavanaugh (2008). These creep and shrinkage models were incorporated into a modified computer program developed by Schrantz (2012) to predict prestress losses. However, a calculation error was found in the temperature corrections for measured camber and internal strain values. The slope of the temperature gradient in the girders web was calculated opposite than assumed. This is discussed further in Section 6.2. Also, the concrete coefficient of thermal expansion values assigned to both SCC and VC girders were found to decrease the level of accuracy in the temperature corrections for camber and internal strain. This is further discussed in Section 6.2.3. Johnson determined that the ACI and AASHTO 2010 methods significantly under-predicted effective prestress at later ages. Although, it was also found that all of the prediction methods over-predicted effective prestress in the first months after transfer while mostly under-predicting effective prestress at later ages.

Another question that arises is how the level of accuracy using measured material properties differs from using design values. Johnson (2012) used the AASHTO 2010 creep and shrinkage prediction models to compare time-dependent deformations using measured concrete material properties to design material properties. It was determined that a significant reduction in the accuracy of predictions occurs when specified strength and computed stiffness values were used. These resulting prediction errors are at least as large as the errors associated with creep and shrinkage models. This is true regardless of whether the concrete is VC or SCC.

Stallings et al. (2003) determined that accurate predictions require the use of accurate material parameters. Cambers that were calculated using standard material parameters consistently exceeded measured values, and these errors resulted primarily from overestimating creep and shrinkage characteristics of the concrete (Stallings 2003). These findings were from bridge girders that contained high-performance VC girders. Stallings et al. (2003) made it clear that under-predicted prestress values at later girder ages might discourage some designers from using high performance concrete in long-span prestressed bridge girders. Therefore, based on these past studies only measured concrete material properties were used in this investigation. Barr et al. (2008) found that the AASHTO prediction methods over-predicted the average prestress losses for highly stressed girders by 20%. The error seems to be occurring in the creep and shrinkage prediction models, so most of the research conducted recently has been geared toward comparing the creep and shrinkage characteristics of SCC and VC.

Levy et al. (2010) determined that creep and shrinkage strains of SCC elements were no larger than conventional-slump concrete at similar levels of concrete strength

and applied prestress force. Similarly, Kavanaugh (2008) found that all of the SCC mixtures tested exhibited creep values similar to or less than VC mixtures. In accelerated-cured specimens, the creep strains of all of the SCC mixtures were less than those of VC concretes (Kavanaugh 2008). Shrinkage strains in the SCC mixtures were found to be similar in magnitude to the shrinkage strains of the VC mixtures (Kavanaugh 2008).

Past studies have also incorporated earlier versions of AASHTO prediction models to determine which methods are most accurate in predicting long-term strain changes in both high-performance VC and SCC concretes. Levy et al. (2010) found that ACI 209 and AASHTO long-term creep and shrinkage predictions of SCC mixtures including slag cement as a supplementary cementing materials (SCM) were much larger than measured values. The same result was found for high-strength SCC mixtures (Levy et al. 2010) with slag cement or fly ash as SCM. Kavanaugh (2008) concurred with Levy about the ACI 209 prediction model, concluding that it could not accurately predict the creep strain of high-strength concrete. Levy et al. (2010) concluded that the AASHTO 2010 model provided better shrinkage strain predictions than AASHTO 2004 predictions, but the creep predictions were very similar. Kavanaugh (2008) concluded that the AASHTO 2010 method overestimated creep in accelerated-cured concrete. The MC 90 was found to be the most accurate model to predict creep strains for both VC and SCC mixtures (Kavanaugh 2008). However, the MC 90 models evaluated were updated in 1999, and comparisons were not made to the newer models.

2.5 Summary

The AASHTO 2012 Bridge Design Specification method to predict prestress losses allows for the use of several different prediction models to develop predictions for creep and shrinkage strains. While various studies have sought to determine which of these creep and shrinkage prediction models produces the most accurate predictions, the results of these studies are largely inconclusive. Many of the models do not provide predictions that correspond to measured deformations in full-scale in-service girders. Also, very few investigations have compared time-dependent deformations of in-service precast, prestressed bridge girders composed with SCC to VC. Therefore, this investigation will predict time-dependent deformations of in-service girders using the creep and shrinkage prediction models found in the AASHTO 2012 Bridge Design Specification. These predictions will be compared to measured deformations of large in-service girders manufactured with SCC and VC. The research below will also seek to compare the in-service performance of girders constructed with SCC to VC.

Chapter 3 Design and Construction of Experimental Specimens

3.1 Introduction

The girders used in this research for the bridge over Hillabee Creek on Alabama Highway 22 in Tallapoosa County, Alabama were constructed at Hanson Pipe and Precast in Pelham, Alabama during the fall of 2010. The bridge extends 470 ft between abutments and is shown in Figure 3-1. All twenty-eight girders were PCI Bulb-Tee girders. Spans 1 and 4 contained seven BT-54 girders 97 ft 10 in. in length (Figure 3-2) and spans 2 and 3 contained seven BT-72 girders 134 ft 2 in. in length (Figure 3-3). Two different types of concrete were used to manufacture these girders. The girders in spans 1 and 2 were cast using a self-consolidating concrete (SCC) while the girders in spans 3 and 4 were cast using a conventionally vibrated concrete (VC). A description of the girders, deck, webwalls, and diaphragms of each span follows.

Figure 3-1: Hillabee Creek Bridge (Span 1 in Foreground)

Figure 3-2: Exterior CVC BT-54 Girder in Span 4

Figure 3-3: Span 2 BT-72 Girders

3.2 Bridge Description

A plan view of the bridge with respect to Hillabee Creek can be seen in Figure 3-4. Each span contains seven precast, prestressed concrete girders spaced at 6 ft. 6 in. on center. Spans 1 and 2 contain girders constructed with SCC, while spans 3 and 4 contain girders constructed with VC. The girder framing scheme can be seen in Figure 3-5, where girders in spans 1 and 2 are labeled 1 thru 7, and girders in spans 3 and 4 are labeled 8 thru 14. The girders rest on neoprene bearing pads which are supported by reinforced cast-in-place, vibrated-concrete (VC) bents and columns between spans and reinforced cast-in-place, VC abutments at each end of the bridge. The roadway has a transverse width of 44 ft. between ALDOT standard drawing number I-131 traffic barriers with a 7 in. thick VC deck as shown in Figure 3-6. The bridge was constructed on a 15-degree skew. Typical girder cross sections are shown in Figure 3-7 and Figure 3-8.

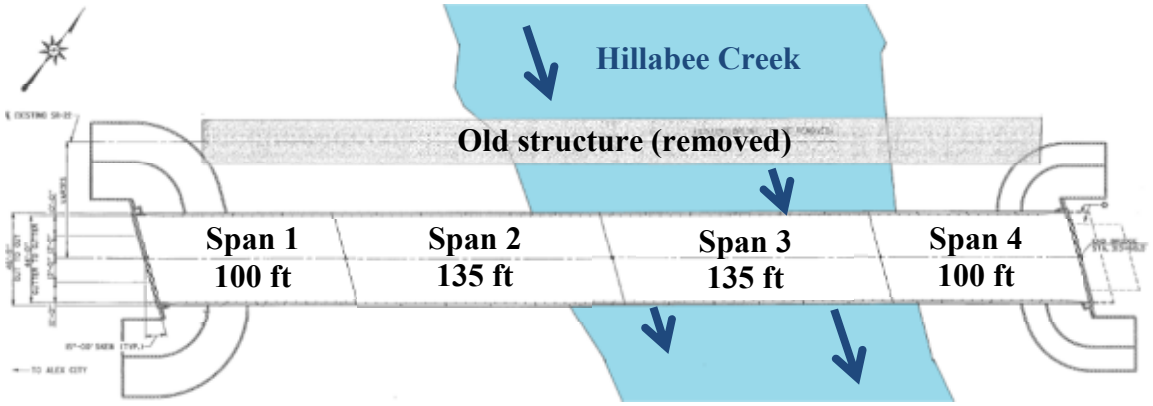

Figure 3-4: Plan View of Bridge with Respect to Hillabee Creek

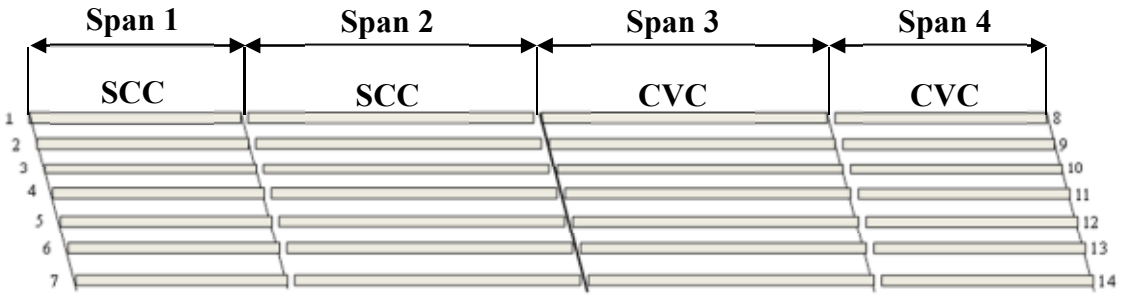

Figure 3-5: Girder Framing Scheme

Figure 3-6: Bridge Deck and Barriers in Place

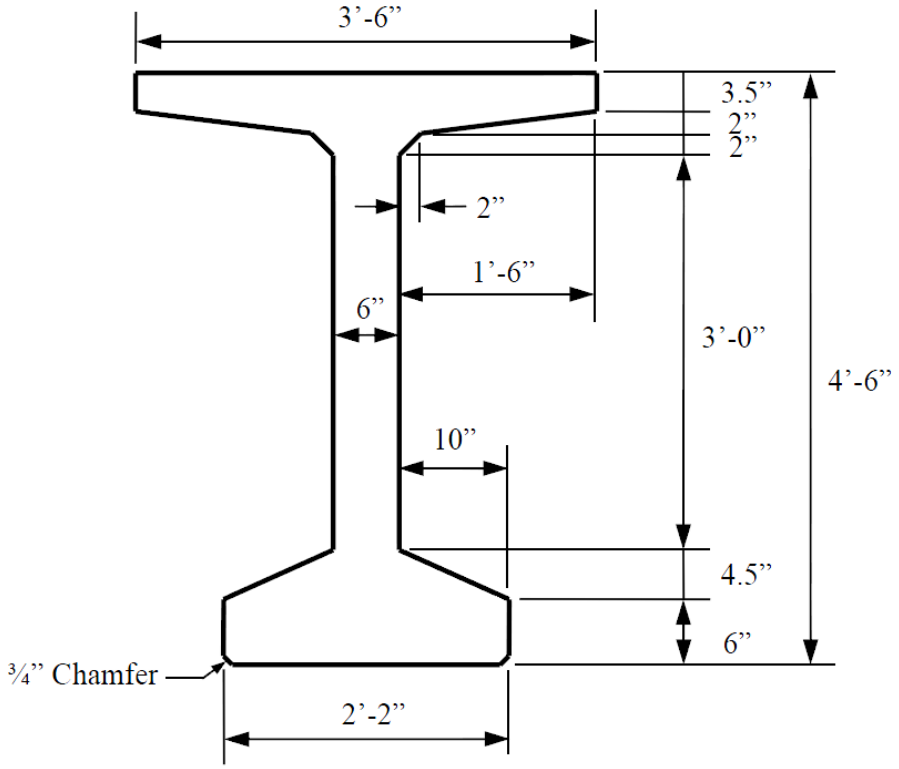

Figure 3-7: BT-54 Cross Section

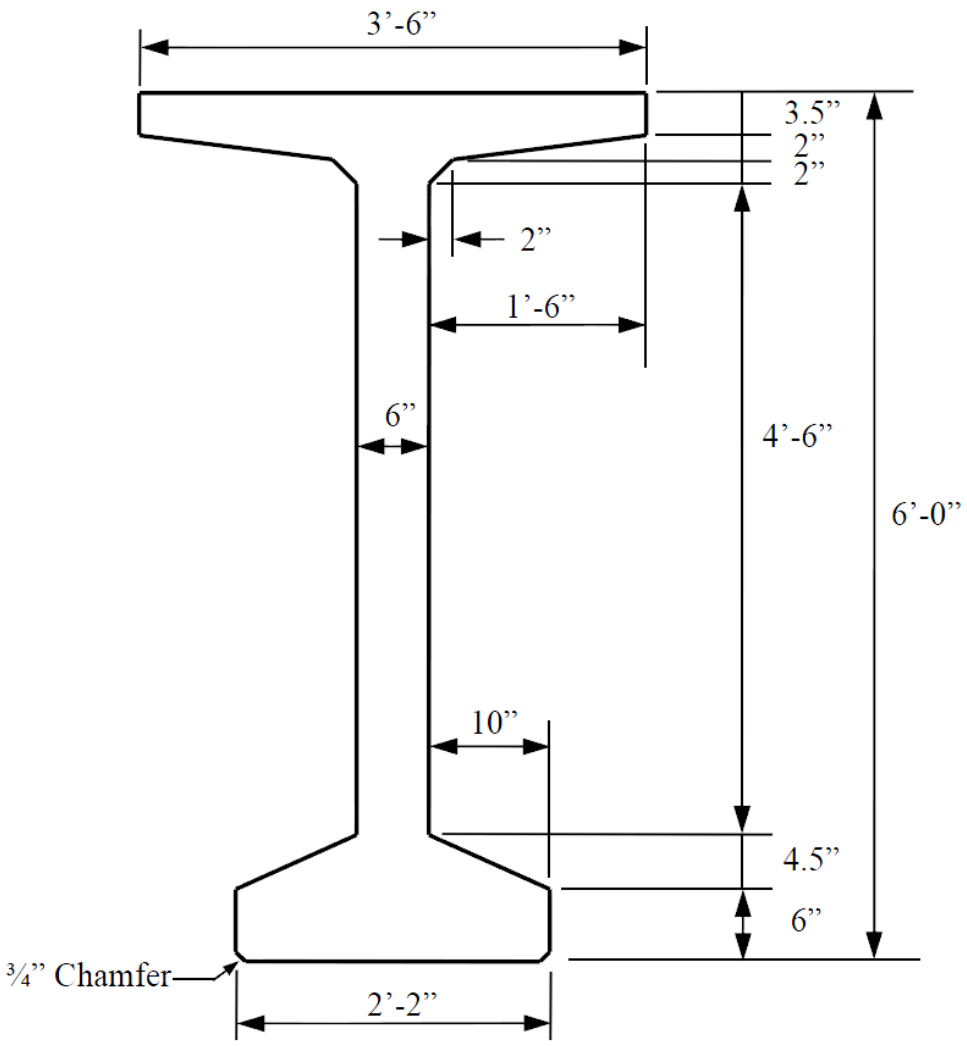

Figure 3-8: BT-72 Cross Section

The girders were cast over a thirty-eight day period between September 21 and October 28, 2010. The girders were erected on four days between May 5 and May 10, 2011 (Figure 3-9). Cast-in-place, vibrated-concrete diaphragms or “webwalls” were then gradually added, connecting to the girders using reinforcing bars, between June 6 and June 21, 2011. Diaphragms are located at the ends of each girder, at the midspan points of the girders in spans 1 and 4, and at the quarterspan and midspan points of the girders in spans 2 and 3. The four bridge deck spans were cast on four separate days between

August 3 and August 16, 2011. The deck was cast to achieve composite action with the girders and diaphragms using vibrated concrete. There is no structural continuity between any of the four spans due to the open deck joint at the end of each. Lastly, traffic barriers were slip-form cast over reinforcement protruding from the deck on November 1, 2011.

Figure 3-9: Erection of a VC Girder in Span 3

3.3 Girder Identification

A specimen identification scheme was developed for this project by Dunham (2011), and adapted for use in this report. Figure 3-10 illustrates the specimen identification scheme used in this project. Two different PCI Bulb-Tee sections were used in this project; half of the girders had heights of 54 in., and the other half had

heights of 72 in. The specimen heights are the first number in the specimen identification scheme. The girder number corresponds to the numbering system set forth on the bridge erection plan. The girder numbers range from 1 to 14. The letter immediately following the girder number indicates the type of concrete used in the girder. Girders 1 through 7 of the 54 in. and 72 in. girders were cast using SCC. Girders 8 through 14 of both the 54 in. and 72 in. girders were cast using VC. This scheme was adapted from the precast concrete producer's numbering scheme in order to more readily relate information about the girder being identified. By adapting an identification scheme similar to the precast concrete producer's identification scheme, researchers and the workers at the precast concrete plant were able to communicate efficiently.

In addition to labeling each specific girder with a unique number, it was necessary to group girders according to their casting group. For the 54 in. girders, three girders were cast on the same casting line, while only two 72 in. girders were on the same line. Table 3-1 groups the specific girders into casting groups, which aids in reporting the properties of the concrete used in each girder. The girders in each group were all cast on the same day.

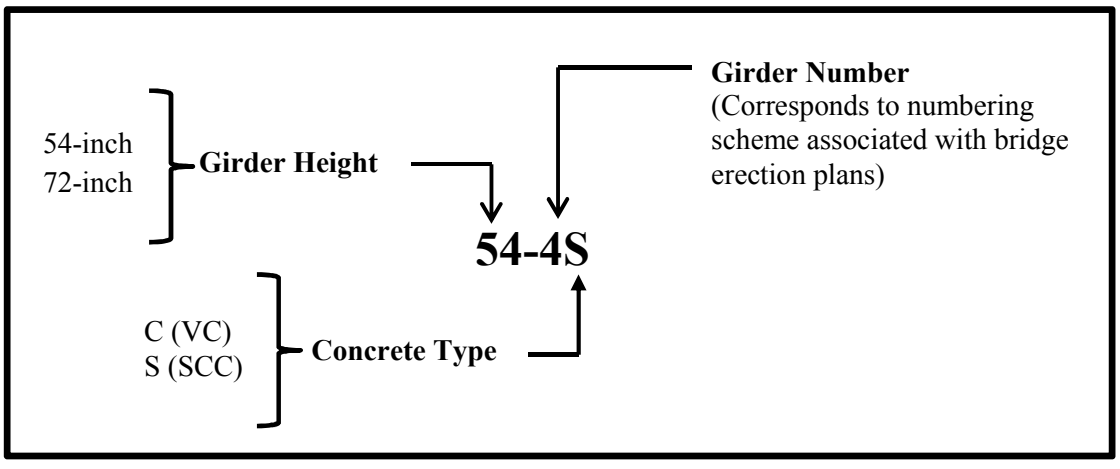

Figure 3-10: Girder Identification Scheme

Table 3-1: Casting Group Designations

Casting Group	Girders
A	54-2S 54-5S 54-6S
B	54-9C 54-10C 54-13C
C	54-1S 54-3S 54-4S
D	54-11C 54-12C 54-14C
E	54-7S 54-8C
F	72-1S 72-7S
G	72-8C 72-14C
H	72-3S 72-4S
I	72-10C 72-13C
J	72-2S 72-5S
K	72-11C 72-12C
L	72-6S 72-9C

3.4 Girders

Two sizes of PCI Bulb-Tee girders were used in the bridge project. Spans 1 and 4 each contained seven BT-54s whose cross section dimensions are shown in Figure 3-7. Each BT-54 was 97'-10" in length with a bearing length of 96'-4". Seven PCI Bulb-Tee 72s were used in spans 2 and 3; cross-section dimensions are shown in Figure 3-8. Each BT-72 is 134'-2" in length with a length of 132'-8" between bearing pad centers. All girders were placed on a 15 degree skew to provide proper alignment for the approaches to the bridge.

3.4.1 Girder Strand Arrangement

Two different strand arrangements were used for the girders depending on the section size. Seven-wire, Grade 270, low-relaxation, ½ -inch diameter strands with an area of 0.153-squre inches each were used in the BT-54 girders. Seven-wire, Grade 270, low-relaxation, ½ -inch "special" diameter strands with an area of 0.167- square inches each were used in the BT-72 girders. The specified jacking stress (f_{pj}) was 202.5 ksi for the bottom strands and draped strands and 32.7 ksi for the lightly tensioned top strands in all of the girders. A two-point draping configuration was used in both the BT-54 girders and BT-72 girders as shown in Figure 3-11 and Figure 3-12.

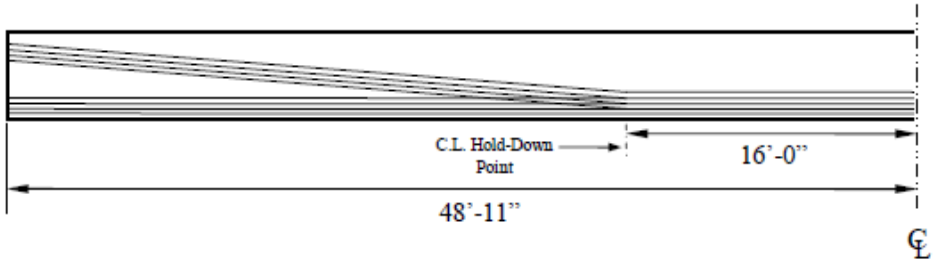

Figure 3-11: BT-54 Draping Configuration

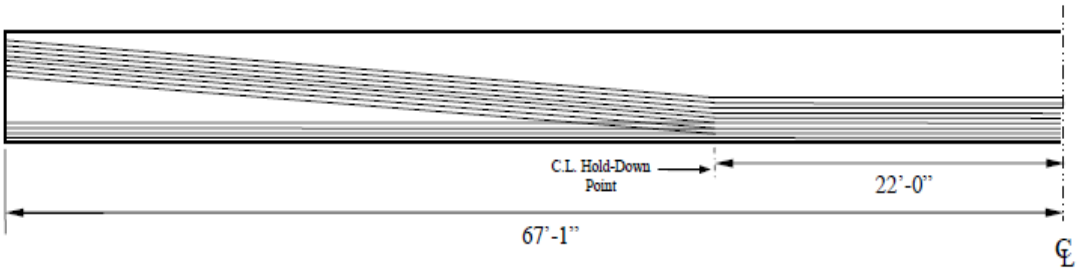

Figure 3-12: BT-72 Draping Configuration

The BT-54 girders contained forty strands including twenty-eight ½ -inch diameter strands in the bottom of the section, eight ½ -inch diameter strands draped along the length of the member, and four ½ -inch diameter lightly tensioned strands in the top of the member. The strands in the bottom of the section as well as the draped strands were tensioned to 202.5 ksi each while the lightly tensioned top strands were tensioned to 32.7 ksi each. The locations of each strand in the BT-54 members at midspan are shown in Figure 3-13 and the locations at the ends of each section are shown in Figure 3-14.

The BT-72 girders contained 50 strands including twenty eight ½ -inch "special" diameter strands in the bottom of the section, eighteen ½ -inch "special" diameter strands draped along the member, and four ½ -inch diameter lightly tensioned strands. The bottom strands and draped strands were tensioned to 202.4 ksi each while the top strands were tensioned to 29.9 ksi each. The locations of the strands at both midspan and the end of the section are illustrated in Figure 3-15 and Figure 3-16.

Figure 3-14 and Figure 3-16 indicate the presence of debonded strands in the girder ends of both the BT-54 girders and the BT-72 girders. The debonding of strands was accomplished by encasing the strand in plastic casing and sealing it with tape. This was done for four strands in the BT-54 girders and six strands for the BT-72 girders for 10 feet from each girder end.

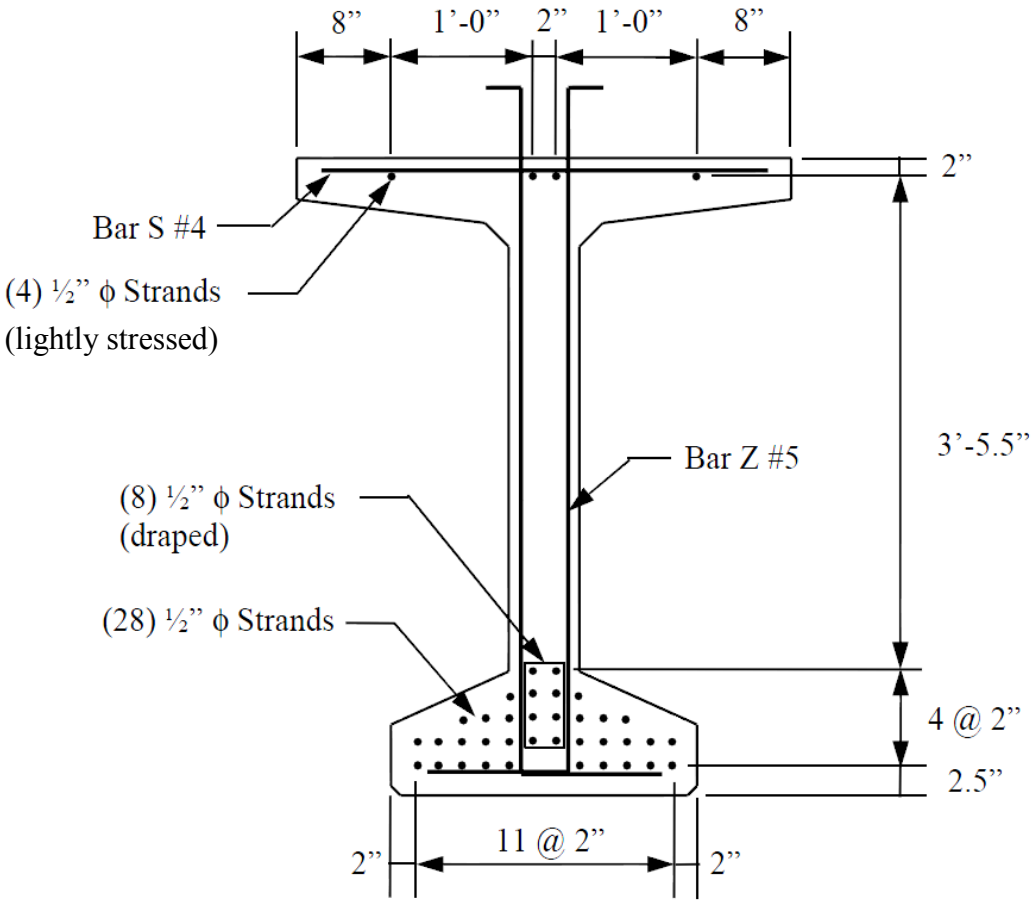

Figure 3-13: BT-54 Reinforcing Bars and Prestressed Strands (Midspan)

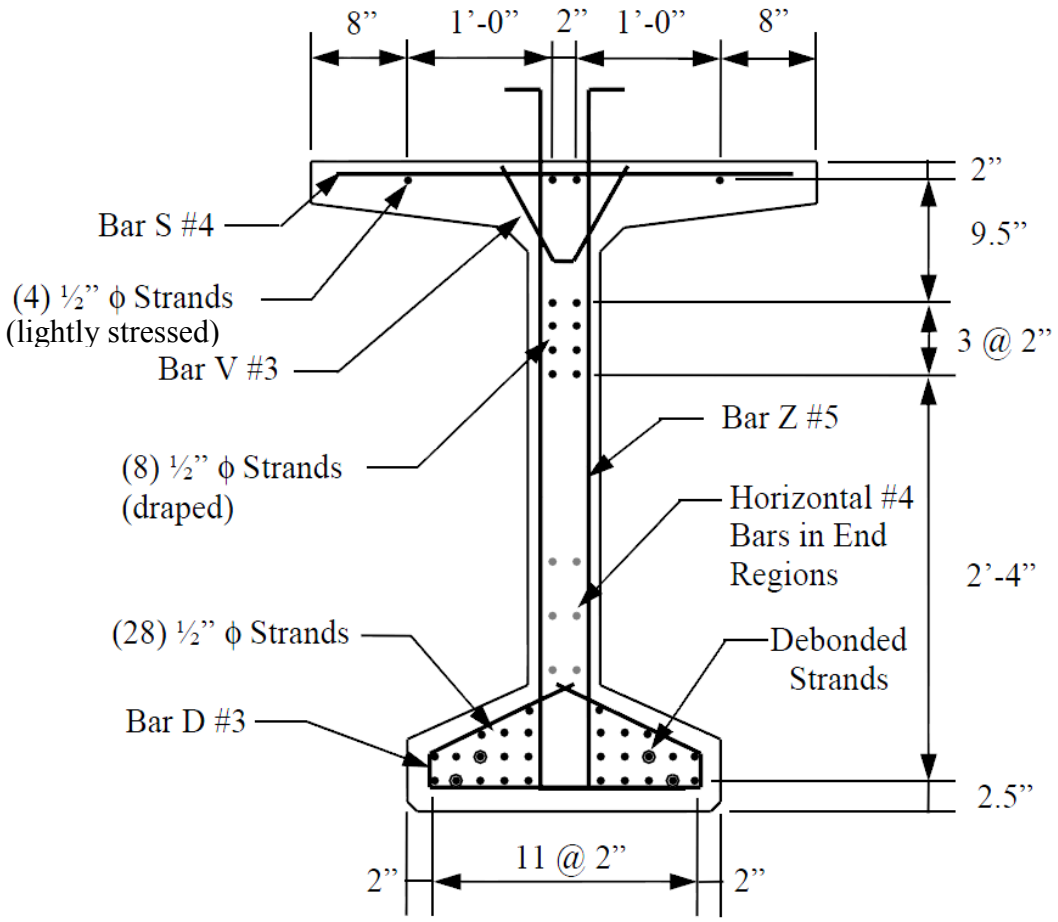

Figure 3-14: BT-54 Mild Steel and Strand Arrangement (End of Span)

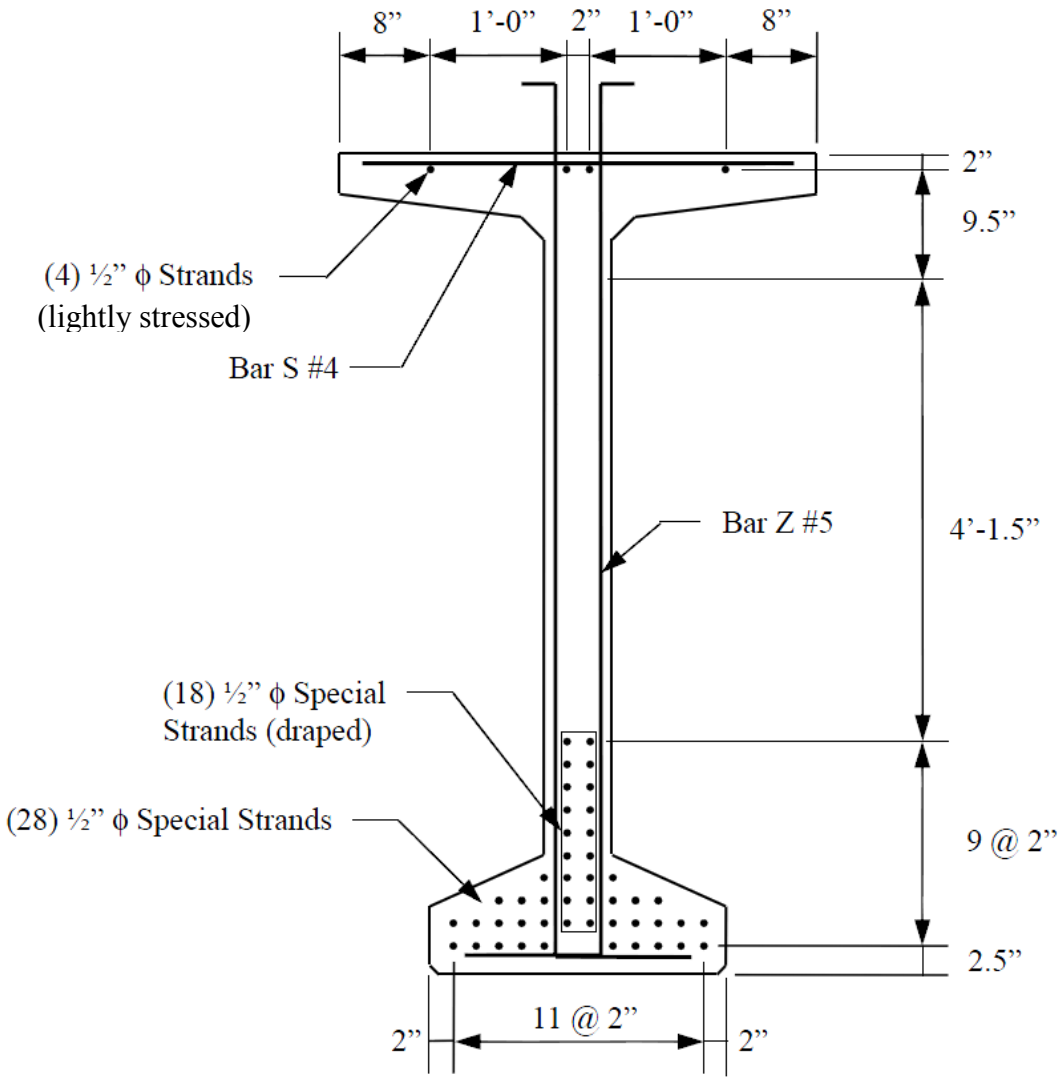

Figure 3-15: BT-72 Mild Steel and Strand Arrangement (Midspan)

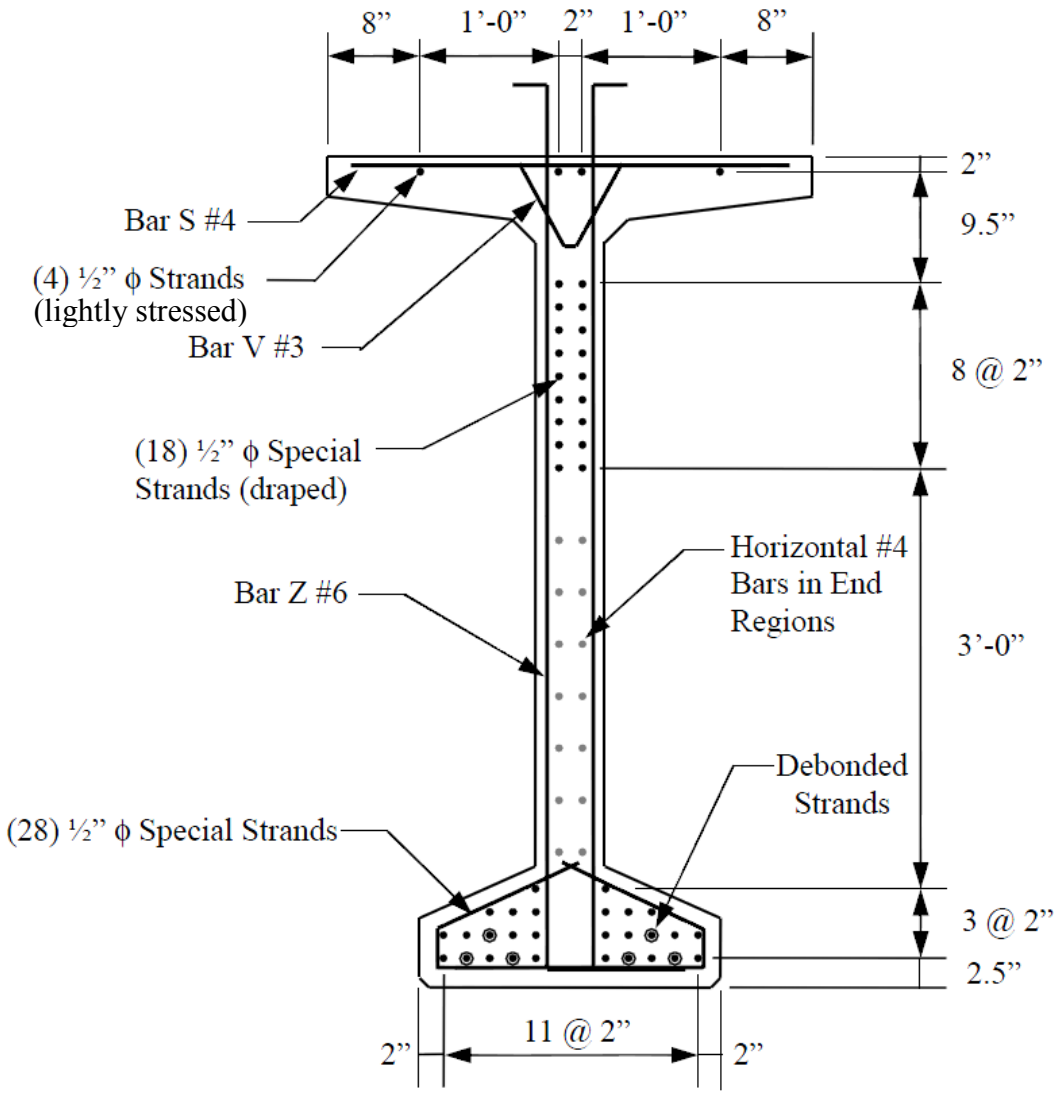

Figure 3-16: BT-72 Mild Steel and Strand Arrangement (End of Span)

3.4.2 Nonprestressed Reinforcement

Nonprestressed reinforcement was needed in the girders to resist shear forces over the girder length as well as anchorage zone forces in the girder ends. The configuration of the mild steel reinforcement in the girders is depicted in Figure 3-13 through Figure 3-16. The four different bar shapes used in both the BT-54 girders and BT-72 girders include Z-bars, bottom steel confinement bars (D-bars), straight bars (S-bars), and V-

bars. Bar spacing along the girder length changed for the BT-54 girders as compared to the bar spacing for the BT-72 girders, as illustrated in Figure 3-17 and Figure 3-18.

At the girder ends, additional horizontal reinforcement in the form of S-bars was required in both the BT-54 and BT-72 girders. The vertical locations of these horizontal bars are shown in Figure 3-14 and Figure 3-16, and their location along the span of the girders is shown in Figure 3-17 and Figure 3-18. It should also be noted that the nonprestressed reinforcement was heavily concentrated at the girder ends. This was due to both the higher shear forces at the ends of the simply-supported girders as well as the spalling and bursting stresses in the girder ends due to the anchorage of the prestressing strands. The bottom steel confinement bars (D-bars) and V-bars were only located at the girder ends, none were required along the girder length closer to midspan.

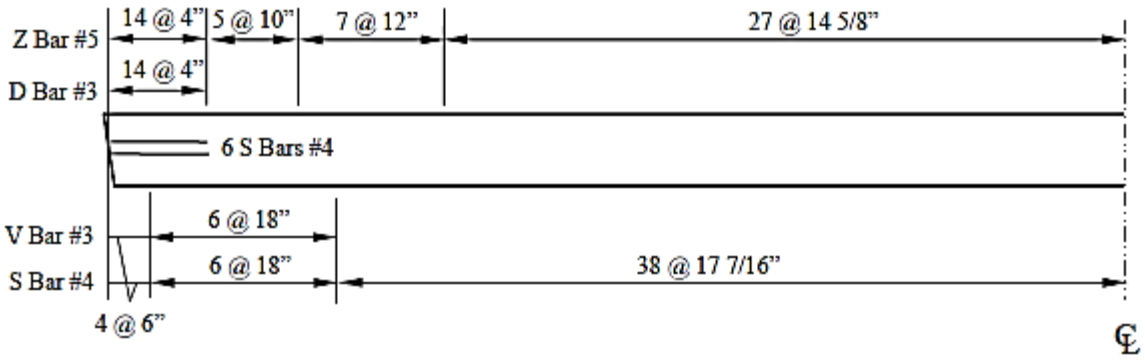

Figure 3-17: BT-54 Reinforcing Bar Spacing

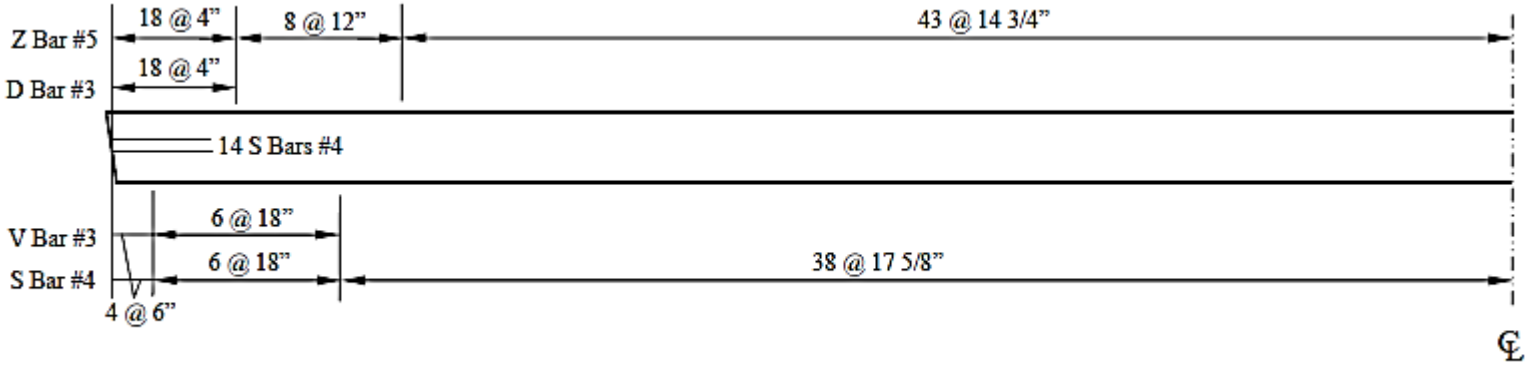

Figure 3-18: BT-72 Reinforcing Spacing

3.5 Webwalls, Haunch, Deck, and Barriers

Each span in the bridge over Hillabee Creek has webwalls at each end connecting all seven girders. In Figure 3-19 the webwall reinforcement configuration and formwork can be seen. Shown in Figure 3-20 and Figure 3-21are the web wall locations for all four spans. A cross-section depiction of the webwall at the bearings is shown in Figure 3-22. The webwalls are 0'-8" thick and span between girders along the skew, achieving composite action with the girders through rebar inserts into the girders. The webwalls achieve composite action with the deck through #5 stirrups and have a bottom face located 0'-10 ½" above the bottom face of the adjacent girders. Spans 1 and 4 contain midspan webwalls in addition to end webwalls. Spans 2 and 3 contain midspan and quarterspan webwalls in addition to end web walls. The midspan and quarterspan webwalls shown in Figure 3-23 have similar characteristics as the end webwalls described above except they do not follow the skew of the bridge. Each of these webwalls is oriented perpendicular to the adjacent girders, but staggered along the skew line.

Figure 3-19: BT-54 Webwall Reinforcement Configuration and Formwork (from Above)

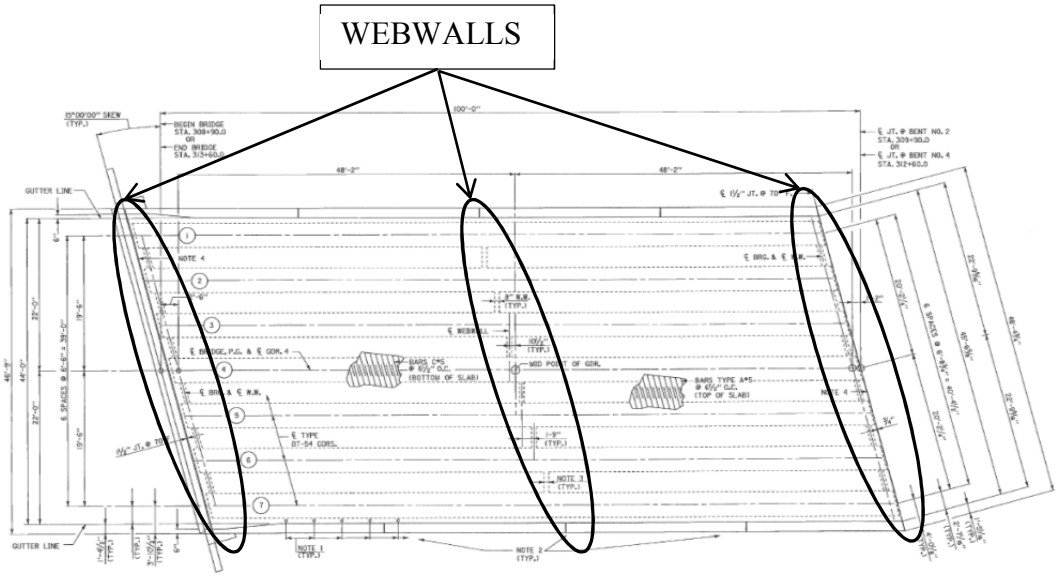

Figure 3-20: Webwall Locations Spans 1 and 4

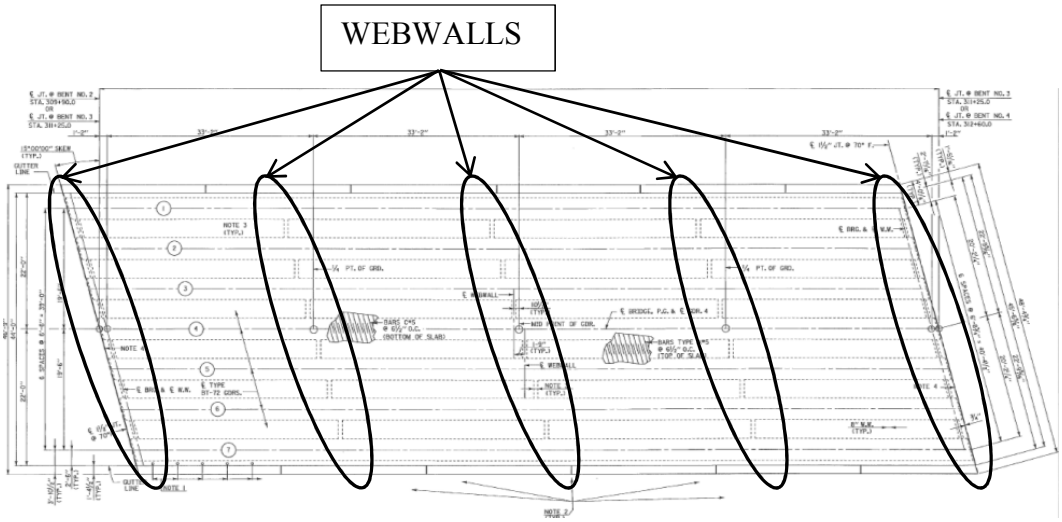

Figure 3-21: Webwall Locations Spans 2 and 3

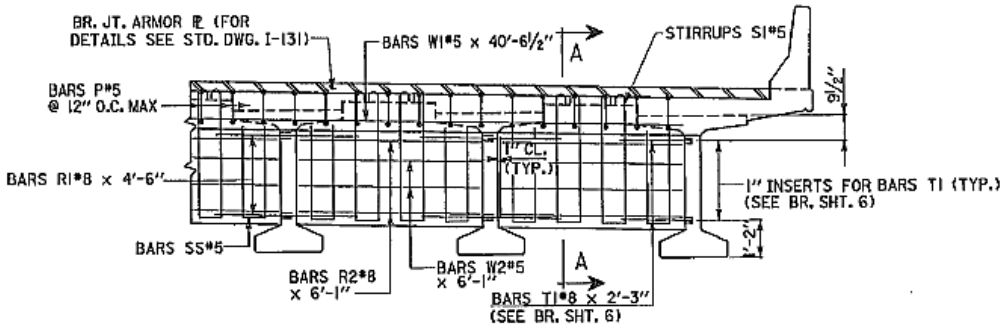

Figure 3-22: Webwall Details (Ends of Span)

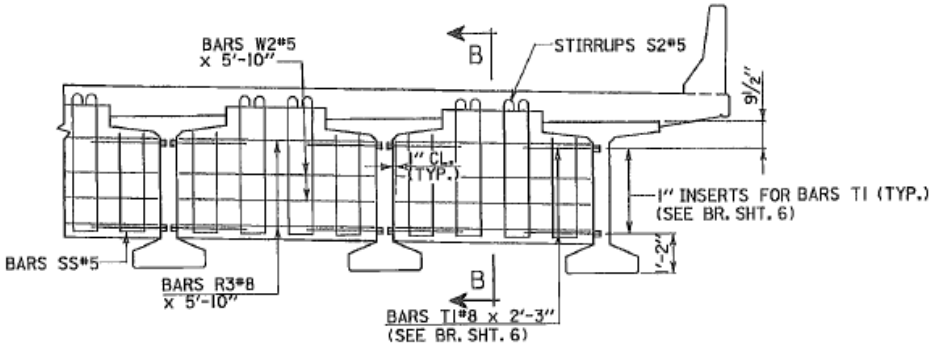

Figure 3-23: Webwall Details (Midspan and Quarterspan)

As in most prestressed bridge girder applications, the bridge over Hillabee Creek has a thin concrete section that lies between the top of a girder and the bottom of the

deck. This section of concrete is most commonly referred to as the girder haunch. Haunch thicknesses vary along the girders length in order to accommodate for camber and geometric profiles of the deck surface. These geometric profiles include the vertical and horizontal curves along the length of the bridge. An example of a haunch build up can be seen as the section of concrete located between the top of girder and bottom of deck in Figure 3-23.

The bridge over Hillabee Creek has a 46'-9" wide deck with a 44'-0" wide roadway surface between the barriers. The 7" slab, whose cross section is shown in Figure 3-24 and Figure 3-25, contains two layers of longitudinal, nonprestressed steel. The top layer contains #4 bars throughout while the bottom layer contains #5 bars. The deck also contains two transverse layers of nonprestressed steel. The top layer rests upon the top longitudinal layer of steel, has 2" of clear cover and consists of #5 bars spaced at 0'-6 ½" on center. The bottom layer of steel, located immediately below the bottom layer of longitudinal steel, has 1" of clear cover and contains #5 bars spaced at 0'-6 ½" O.C. The deck is not continuous between spans.

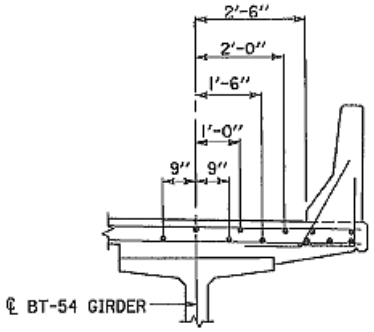

Figure 3-24: Deck Reinforcement Configuration near the Barriers

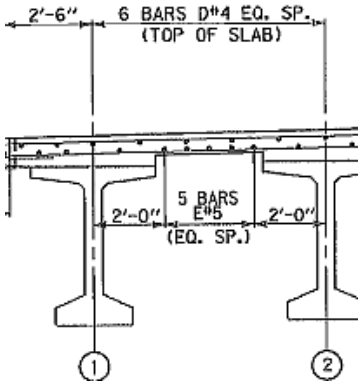

Figure 3-25: Deck Reinforcement Configuration between Interior Girders

There is a continuous, composite barrier on both the upstream and downstream sides of the bridge over Hillabee Creek. Composite action was achieved by slip-form barrier placement over #4 and #5 bars previously cast into the deck. The barrier contains ¾" wide joint openings spaced at 25 ft. for spans 1 and 4 and 22.5 ft. for spans 2 and 3 (Alabama Department of Transportation 2012). A typical cross-section of a thru rail is shown in Figure 3-26, and was taken from ALDOT Standard Drawing No. I-131.

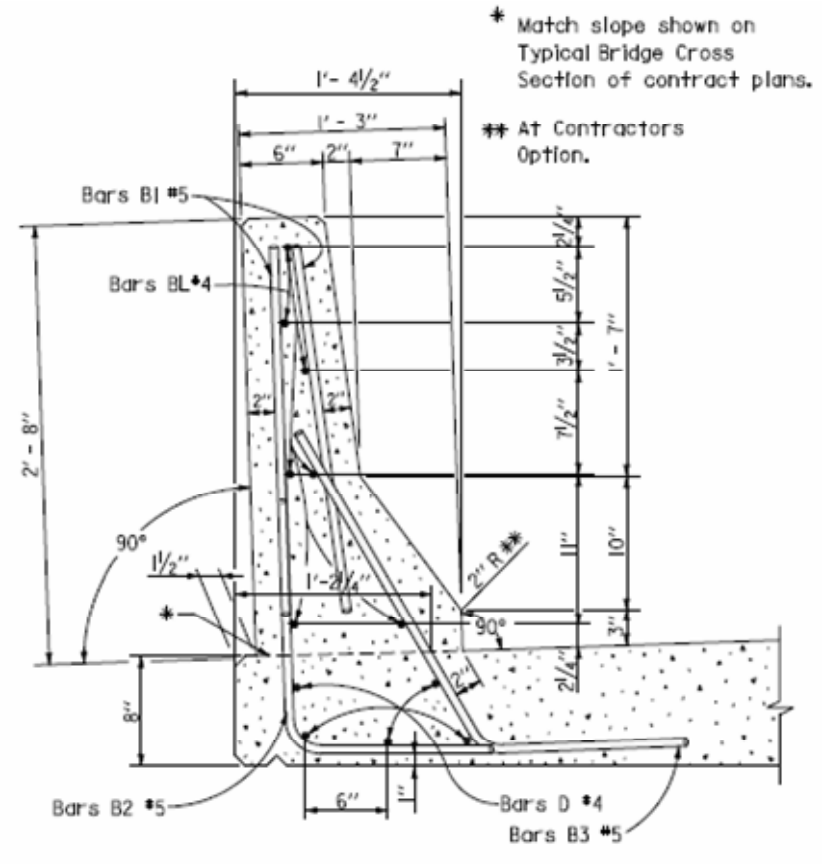

Figure 3-26: Typical Barrier Cross Section

3.6 Material Properties

The primary materials used to construct the bridge superstructure included conventionally vibrated concrete (VC), self-consolidated concrete (SCC), prestressing strand, and nonprestressed reinforcement. The properties for these materials are discussed in this section.

3.6.1 Concrete

Both the VC and SCC mixtures contained Type III portland cement and slag cement. It was necessary to add chemical admixtures to both mixtures to obtain desired fresh concrete properties. Chemical admixtures employed in both mixes included an air-entraining admixture (Darex AEA EH), a high-range, water-reducing (HRWR) admixture (ADVA Cast 575), a viscosity modifying admixture (V-Mar 3), and a hydration stabilizing mixture (Recover). All admixtures were supplied by W.R. Grace.

There were three main differences between the VC and SCC for the girders. The first was the amount and type of admixtures varied to bring about the desired properties for each mixture. The second was that the SCC mixture used #78 limestone as coarse aggregate whereas the VC mixture used # 67 limestone as its coarse aggregate. The third main difference between the two mixtures was that the sand-to-total aggregate ratio for SCC was much greater than that of the VC mixture. The constituents of each mixture are summarized in Table 3-2. The fresh properties of each casting group can be found in Table 3-3.

Table 3-2: Summary of Girder Mixture Proportions

Item	BT-54		BT-72	
	SCC	VC	SCC	VC
Water Content (pcy)	266	238	265	234
Cement Content (pcy)	758	696	760	708
GGBF Slag Content (pcy)	134	124	135	125
w/cm	0.30	0.29	0.30	0.28
SSD Coarse Agg. #78 (pcy)	1528	0	1550	0
SSD Coarse Agg. #67 (pcy)	0	1923	0	1950
SSD Fine Agg. (pcy)	1384	1163	1370	1179
s/agg (by weight)	0.48	0.38	0.47	0.38
Air-Entraining Admixture (oz/cy)	0.3	0.3	0.2	0.2
HRWR Admixture (oz/cy)	11	8	11	7
Viscosity-Modifying Admixture (oz/cy)	2	0	4	0
Hydration-Stabilizing Admixture (oz/cy)	2	1	2	1
Total Air Content (%)	4.1	4.2	4.0	3.2

Table 3-3: Fresh Property Ranges per Span

Span	Unit Weight (lb/ft^3)	Slump (in.)	Slump Flow (in.)	Air (%)	T50 (sec.)	VSI
1	149.1	-	26.0-27.5	2.6-5.5	6-8	1.0-1.5
2	148.1-150.1	-	23.0-28.0	3.3-4.8	5-15	1.0-1.5
3	153.3-153.4	8.25-9.25	-	2.2-4.3	-	-
4	152.3-153.2	8.50-10.00	-	3.9-4.5	-	-

The webwalls, deck, and barriers were all cast-in-place and all utilized the same ALDOT AF-1c mixture proportions. The mixtures contained Type I/II portland cement,

Class C fly ash, #100 sand fine aggregate, and #67 limestone coarse aggregate. Admixtures were also added including the air-entraining admixture MB AE 90, the water reducer Pozzolith 322N, and the midrange water reducer Polyheed 1025, all provided by BASF, Cleveland, Ohio. The mixture proportion summary can be found in Table 3-4.

Table 3-4: Mixture Proportions used for Deck, Webwalls, and Barriers

ITEM (One cubic yard)	**AF-1c**
CEMENT (lb)	496
CLASS C FLY ASH (lb)	124
AIR ENTRAINING ADMIXTURE (oz)	1.2
MAXIMUM WATER (gallons)	33.1
FINE AGGREGATE (lb)	1,200
COARSE AGGREGATE (lb)	1,870
TOTAL AIR (%)	2.5%-6.0%
ALLOWABLE SLUMP (in)	3.5
WATER REDUCER (oz)	18.6
MID RANGE WATER REDUCER (oz)	31.0

Note: Water amounts may differ for workability

In addition to testing fresh properties, Auburn University researchers molded concrete cylinders to determine hardened properties of concrete each girder, span of deck, and barrier. The 6" x 12" girder concrete cylinders were steam cured along with the girders under the curing tarps, while the deck and barrier cylinders were field cured on the Hillabee Creek bridge construction site. The girder cylinders were then tested at various ages including compressive strength at prestress transfer and 28 days and modulus of elasticity at transfer and 28 days. The deck cylinder compressive strength and modulus of elasticity values were tested at 3 days, 7 days, 28 days, and 91 days. All cylinders were strength tested in accordance with ASTM C39 (2005). Modulus of elasticity testing was performed in accordance with ASTM C469 (2002). The averaged results for both strength and modulus of elasticity testing of all girders are summarized in

Table 3-5. The results for both strength and modulus of elasticity for the deck and barriers are summarized in Table 3-6.

Table 3-5: Girder Hardened Concrete Properties

	Release			28 Days	
Casting Group	**Age (hrs)**	**f'_{ci} (psi)**	**E_{ci} (ksi)**	**f'_c (psi)**	**E_c (ksi)**
A (SCC)	24	9010	6200	10240	6400
B (VC)	23	8790	7100	10590	7400
C (SCC)	24	8680	6300	10800	6600
D (VC)	24	7860	6700	9670	6900
E (SCC)	24	7940	6100	10180	6200
E (VC)	25	8760	6400	10360	6800
Specified BT-54	-	5200	-	6000	-
F (SCC)	24	8120	5800	10490	6300
G (VC)	23	8290	6700	10770	7000
H (SCC)	19	7860	5900	10770	6400
I (VC)	22	8770	7100	10850	7300
J (SCC)	22	8220	5800	10550	6400
K (VC)	20	8320	6800	11050	7700
L (SCC)	19	6930	5700	10070	6000
L (VC)	20	7710	6600	10510	6900
Specified BT-72	-	5800	-	8000	-

Table 3-6: Deck and Barrier Material Properties

	3 Days		7 Days		28 Days		91 Days	
	f_c (psi)	E_c (ksi)	f_c (psi)	E_c (ksi)	f'_c (psi)	E_c (ksi)	f_c (psi)	E_c (ksi)
Span1	4370	5300	4750	5800	6030	6300	6750	6600
Span 2	4650	5300	5280	6100	6510	6400	7410	6900
Span 3	4320	5400	4900	5600	6060	6100	6940	7000
Span 4	4370	5300	4720	5900	5910	6400	6430	6500
Barriers					5860	6000		

3.6.2 Prestressing Strand

As mentioned earlier, the prestressing strand used in this project was low-relaxation, Grade 270, seven-wire strand. The strand used in the BT-54 sections was ½-inch diameter strand with an area of 0.153-square inches each provided by Strand-Tech Martin, Inc. from Summerville, South Carolina. The BT-72 girders used ½-inch "special" strand with an area of 0.167-square inches each provided by American Spring Wire from Houston, Texas. Prior to being used in the girders, the strand was stored outdoors in accordance with standard ALDOT procedure. As evident in Figure 3-27, the prestressing strand exhibited slight weathering effects.

Figure 3-27: Prestressing Wire Surface Condition

Prior to girder fabrication, strand pull-out testing was performed on samples of the strand that would be used in the project. This testing was done to ensure that the bond between the concrete and strand would be adequate but not excessively strong. The pull-out tests were performed on September 14, 2010 at Hanson Pipe and Precast in Pelham, Alabama. The bond quality of both the ½-inch and ½-inch "special" strands was found to be adequate, as reported in Dunham (2011, Appendix C).

3.6.3 Nonprestressed Steel Reinforcement

Nonprestressed steel reinforcement was used in the girders to reinforce against shear forces and anchorage zone forces. ASTM A615 Grade 60 steel was used. Figure

3-13 through Figure 3-16 show the shape and locations of the nonprestressed reinforcement and Figure 3-17 and Figure 3-18 show the spacings along the girder for this reinforcement.

3.7 Specimen Fabrication

This section will detail the fabrication process used in making the twenty-eight precast, prestressed girders for the bridge on State Route 22 over Hillabee Creek. There are some key differences in the way that the girders fabricated with VC were made versus those that were made using SCC. The process for making BT-54 girders is very similar to that for making BT-72 girders, and that process is detailed below.

3.7.1 Casting Configuration

Two adjacent casting lines were utilized at the plant for to help complete fabrication more efficiently. The BT-54 sections were 97 ft 10 in. in length, and therefore could be cast with three girders on the same line at the same time, as shown in Figure 3-28. Casting began on September 21, 2010 with the first three SCC girders and then alternated between VC and SCC girders. Four total castings were performed with three BT-54 girders each to yield twelve girders. On the last day of casting the BT-54 girders, only two were cast on the line as shown in Figure 3-29. This pair consisted of a VC girder and an SCC girder, with the VC being cast first so that the vibration during placement would not affect the fresh SCC. All of the BT-54 girders were completed before work began on the BT-72 girders.

Figure 3-28: Casting Configuration of Three BT-54 Girders

Figure 3-29: Casting Configuration of Two BT-54 Girders

The BT-72 girders were 134 ft 2in. in length, and so only two could be cast on the same casting line at one time. Figure 3-30 depicts the casting line for the BT-72 girders. The casting for the BT-72 girders began on October 14, 2010 with the casting of two SCC girders. Pairs of SCC and VC girders were cast alternating between the types of concrete, which was similar to the process used for the BT-54 girders. On the final day of casting for the BT-72 girders, which was October 28, 2010, one VC girder and one SCC girder were cast on the same line, again placing the VC first to avoid vibrating the SCC.

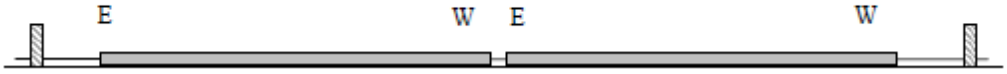

Figure 3-30: Casting Configuration of BT-72 Girders

3.7.2 Fabrication of Precast, Prestressed Bridge Girders

The test specimens used in this project were designed and built to be used in an actual bridge on State Route 22 over Hillabee Creek near Alexander City, Alabama. Care had to be taken to ensure that experimental testing equipment and procedures did not interfere with the standard plant operations during fabrication. While some standard procedures did have to be altered in small ways, these alterations were deemed to be acceptable and to not have any adverse effects on girder performance.

The first step in the process involved aligning and cleaning the casting bed. Next, wooden headers with holes for the prestressing strands were placed on the casting lines to

form the girder ends so that the girders would be the correct length. Hold-down anchors used for the draped strands were positioned and secured to the casting bed. Hold-up anchors were located in a lowered position so that after the strands were tensioned, they could be raised up to drape the strands. Strands were then pulled through all of the headers and hold-up/down anchors.

After all of the strands were positioned properly, they were tensioned to a specified jacking stress using a hydraulic jack and checked according to ALDOT standards for the proper tension and elongation. The strands were partially stressed at first in order to straighten them and detect potential flaws. Once it was determined that the strand did not have any major flaws, the full jacking stress was imparted to the strand. Once all of the strands were properly tensioned, the hold-up anchors were raised to the correct elevation for draping using a mobile crane. After tensioning the strands, insulating foam was applied on the outside holes in the wooden headers through which the strands had been run in order to prevent concrete and bleed water from leaking out of the formwork.

At the ends of each girder some strands were designed to be debonded for a length of 10 feet. Figure 3-14 shows that four total strands would be debonded at the ends of the BT-54 girders and Figure 3-16 shows that six total strands would be debonded at the ends of the BT-72 girders. Debonding was achieved by securing a plastic sheath around the specific strands as shown in Figure 3-31. The plastic sheath prevented the concrete from coming into contact with the strand and bonding to it.

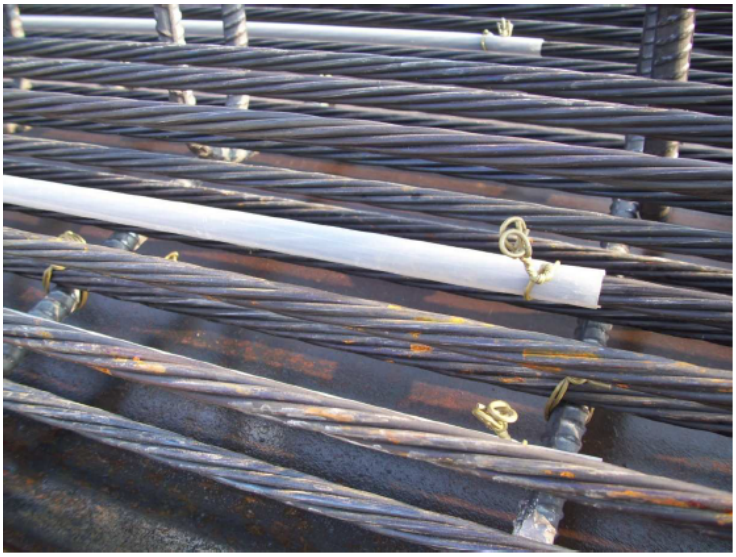

Figure 3-31: Strand Debonding

After the prestressing strands were positioned and tensioned, the mild steel reinforcement discussed in Section 3.4.2 above was tied into place. The pre-bent reinforcing bars were secured to the prestressing strands with wire ties at the specified locations and spacing. Once the nonprestressed steel was securely in place, the vibrating-wire strain gauges (VWSGs) that were used in each girder were installed by Auburn University researchers. The gauges were installed at midspan or at quarterspan of the girders using wire ties, zip-ties, and in some cases small pieces of reinforcing bar for proper alignment. This process is discussed in detail later in Section 5.3.

The final preparations before concrete placement could begin included applying form release agent to the bottom of the casting bed. Care was taken to avoid getting the release agent on the prestressing strands, as this would compromise their bond to the concrete and have detrimental effects to the performance of the girder. The release agent was also sprayed onto the side forms before they were installed. The side forms were then put into place and secured, again making sure that the release agent did not come into contact with any of the prestressing strand or nonprestressed reinforcement. Figure

3-32 depicts the installation of a side form. Cables connecting the VWSGs to the data acquisition system had to be run over the top of the side forms, and behind the vibrator tracks located on the outside of the side forms. This was done to ensure that the VWSG cables would not interfere with or be damaged by the vibration of the VC.

Figure 3-32: Side Form Installation

All concrete used in the girders was batched on site at the plant. Specialized concrete delivery trucks with a 4 yd^3 capacity transported concrete from the mixing tower to the casting line. The concrete was placed in the girder forms from the trucks through

the use of an auger-driven chute attached to the front of the truck, as seen in Figure 3-33. Throughout the casting process each day, trucks would be stopped periodically to perform tests on the fresh concrete, the results of which are discussed in Section 3.6.1. The same trucks would also be stopped to obtain concrete samples to use in making test cylinders to determine hardened concrete properties. These samples were taken from the trucks after they had discharged roughly half of their concrete into the girder.

Figure 3-33: Concrete Delivery Truck

The process used to place the VC was different than the process used to place the SCC because of the physical differences in the fresh concrete. To place the VC, the delivery trucks positioned the chute over the girder starting at one end of the girder and discharged enough concrete to fill up the bottom bulb and web of the girder in that area before moving down the girder a few feet and discharging more concrete. The VC was

not able to flow through the reinforcement, causing the trucks to have to discharge concrete every few feet along the girder. Then a second truck would come behind the first one and fill the top flange with concrete. The placement began at one end of the girder and progressed down to the other end.

As the forms were filled with concrete, vibration needed to be introduced to the concrete in order to adequately consolidate the VC. Internal and external vibration techniques were used. Figure 3-34 shows the internal vibration applied by a worker walking along the top of the formwork. Figure 3-35 shows the external vibrator in a track on the side of the formwork as concrete is being placed in the girder.

Figure 3-34: Internal Vibration Used in VC Placement

Figure 3-35: External Vibration

For SCC girders, the concrete placement process was less complex than the VC placement process. The placement of SCC did not involve as many laborers because it did not require any external or internal vibration. When the delivery trucks placed the concrete into the forms, it flowed easily around the reinforcement. This allowed the delivery trucks to not be as precise as to where they placed the concrete because the SCC would simply flow around the reinforcement and along the length of the girder.

Once a girder was completely filled with concrete, and all vibration had been completed in the case of the VC girders, the top surface of each girder was roughened by the use of a wire rake. In the case of the SCC girders, the top surface was roughened using the wire rake after some time was allowed to pass so that the SCC would stay in a roughened state as opposed to consolidating back down into a smooth top surface. Figure 3-36 shows the surface roughening process. After surface roughening had been accomplished in accordance with ALDOT specifications, metal deck clips and overhang

brackets were installed on the top flanges of the girder by inserting them into the fresh concrete. These accessories would be used later to facilitate installation of formwork for the bridge deck. As the deck clips and overhang brackets were being installed, steel bolts were inserted into the tops of the girders as part of the camber measurement system discussed in detail in the next chapter. Figure 3-37 shows one of these bolts installed in the girder and illustrates the surface roughness of an SCC girder.

Figure 3-36: Surface Roughening of SCC Girders

Figure 3-37: Camber Measurement Marker

After the top of the girder was roughened and the accessories and camber measurement bolts had been installed, a curing blanket and protective tarp were prepared to cover the girders during curing. Prior to the blanket and tarp covering, the concrete cylinders that had been prepared from the concrete used in the girders were placed beside the formwork for the girders so that they would be subjected to the same steam curing as the girders. Once the cylinders were positioned, the curing blanket and tarp were pulled over the formwork by the use of a crane as seen in Figure 3-38. The curing blanket and tarp remained on the girders for one night and were removed the following morning.

Figure 3-38: Curing Blanket and Tarp Covering

The morning after concrete placement, the curing blanket and protective tarp were removed from the formwork and the forms were stripped from the sides of the girders. Care was taken to temporarily disconnect the VWSG cables from the data acquisition system while the forms were being stripped because the wires had been run underneath the vibrator track on the forms. Once the forms had been removed, the gauges were reconnected in order to collect data before and during prestress transfer.

Some cracking in the girders occurred after the removal of the formwork prior to prestress transfer. The girders had two or three cracks that ran from the top surface down to the web. There did not seem to be any difference between VC or SCC girders in the cracking pattern or number of cracks. In Figure 3-39, a typical crack that has been highlighted by marker ink can be seen. Cracks were widest at the top of the girder. The width of this crack (in a VC girder) can be seen in Figure 3-40. Most of the cracks were

approximately 0.02 in. wide, with the largest crack 0.04 in. wide. The cracks closed during prestress transfer. Some possible reasons for why these cracks developed as well as their possible influence on the research for this project are discussed in Johnson (2012).

Figure 3-39: Crack in BT-54 Prior to Prestess Transfer

Figure 3-40: Crack Width in BT-54 Girder Prior to Prestress Transfer

After the forms were stripped, baseline camber readings were taken using the surveying camber measurement system. This camber measurement system is discussed in detail in the next chapter.

As the camber baseline measurements were made, concrete cylinders that had been steam-cured alongside of the girders were tested in order to verify that the girder concrete had reached the minimum strength required to transfer the prestress force through strand release. Releasing the strands was accomplished by cutting them with oxyacetylene torches. Flame-cutting the strands required a worker at each end of the casting line as well as between each girder. The strands and hold-downs were cut in a specific order. Each individual strand was cut by each worker with the torch before moving on to the next strand. First, the bottom-most outside strands were cut. Next, the top strands were cut. These were followed by the draped strands. Finally, the remaining

strands in the bottom flange were cut. Figure 3-41 shows the flame-cutting sequence for the BT-54 girders and Figure 3-42 shows the flame-cutting sequence for the BT-72 girders.

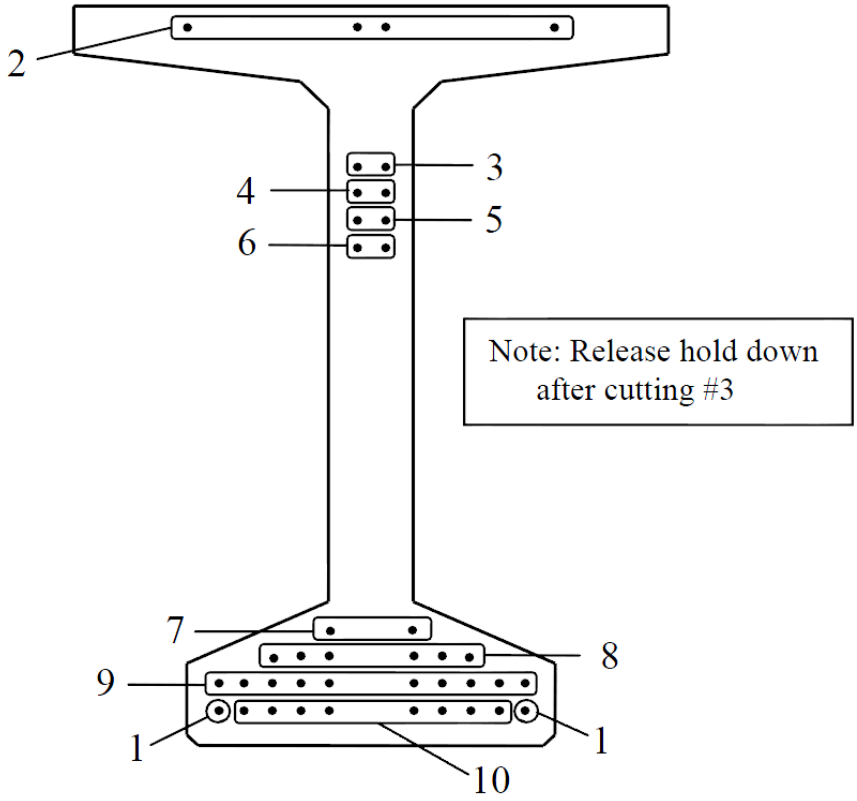

Figure 3-41: Flame-Cutting Sequence for BT-54 Girders

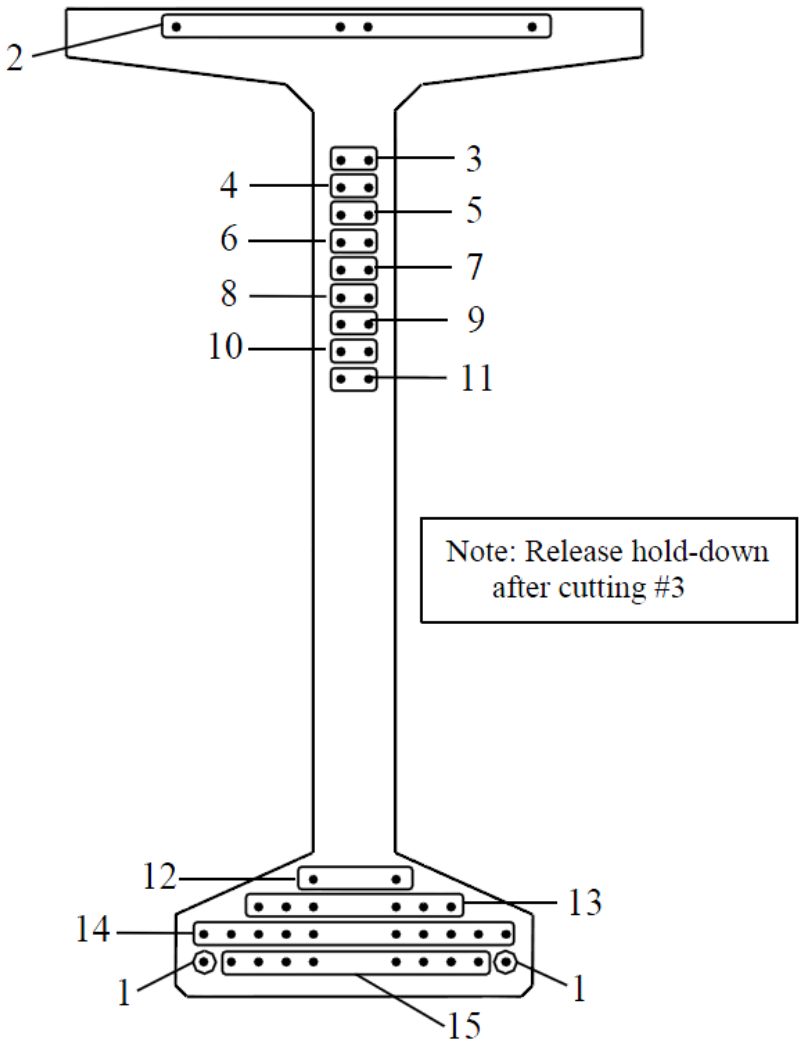

Figure 3-42: Flame-Cutting Sequence for BT-72 Girders

Immediately after all of the strands and hold-downs were released, camber measurements were taken using the surveying system. After these measurements were recorded, the girders were ready to be moved to storage. Once again, the VWSG wires were disconnected while the girders were transported to storage. One crane was used to move each BT-54 girder while two cranes were used to move each BT-72 girder. Storage conditions were arranged so that the girders would be supported with the same span length that they would have in the bridge. This meant that a length of 9 inches of the

girder was resting on the support. The support conditions are shown in Figure 3-43. After being placed in storage, the VWSG cables were reconnected to the data collection system and another set of camber measurements were taken.

Figure 3-43: Support Conditions in Storage

Chapter 4 Camber Measurement Program

4.1 Introduction

The precast, prestressed bridge girders used in this study were originally measured for camber using two different methods: tensioned wire method and a surveying method. Based on the investigation by Johnson (2012), the tensioned wire method provided inaccurate measurements. Also, due to construction of bridge components, the tension wire method was deemed unusable after erection. Therefore, camber measurements utilizing the surveying method were used in this investigation. This chapter will describe in detail the implementation of the surveying method.

4.2 Surveying Method: Casting Until Erection

The twenty-eight girders that were studied in this project were measured for camber using the surveying method. This method involved the use of specific targets placed on the surface of each girder, a prism rod with an attached prism, and a total station. The targets provided a specific and consistent location for prism rod placement for each total station reading before deck casting. These targets consisted of hexagonal-head bolts that were embedded in the top of the fresh concrete at specific locations along the length of each girder after the concrete surface had been roughened. Then, each bolt was marked on top with a sharpie to provide a more specific target to place the tip of the prism pole. One of these bolts embedded in the concrete is shown in Figure 4-1. These targets were placed on specific points along the girder surface: 9 inches from each end, the $1/6^{th}$ and $5/6^{th}$ span locations, and midspan.

Figure 4-1: Surveying Target in Place

Camber measurements were taken at specific times as the girders aged. The baseline set of readings were taken after the concrete had cured just prior to prestress transfer. The first true cambers were measured just after transfer had taken place. Camber was measured again after the girders were moved from the casting bed to their storage location in the plant. Camber measurements were then taken when the girders reached ages of 7 days, 14 days, and 28 days. After the girders reached 28 days, intermittent readings were taken while the girders remained in storage. In most cases, cambers were measured every two weeks after the girders reached an age of 28 days. These measurements were taken as early in the day as feasible so as to minimize temperature effects due to sunlight.

The first step in the measurement of camber using the surveying method used in the investigation by Johnson (2012) involved the setup of the total station. An effort was made to set up the total station in locations that were not too close to the girders, as large horizontal angle changes between the end targets might have decreased accuracy in the measurements. Furthermore, when measurements were taken on girders in storage, a single setup location was often used to make measurements on multiple girders. On many occasions, the location of the total station was constrained by plant operations.

Once the total station was set up and leveled, measurements were taken. First, the prism pole was placed on the bolt installed at the mark end of the girder. Once the prism was correctly positioned on the bolt and held level, the total station measured the horizontal angle, the horizontal distance, and the vertical distance to the prism. This is shown in Figure 4-2. Once this was completed, the values were manually recorded, and the prism pole was moved to the $1/6^{th}$ -span location. The measurement process was then repeated for every location on the girder, ending with the far end. All of the calculations to determine camber were relative to the endspan target locations. Specifically, the horizontal angle measured and recorded for the mark end target for each set of measurements was the baseline angle for that set of measurements. The change in horizontal angle from the mark end target to the other targets was the important value to calculate the camber change. In many cases, the horizontal angle for the first reading was set to 0°0’0” in order to simplify the other angle measurements for that girder.

Figure 4-2: Surveying Method During Storage

A computer spreadsheet was developed to determine the camber values for each girder based on the surveying method measurements. The first set of measurements taken for each girder were taken just prior to transfer. The computer program used these first measurements as baseline readings. The offset of the $1/6^{th}$ -span, midspan, and $5/6^{th}$ -span targets off of a straight line drawn between the two end span targets was calculated. If the target was above the imaginary straight line, then the offset was a negative value. If the target was below the line, the offset was positive. After transfer, the offsets of the interior targets were again calculated from an imaginary straight line drawn between the end span targets. These measured offsets were subtracted from the initial offsets in order to determine the change in camber during the measurement time interval.

4.3 Surveying Method: Erection through Casting of Barriers

After the girders were erected, construction practices interfered with collecting camber measurements as detailed above. The bolts that were cast into the top of the girder were no longer easily accessible, and eventually would be covered up by the deck. Therefore, a method was developed to collect camber measurements by taking measurements from the underside of the girder. First, the girder thickness was determined at each end point and at midspan. This girder thickness was needed in order to correct measurements so they would reflect what readings would to the top of the girders. A special apparatus was developed by Auburn University researchers to collect these underside readings, and is shown in Figure 4-3. The average of multiple girder thickness readings were taken for each girder at the ends and midspan locations. The total station was set up at a convenient location at ground level and measurements were taken at the ends and at midspan.

Figure 4-3: Underside Camber Measurement Apparatus

A computer spreadsheet was developed to determine the camber values for each girder based on the surveying method measurements. The computer program calculated the change in camber in a similar fashion as outlined in the previous section, but with a couple modifications. First, underside measurements were corrected for the girder

thickness to reflect what the readings would be at the top of the girder. Second, only the ends and midspan measurements were taken and used in the computer spreadsheet. Even after the deck was cast construction practices interfered with taking measurements from the top of deck, so this method was used until the barriers were cast.

4.4 Surveying Method: After Casting of Barriers

After the barriers were cast, construction traffic was reduced to a level so that camber measurements could be taken from the top of the deck. After ALDOT grooved the deck, a cordless hammer drill was used to notch the deck approximately 1/8 in. so that surveying points could be easily found. These notches were placed directly over the girders, and were placed at the end of spans and at midspan. In order to relate measurements to the top of the girders, the deck and haunch thickness at the ends and midspan was determined. This was achieved by taking a reading to the top of deck and using the underside apparatus to collect a total thickness. The girder thickness values collected earlier were then subtracted from the total thickness to determine the deck plus haunch thickness. After this thickness was determined for each girder camber measurements could then be taken from the top of the deck.

A total station was set up on one side of the bridge, and readings were taken for each girder using a prism attached to a prism rod at the ends and midspan. Figure 4-4 shows the method used to take camber measurements from the top of the deck.

Figure 4-4: Deck Surveying Method Camber Measurements

In preparation to open the bridge to traffic, ALDOT workers placed dashed traffic striping which covered up some of the drilled holes in the deck above the center girders of the bridge. To account for this, measurements were taken adjacent to the tape at the approximate location of the drilled notches. Once the bridge was opened for traffic, measurements were taken during traffic lulls.

A computer spreadsheet similar to that developed for the underside surveying method was used to determine camber values for each girder. The difference being that collected measurements were adjusted for the deck plus haunch thickness to reflect what readings would be at the top of the girder. Just like the previous two surveying methods, the measured offsets were subtracted from the initial offsets in order to determine the change in camber during the measurement time interval.

Chapter 5 Strain Measurement Program

5.1 Introduction

Vibrating-wire strain gauges (VWSGs) were installed in various cross sections and locations within the girders and deck in order to measure internal strains and temperatures. The internal temperatures were used to develop a temperature profile and adjust camber and strain measurements to reflect thermal influence. The internal strain measurements were used to measure the amount of prestress loss present in the girders. The measurement of internal strain was important in this project for two reasons. First, the gauges were positioned within the VC and SCC girders in such a way as to provide a direct comparison between the strains and prestress losses measured in each. Second, predicted prestress losses for the girders were calculated using the *AASHTO LRFD Bridge Design Specifications* 2012. Part of the scope of the project was making comparisons between the measured prestress losses to the predicted losses based on the AASHTO 2012 prediction model.

5.2 Vibrating-Wire Strain Gauges

The vibrating-wire strain gauges used in this project were Geokon, Inc. VCE-4200 gauges. According to the Geokon manual, these gauges are ideally suited for long-term strain measurements in mass concrete. The strain measurement was accomplished through the vibrating wire. A steel wire is tensioned between the two end blocks of the gauge. Once the gauge is embedded in the hardened concrete the gauge will undergo shortening and lengthening along with the concrete, which will increase or decrease the

tension in the wire accordingly. Electromagnets incorporated into the gauge pluck the wire and subsequently measure the wire's natural frequency of vibration. The change in the natural frequency of the wire reflects the change in tension that the wire has undergone, which can in turn yield the change in strain of the wire (Geokon). Figure 5-1 is a detailed drawing showing the various components of these gauges.

Along with the vibrating wire scheme, a thermistor is incorporated into each gauge. The thermistor measures the temperature of the gauge at the same time that the strain measurement is being taken using the vibrating wire assembly. The temperature of the gauge at the time of a strain reading was important information to record, as corrections due to temperature were calculated and applied to the strain readings. These corrections will be discussed in the following chapter.

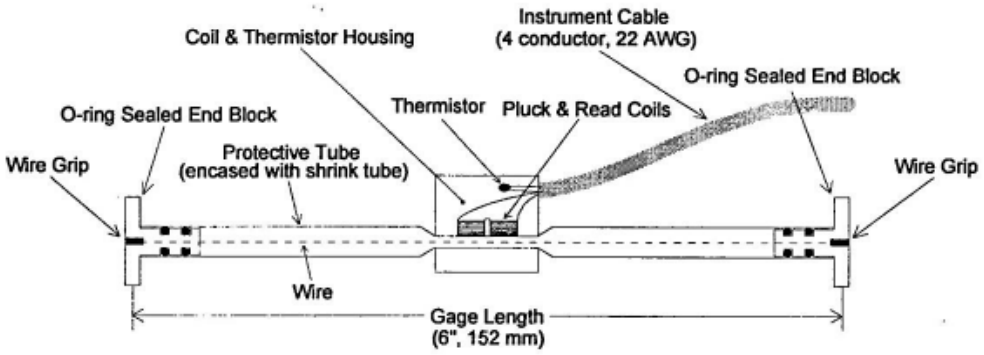

Figure 5-1: VCE-4200 Vibrating-Wire Strain Gauge Schematic (Geokon 2010)

5.3 Vibrating-Wire Strain Gauge Locations

The bridge symmetry allowed for a girder layout conducive to direct comparisons between those composed of VC to those composed of SCC. Span 1 and Span 2 consisted of SCC girders while Span 3 and Span 4 contained VC girders.

Special consideration was taken when placing the VWSGs within the girders to allow for strain comparisons between girders undergoing similar loading but composed

of different types of concrete. Specifically, more strain gauges were placed in girders with numbers from 4 to 7 on Spans 1 and 2, and from 8 to 11 on Spans 3 and 4. This was done to allow for a more direct comparison between girders of different spans under load testing and traffic loads due to the bridge skew. Figure 5-2 is a simplified schematic illustration of the girder configuration in the bridge. This view also shows the gauge layouts that were used in each girder.

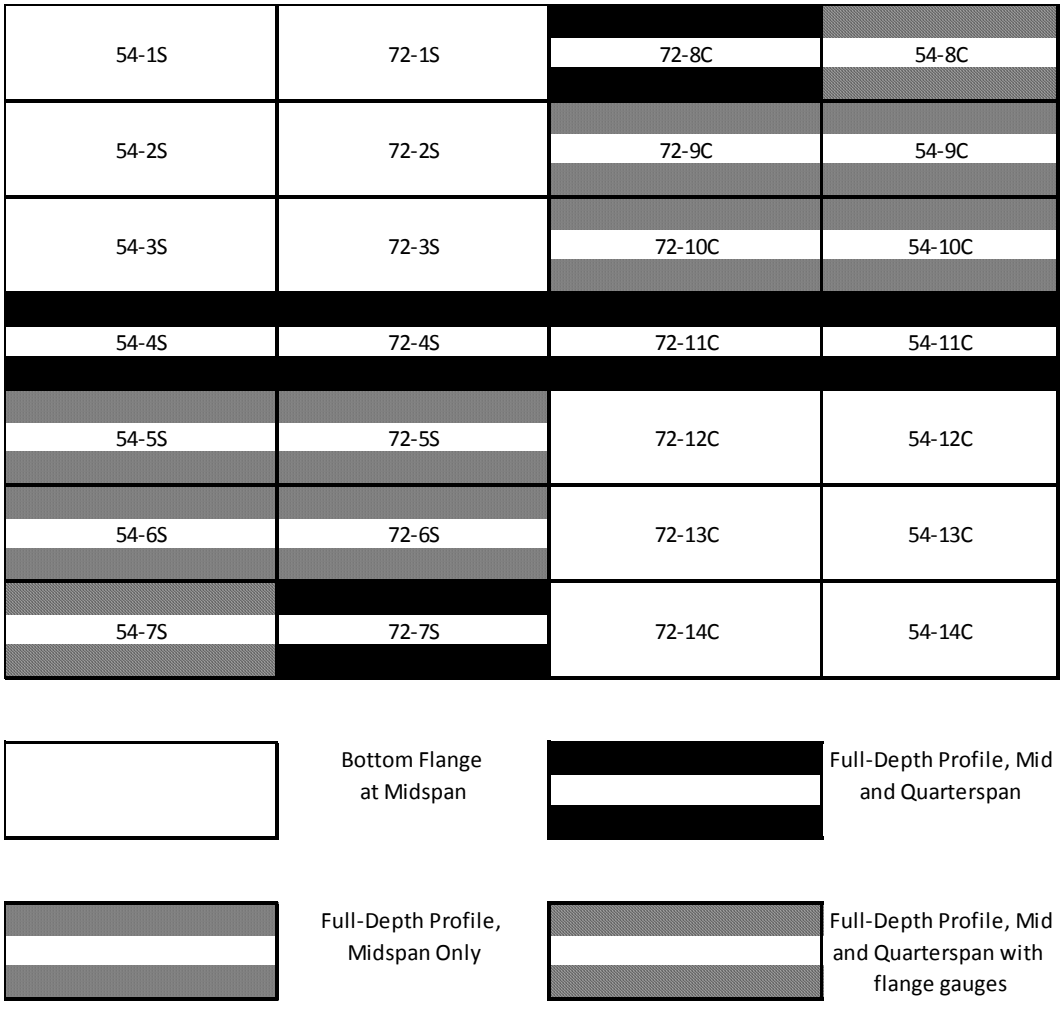

Figure 5-2: VWSG Installation Schematic by Girder ID

The VWSGs that were placed in girders containing only one gauge (bottom flange at midspan) were placed at the centroid of the prestressing strands that were contained

within the bottom bulb. This included the draped strands because they were located in the bottom bulb at the midspan of the girder. These centroids, shown in Figure 5-3 and Figure 5-4, were located at a height of 6 in. for the BT-54 girders and a height of 8.8 in. for the BT-72 girders. Figure 5-5 and Figure 5-6 depict the gauge locations for the girders that contained gauges to measure strains across a full-depth profile at midspan. The bottom-flange gauges were again placed at the centroid of the bottom prestressing steel. The gauges in the web were placed one quarter of the web height above the bottom bulb as well as below the top flange. Finally, the top gauge was placed at the centroid of the prestressing steel that ran through the top flange. After the girders were erected gauges were installed within the deck to collect strain and temperature measurements. The deck gauges were installed 3.9 in. from the top of the deck, and the deck gauge locations are included in Figure 5-3 through Figure 5-6.

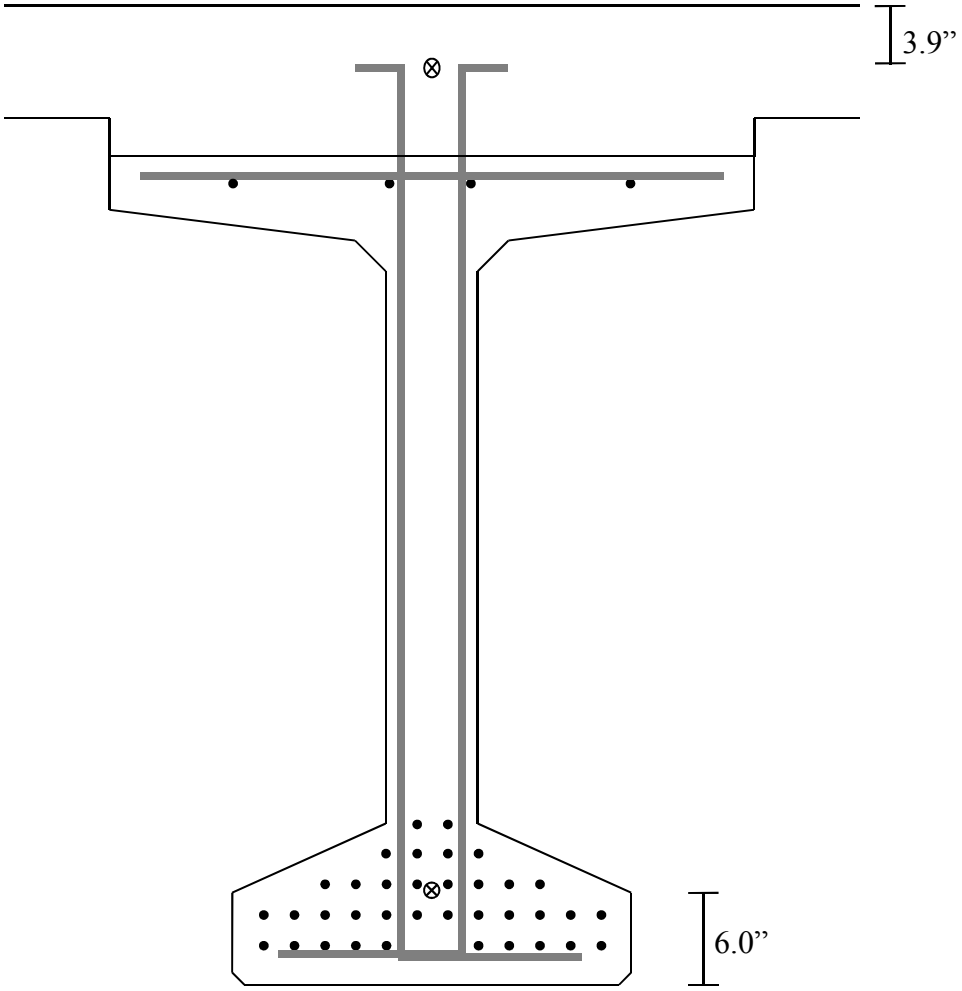

Figure 5-3: BT-54 Midspan Cross Section with a Bottom-Bulb and Deck VWSG

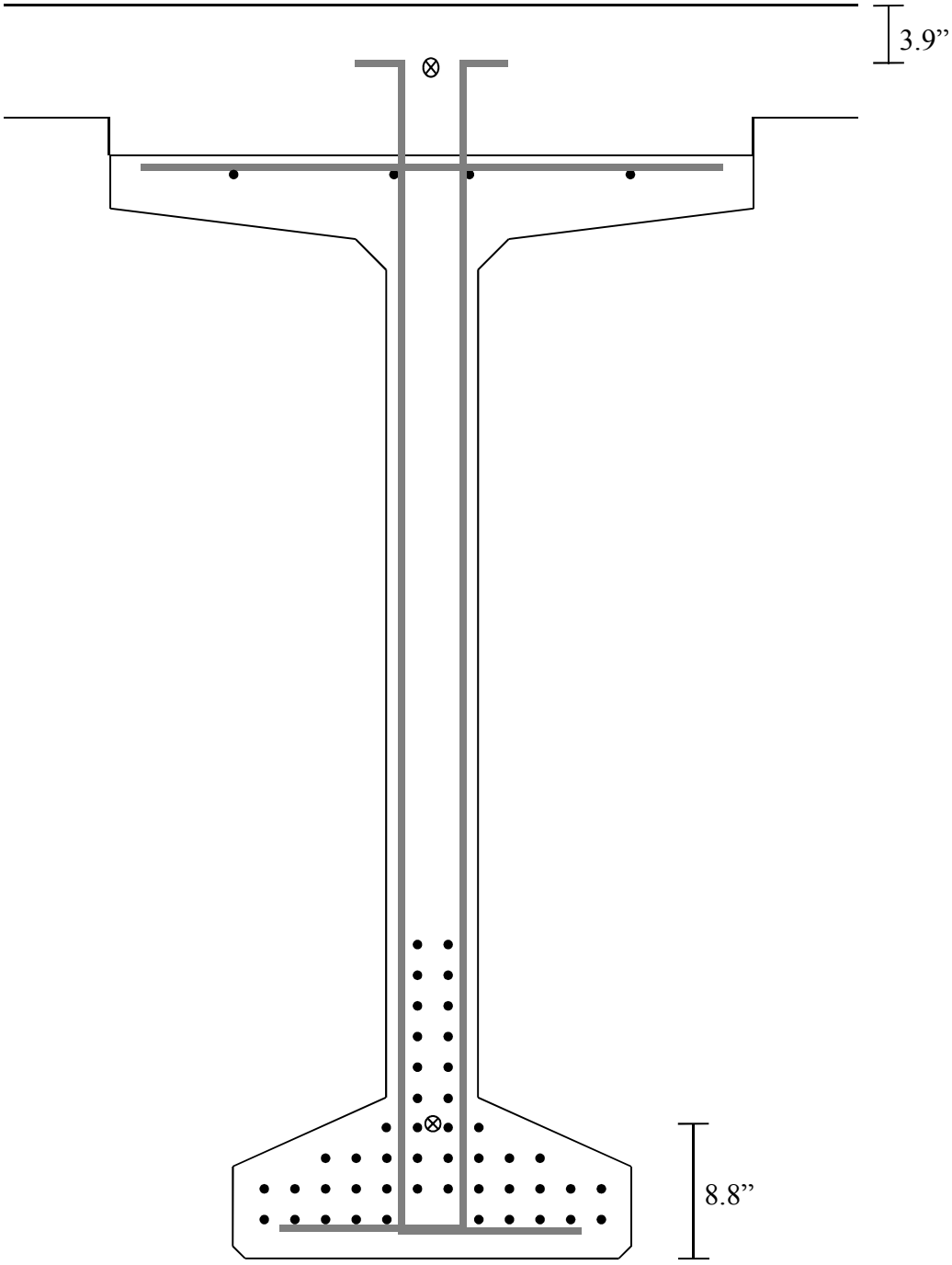

Figure 5-4: BT-72 Midspan Cross Section with a Bottom-Bulb and Deck VWSG

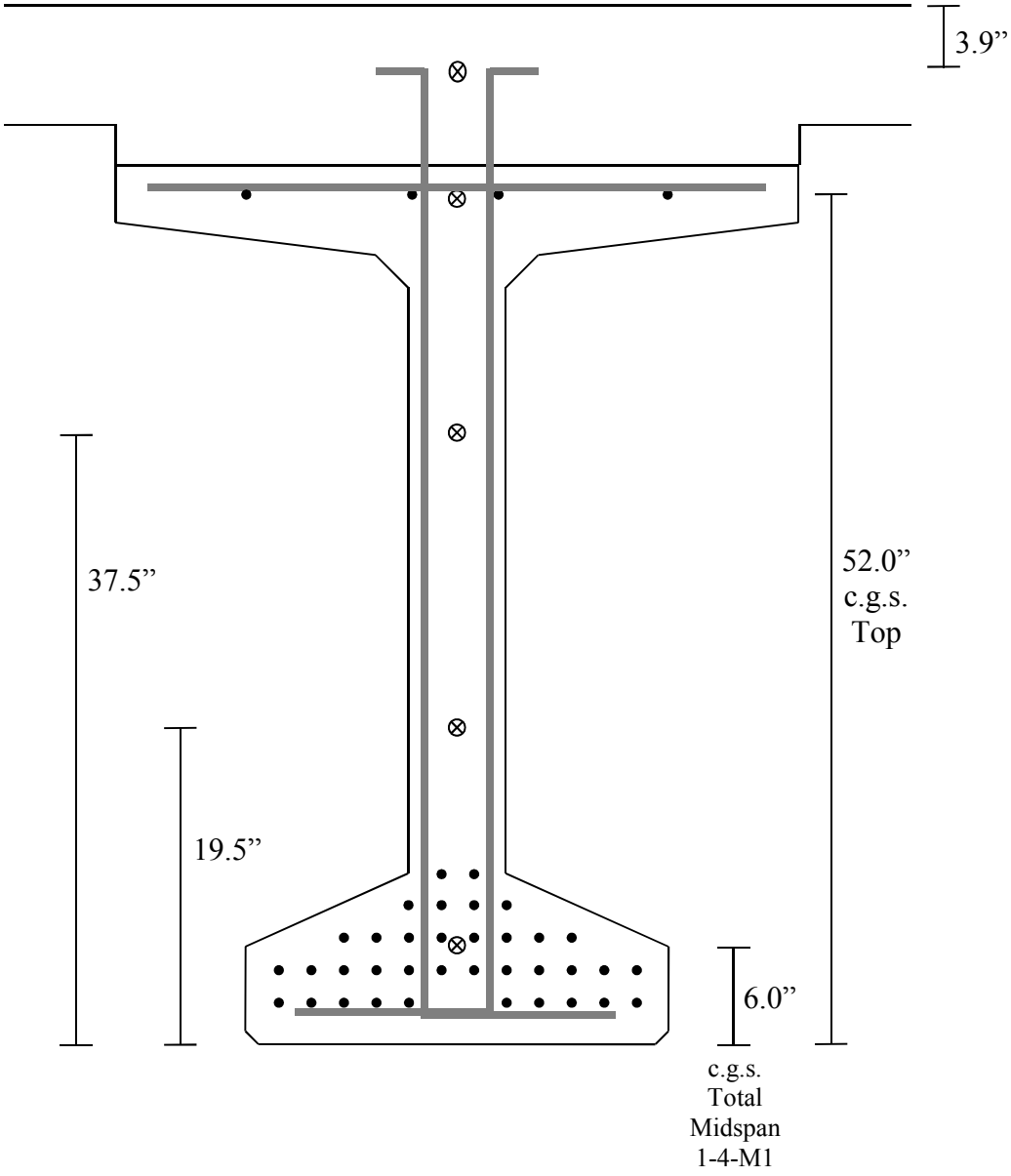

Figure 5-5: BT-54 Midspan Full Profile VWSG Layout

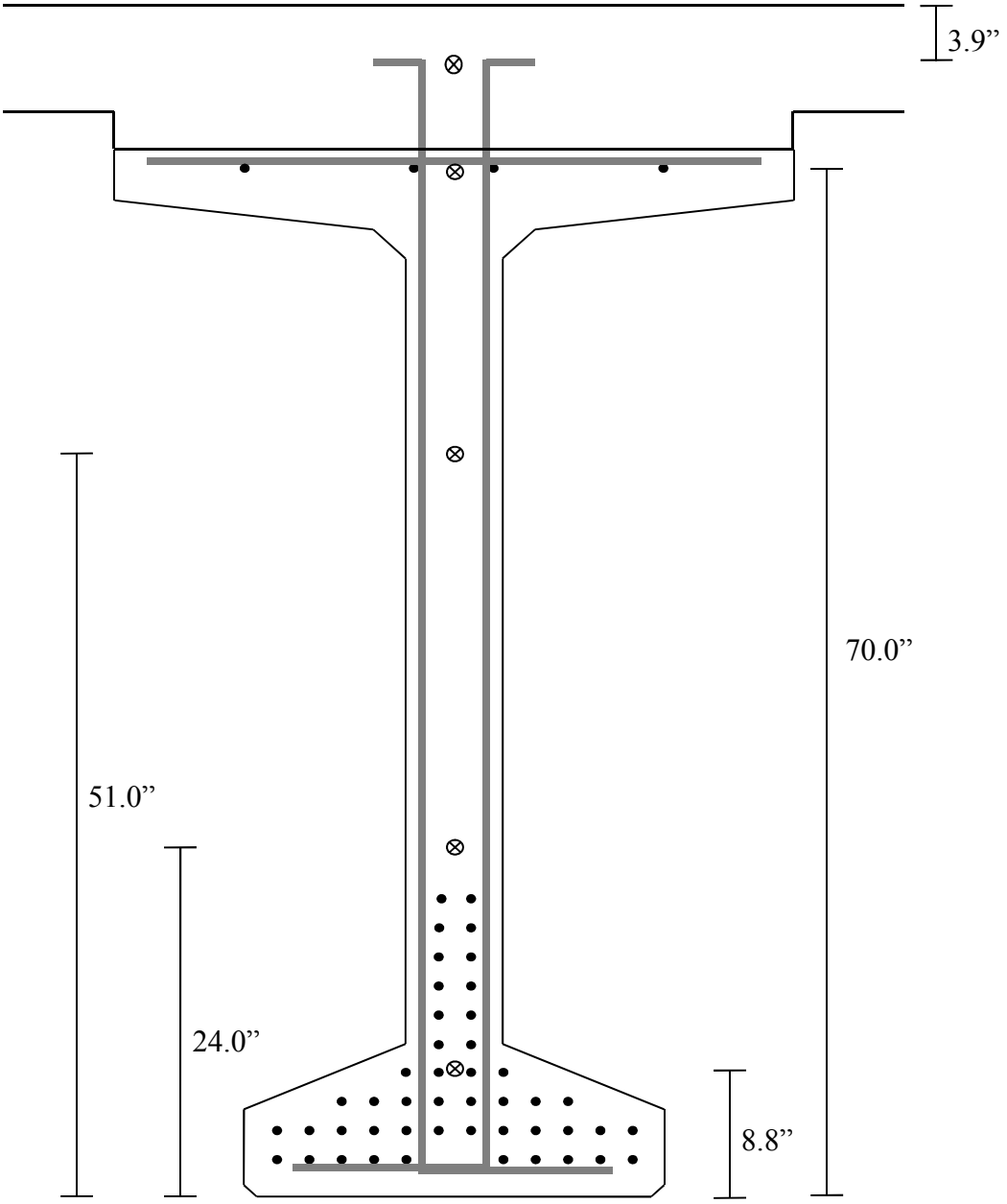

Figure 5-6: BT-72 Midspan Full Profile VWSG Layout

5.4 Vibrating-Wire Strain Gauge Installation

Great care was taken to place the VWSGs in a manner in which they were secured at the proper location and would be able to bond with the concrete. The gauges were secured into place using various materials including plastic cable-ties, steel wire, and small segments of reinforcing steel. Gauges located in the bulb section of the girder were

secured into place using zip-ties tied around the prestressing strand. Figure 5-7 shows a gauge located in the bottom bulb of a girder. Gauges placed in the top flange of a girder were secured in the same manner.

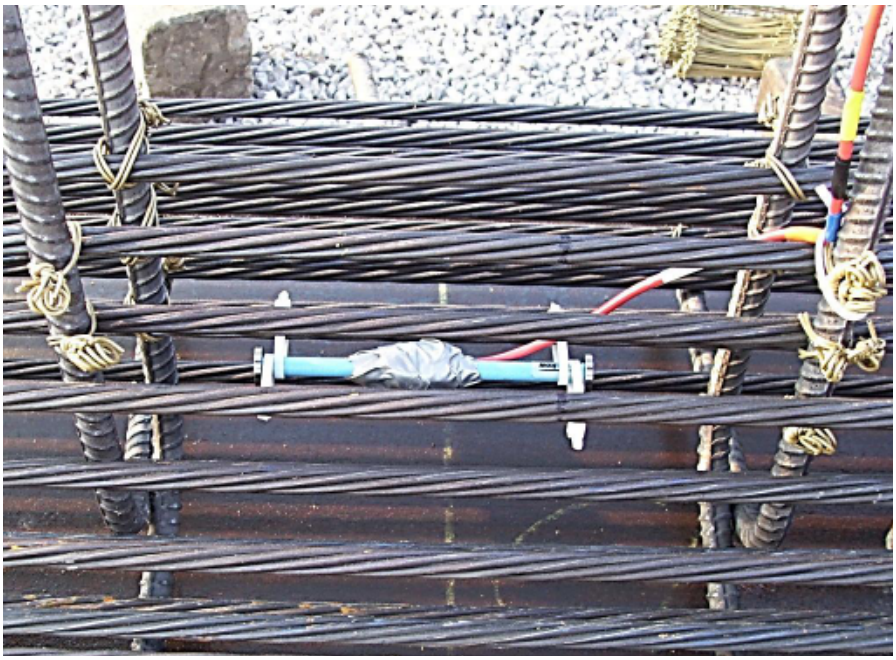

Figure 5-7: VWSG Secured in Bottom Bulb

Gauges that were to be placed within the web of a girder were more difficult to secure because there were no prestressing strands to tie directly to. An assembly of small sections of reinforcing bar along with steel wire was fabricated in order to provide a stable suspension system without adding significant longitudinal reinforcement to the cross sections. Figure 5-8 shows a typical example of this method of securing the VWSGs. Wire ties were used to tie small sections of reinforcing steel to the stirrup sections used as reinforcement in the girder. Next, steel wire was wound around the steel sections to connect them together. Finally, plastic cable ties were used to secure the VWSG to the steel wire.

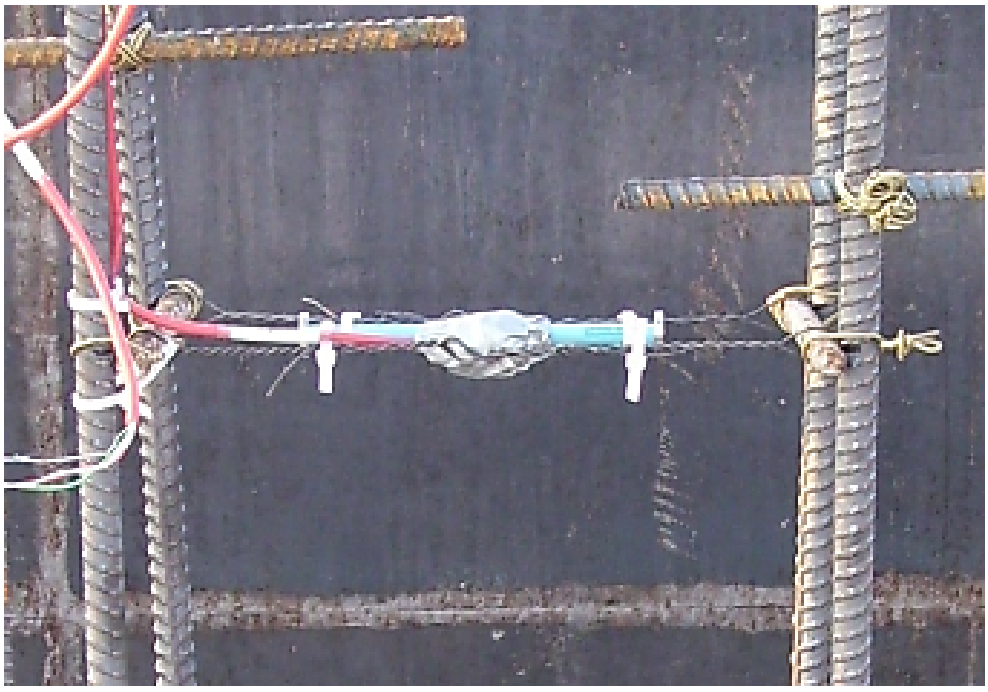

Figure 5-8: VWSG Secured in Web of a Bulb Tee Girder

Gauges located in the deck were secured to the deck reinforcement using plastic cable ties. Figure 5-9 shows a gauge located along the centerline of the girder in the deck.

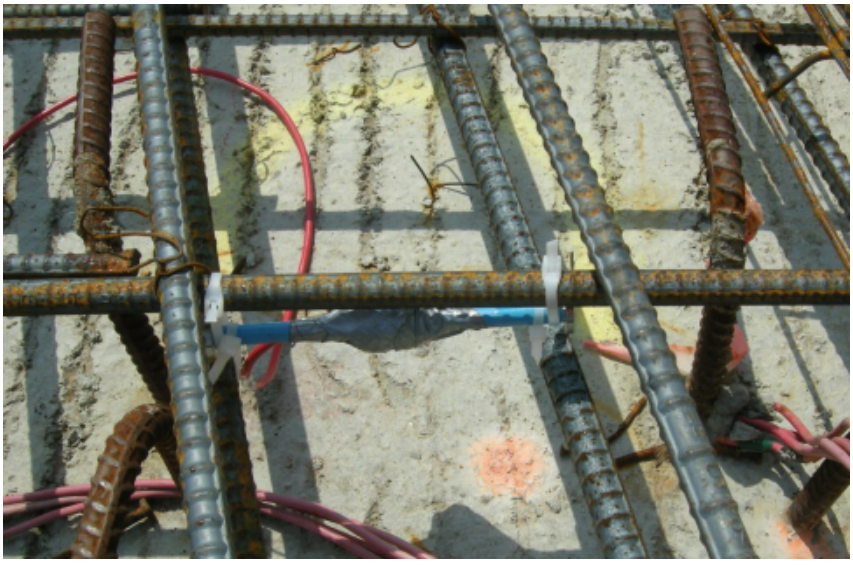

Figure 5-9: VWSG Secured in Deck above Girder

5.5 VWSG Data Acquisition System

Two data acquisition systems (DAS) were used in this research. Each DAS was designed to be a standalone system that could be used to collect data at the prestressing plant as well as on-site at the bridge. The boxes containing the DAS equipment were designed to withstand the rigors of being exposed to the environment for extended periods of time while recording measurements. The design and configuration of the DAS were based on a similar setup by Gross (2000). Each DAS unit contained a CR1000 datalogger, two multiplexers, and a battery system. Figure 5-10 provides a schematic for the layout of each DAS unit.

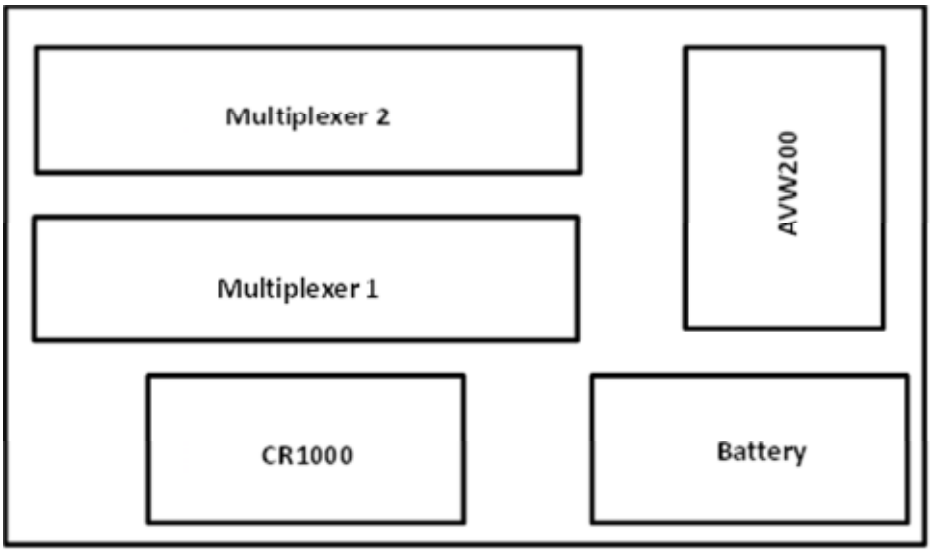

Figure 5-10: VWSG Data Acquisition System Schematic

The CR1000 was programmed to activate each VWSG every six minutes and record the resonant frequency of vibration and thermistor resistance as discussed in Section 5.2. Each multiplexer used had the capacity to record 16 separate VWSGs. This means that each DAS had the capacity to read 32 VWSGs simultaneously. The program calculated the temperature of the gauge using the recorded thermistor resistance by Equation 5-1. The constants A, B, and C were provided in the instruction manual

included with the gauges, and Equation 5-1 is located in Appendix C of the Geokon Instruction Manual (2010).

$$T = \frac{1}{A + B(lnR) + C(lnR)^3} - 273.15 \qquad \text{Equation 5-1}$$

Where

T = the gauge temperature (℃)

R = the thermistor resistance

A = 1.4051 x 10^{-3}

B = 2.369 x 10^{-4}

C = 1.019 x 10^{-7}

The gauge strain was determined in a similar manner using the recorded natural frequency of vibration. The process outlined below is found in Appendix B of the Geokon Instruction Manual (2010) that was included with the gauges. The natural frequency of vibration of a wire is related to its tension, length, and mass by Equation 5-2.

$$f = \frac{1}{2L_w}\sqrt{\frac{F}{m}} \qquad \text{Equation 5-2}$$

Where

f = the natural frequency of the wire (Hz)

L_w = the length of the wire (in.)

F = the wire tension (lbs)

m = the mass of the wire per unit length (lb $sec^2/in.^2$)

Re-arranging Equation 5-2, using the relationship that the force in the wire is related to the strain in the wire through the modulus of elasticity of the wire, and using

the correct values for length and mass of the wire, Equation 5-3 can be used to determine the strain in the wire directly from the natural frequency measured.

$$\varepsilon_w = 3.304 \times 10^{-3}(f^2) \qquad \text{Equation 5-3}$$

Where

ε_w = the measured strain in the gauge (10^{-6} in./in.)

f = the frequency (Hz)

Chapter 6 Results and Discussion

6.1 Introduction

This chapter includes predicted and measured results for the studied specimens. In order to make comparisons with the prediction model, the values measured in the field needed to be adjusted to compensate for transient effects of varying temperatures within the bridge components. An effective coefficient of thermal expansion was determined for both SCC and VC girders in order to accurately compensate for thermal effects. The process for determining the effective coefficients of thermal expansion is explained throughout this chapter. Finally, measured and predicted cambers along with prestress losses are presented and discussed.

6.2 Adjustment of Measurements to Account for Temperature Changes

The AASHTO 2012 predicted prestress losses for the specimens in this study were computed assuming a constant temperature throughout the cross section. However, the actual girders were exposed to daily variations in temperature and environmental conditions including sunlight, wind, and precipitation. These environmental conditions induce non-uniform and nonlinear temperature distributions throughout the girder and deck cross section during the measurement of internal strains and cambers. Since both steel and concrete are susceptible to thermal expansion and contraction, measured internal strains and cambers reflected these temperature gradients. It was necessary to take these thermal gradients into account and adjust the strains and cambers measured in order to minimize the influence of these transient thermal effects on the measured long-

term behavior. Camber and strain measurements were adjusted to equivalent measurements expected if the concrete had a uniform internal temperature of 68 degrees Fahrenheit (20 °C).

In order to simplify the analysis for thermal effects, an idealized cross section was assumed for both the BT- 54 and BT-72 cross sections. These idealized shapes were dimensioned in order to very closely resemble the BT-54 section and BT-72 section in such geometric properties as the location of the centroid, the area of the cross section, and the moment of inertia of the cross section. It was assumed that each interior girder supported one half of the deck width to the next girder. Also, as-built haunch buildup thicknesses were determined for each girder by the method outlined in Section 4.4, and were included in the idealized composite cross sections. Figure 6-1 through Figure 6-4 show the idealized girder and composite cross sections. In Figure 6-1and Figure 6-2 the idealized girders are superimposed over the actual girders cross section where the actual girders cross section is shown as a dashed line.

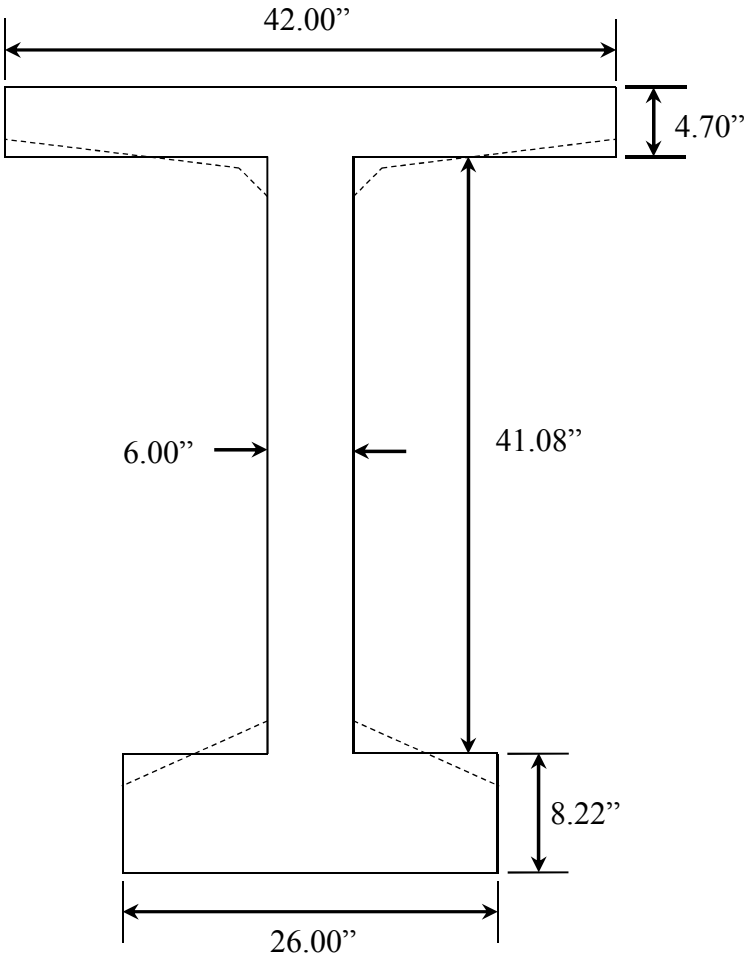

Figure 6-1: Simplified BT-54 Section

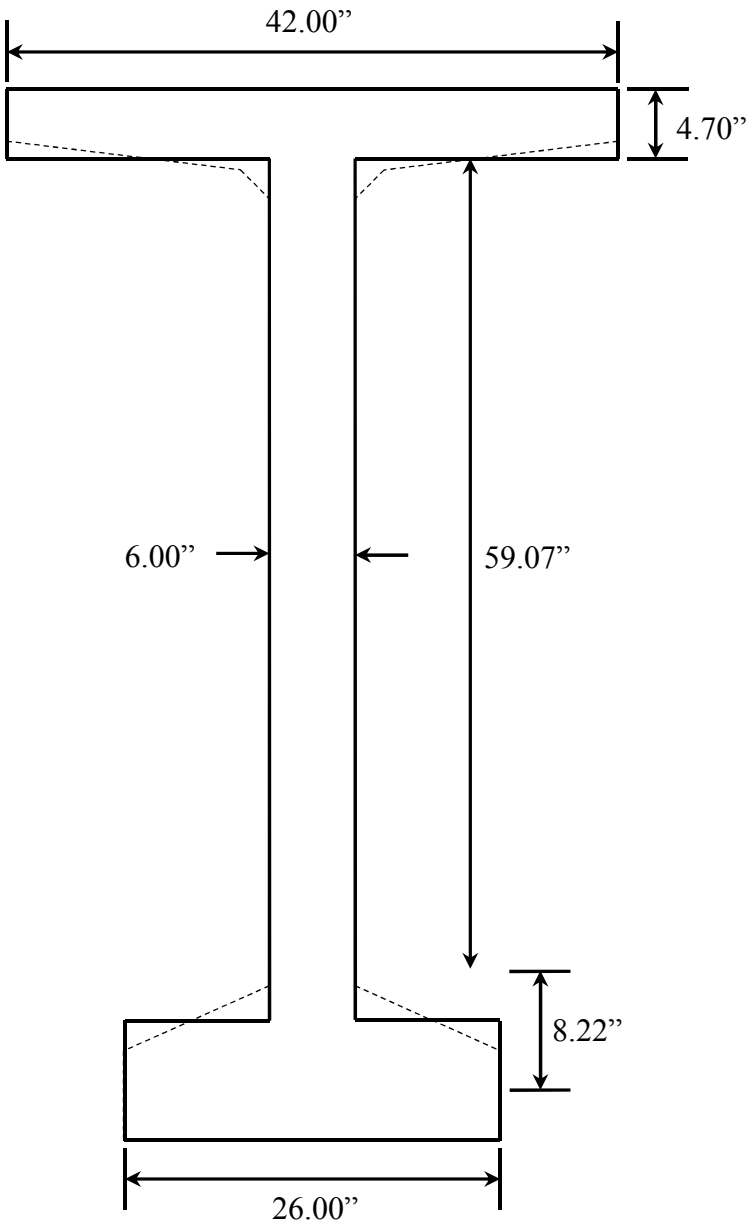

Figure 6-2: Simplified BT-72 Section

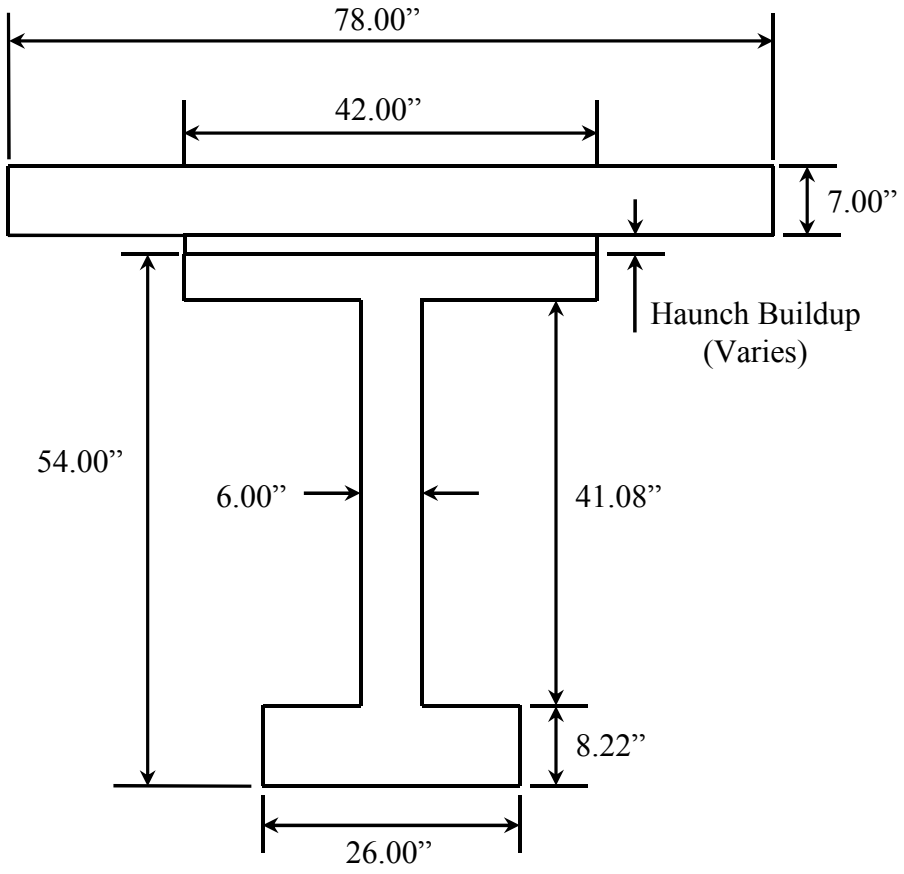

Figure 6-3: Simplified BT-54 Composite Section

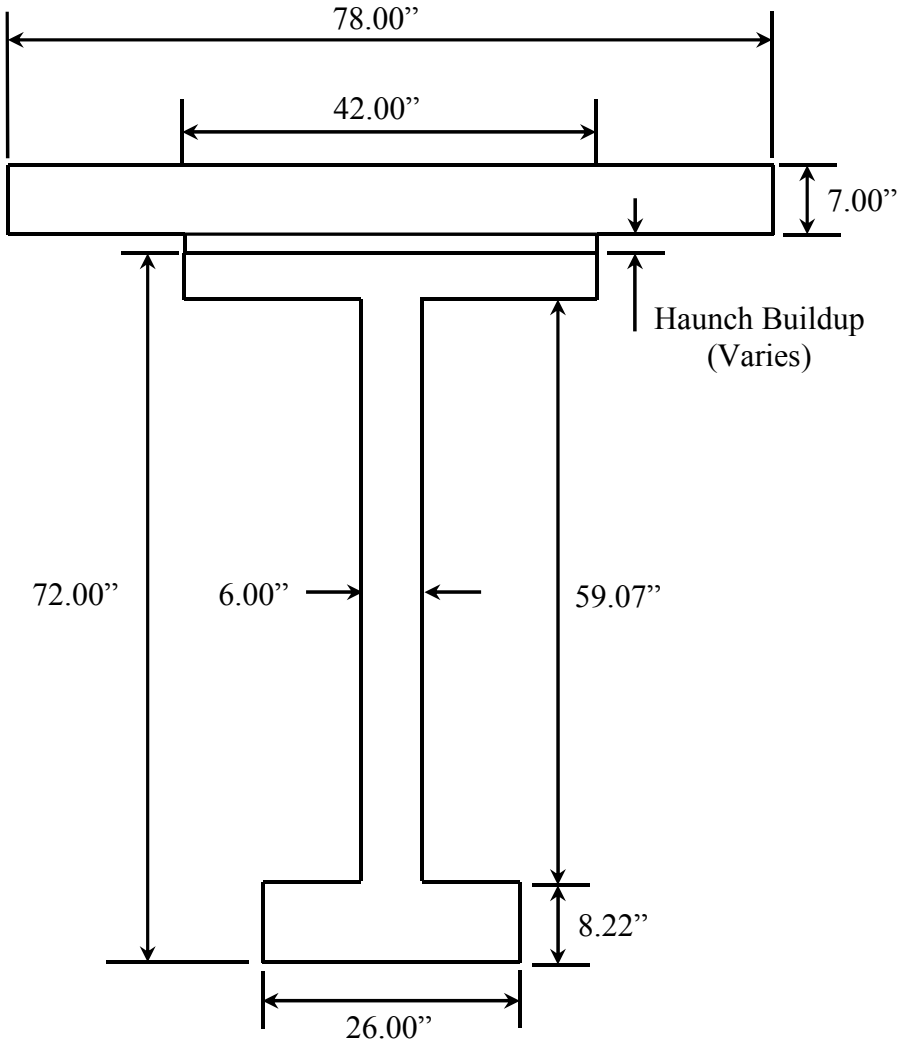

Figure 6-4: Simplified BT-72 Composite Section

As discussed previously, the VWSG gauges installed in the girders and deck measured strain and temperature. Therefore, whenever a strain reading was recorded, the corresponding temperature of the gauge and consequently the temperature of the concrete around the gauge were recorded. This allowed approximate temperature gradients at the time of strain measurements to be constructed based on these temperature measurements. The top and bottom flanges only have one gauge and are relatively thin; therefore temperature gradients were considered constant throughout the top and bottom flanges of

the idealized girder cross sections. The temperature gradient through the haunch was also considered to be constant and equal to the temperature present in the top flange of the girder. The temperature gradient through the middle rectangle, which idealized the web of the girder, was assumed to be linear. This was due to the placement of the two VWSG within the web of actual girders. The temperature gradient through the deck of the idealized composite section was assumed to be linear as well. The slope of the temperature gradient through the deck was determined based on temperature readings from the gauge located in the deck and top flange of the girder. This was due to the fact that the deck is directly exposed to any sunlight, and elevated temperatures could be expected in the top of the deck in relation to the bottom of the deck. Gauge locations were discussed above in Section 5.3. Trial analyses were also conducted assuming linear gradients in both the bottom bulb and the top flange, but results from those models did not differ significantly from the constant temperature assumption in the bottom bulb and top flange.

In order to make accurate comparisons to predicted long-term values, the measured strains and cambers were adjusted so that they would represent what the measured strain or camber would have been if the girder was a uniform 68°F (20°C) throughout its cross section at the time of measurement. These adjustments were made assuming that plane sections remain plane at all times. This means that the change in strain at any level can be determined if the change in strain at the centroid and the change in curvature of the cross section is known, as shown in Equation 6-1.

$$\Delta\varepsilon_c = \Delta\varepsilon_{cen} + (\Delta\phi)y \qquad \text{Equation 6-1}$$

Where

$\Delta\varepsilon_c$ = the change in strain in the concrete (in./in)

$\Delta\varepsilon_{cen}$ = the change in strain at the centroid of the cross section (in./in.)

$\Delta\phi$ = the change in curvature of the cross section

y = the distance from the centroid (positive down) to the concrete being considered (in.)

The change in total strain at any depth of a cross section is the sum of the change in stress-dependent strain and the change in stress-independent strain. The stress-dependent strain is a linear-elastic response to stress, and can be seen in the first part of Equation 6-2. The change in stress-dependent strain includes the effects of prestress transfer and other externally applied loads. Stress-independent strain includes the unrestrained component of strain due to shrinkage and temperature, which makes up the second half of Equation 6-2. For the purposes of this transient temperature correction process, only the short-term strain due to the temperature change is considered.

$$\Delta\varepsilon = \frac{\Delta f}{E} + \alpha_T \Delta T \qquad \text{Equation 6-2}$$

Where

Δf = change in stress at any depth of the cross section

α_T = the coefficient of thermal expansion of concrete (με/°C)

ΔT = change temperature (°C)

Furthermore, as long as there is no externally applied axial force equilibrium requires that the sum of the axial forces on any cross section must equal zero. Thus, the change in stresses on a cross section integrated over the area of that cross section must equal zero, as shown in Equation 6-3.

$$\int_A \Delta f dA = 0 \qquad \text{Equation 6-3}$$

For the case where only the girder cross section is considered, solving Equation 6-2 for the change in stress, using the relationship for the strain at any height as a function of the curvature, and substituting into Equation 6-3 yields the relationship shown in Equation 6-4.

$$\int_A E\left[\left(\Delta\varepsilon_{cen,t} + (\Delta\phi \times y)\right) - \alpha_T \Delta T\right] dA = 0 \qquad \text{Equation 6-4}$$

Finally, for the case where only the girder cross section is considered, Equation 6-4 is rearranged to solve for the change in strain at the centroid of the cross section due to changes in the temperature in the cross section. The explanation for the girders coefficient of thermal expansion for both SCC and VC is explained in Section 6.2.3.

$$\Delta\varepsilon_{cen,t} = \frac{\alpha_T \int \Delta T dA}{A} \qquad \text{Equation 6-5}$$

Where

$\Delta\varepsilon_{cen,t}$ = the strain change at the centroid of the cross section due to temperature changes in the concrete

α_T = the coefficient of thermal expansion of concrete (με/°C)

ΔT = change in temperature (°C)

A = the cross-sectional area (in^2)

For the case where the composite section is considered, an extended approach must be considered when developing a relationship similar to Equation 6-5 for the composite section. Since the girder and deck can have different material properties, the relationship in Equation 6-5 is not valid. Therefore, for a composite section Equation 6-4 is solved for the change in stress for both the deck and the girder separately. Using the

relationship for the strain at any height as a function of the curvature, and substituting into Equation 6-3 yields the relationship shown in Equation 6-6. Which is just an expanded form of Equation 6-4. The subscripts "G" and "D" found in Equation 6-6, represent properties and relationships corresponding to the girder and deck respectively.

$$\int_{A_G} E_G \left[\left(\Delta\varepsilon_{cen,t} + (\Delta\phi \times y)\right) - \alpha_{T,G}\Delta T\right] dA_G + \int_{A_D} E_D \left[\left(\Delta\varepsilon_{cen,t} + (\Delta\phi \times y)\right) - \alpha_{T,D}\Delta T\right] dA_D = 0 \quad \text{Equation 6-6}$$

Equation 6-6 is rearranged to solve for the change in strain at the centroid of the composite cross section due to changes in temperatures on the cross section. A transformed section approach simplifies the expression of Equation 6-7, where properties of the deck concrete were transformed into girder concrete properties. It is important to note that expressions for the girder and deck components in Equation 6-7 are separated to account for differing coefficients of thermal expansion.

$$\Delta\varepsilon_{cen,t} = \frac{(\alpha_T \int \Delta T dA)_{GIRDER} + n(\alpha_T \int \Delta T dA)_{DECK}}{A_{tr}} \quad \text{Equation 6-7}$$

In which

$$n = \frac{E_D}{E_G} \quad \text{Equation 6-8}$$

And

$$A_{tr} = A_G + nA_D \quad \text{Equation 6-9}$$

Where

n = the deck-to-girder modular ratio

E_D = the deck concrete Modulus of Elasticity (ksi)

E_G = the girder concrete Modulus of Elasticity (ksi)

A_{tr} = the transformed composite cross sectional area (in^2)

A_G = the girders cross-sectional area (in^2)

A_D = the deck cross-sectional area (in^2)

For a simply-supported flexural member with unchanging loads, the sum of the change in moment due solely to temperature change on any cross section must also be equal to zero. This was used to determine the change in curvature of each cross section due to a change in the temperatures on the cross section. This means that the integral of the change in stress times the distance from the centroid *y* integrated over the area must equal zero.

$$\int_A (\Delta f \times y) dA = 0 \qquad \text{Equation 6-10}$$

For the case when only the girder section is considered, Equation 6-10 is rewritten in terms of strain change at the centroid and curvature, resulting in Equation 6-11. Notice that the equation below is similar to Equation 6-4 with the exception of the addition of the y term.

$$\int_A E\left[\left(\Delta\varepsilon_{cen,t} + (\Delta\phi \times y)\right) - \alpha_T \Delta T\right] y dA = 0 \qquad \text{Equation 6-11}$$

Distributing the integration to each term yields:

$$\left(E\Delta\varepsilon_{cen}\int y dA\right) + \left(E\Delta\phi \int y^2\, dA\right) - \left(E\alpha_T \int T y dA\right) = 0 \qquad \text{Equation 6-12}$$

The first term in Equation 6-12 is equal to zero, due to the fact that y is defined with respect to the centroid of the girders cross section. In the second term of Equation 6-12, the integral of the y^2 term is equivalent to *I*, the area moment of inertia of the cross section. Therefore, Equation 6-12 is rearranged to solve for the change in curvature of the girder cross section.

$$\Delta\phi_t = \frac{\alpha_T \int (\Delta T \times y) dA}{I} \quad \text{Equation 6-13}$$

Where

$\Delta\phi_t$ = the change in curvature of a concrete cross section due to temperature changes on the cross section (in./in)

α_T = the coefficient of thermal expansion of concrete

ΔT = temperature change in of the concrete (°C)

y = the distance from the idealized girder centroid (in)

A = the idealized girders cross-sectional area (in^2)

I = the idealized girders cross-sectional moment of inertia (in^4)

For the case where the composite section is considered, Equation 6-11 is again rewritten in terms of strain change at the centroid and curvature, resulting in Equation 6-14. As can be seen in Equation 6-14, two separate expressions are developed for the girder and deck to account for the differing material properties. Notice that the equation below is similar to Equation 6-6 with the exception of the addition of the y term.

$$\int_{A_G} E_G \left[\left(\Delta\varepsilon_{cen,t} + (\Delta\phi \times y)\right) - \alpha_{T,G}\Delta T\right] y dA_G + \int_{A_D} E_D \left[\left(\Delta\varepsilon_{cen,t} + (\Delta\phi \times y)\right) - \alpha_{T,D}\Delta T\right] y dA_D = 0 \quad \text{Equation 6-14}$$

Distributing the integration to each term yields:

$$\left[\left(E_G\Delta\varepsilon_{cen,t}\int_{AG} y\,dA_G\right)+\left(E_G\Delta\phi\int_{AG} y^2\,dA_G\right)-\left(E_G\alpha_{T,G}\int_{AG}\Delta T y\,dA_G\right)\right]+\left[\left(E_D\Delta\varepsilon_{cen,t}\int_{AD} y\,dA_D\right)+\left(E_D\Delta\phi\int_{AD} y^2\,dA_D\right)-\left(E_D\alpha_{T,D}\int_{AD}\Delta T y\,dA_D\right)\right]=0 \quad \text{Equation 6-15}$$

A transformed section approach was used to rearrange Equation 6-15, where properties of the deck concrete were transformed into girder concrete properties. The first and fourth terms in Equation 6-15 is equal to zero when y is taken with respect to the centroid of the transformed cross section. In the second and fifth terms of Equation 6-15, the integral of the y^2 term is equivalent to the moment of inertia of the girder and deck respectively. Therefore, Equation 6-15 is rearranged to solve for the change in curvature of the composite cross section due to thermal effects, and can be seen in Equation 6-16. It is important to note that expressions for the girder and deck components in Equation 6-16 are separated to account for differing coefficients of thermal expansion.

$$\Delta\phi_t=\frac{[\alpha_T\int(\Delta T\times y)dA]_{GIRDER}+n[\alpha_T\int(\Delta T\times y)dA]_{DECK}}{I_{tr}} \quad \text{Equation 6-16}$$

Where

y = the distance from the transformed composite section centroid (in)

I_{tr} = the transformed composite cross sectional moment of inertia (in^4)

6.2.1 Temperature Correction for Camber

The first step in correcting the measured cambers for temperature was to correct the baseline camber reading for temperature gradient. These baseline readings were taken just prior to prestress transfer. However, because steam curing had recently ended, there were significantly elevated temperatures (relative to 20°C) throughout the cross

section, and a gradient due to elevated temperatures in the bulb section of the girder. The baseline camber reading was corrected by calculating the curvature due to this initial temperature gradient and transforming it into an expected midspan deflection with Equation 6-17. Curvature due to the non-linear temperature gradient was assumed to be uniform along the girders length for every cross section.

$$\delta_{i,t} = \frac{\Delta\phi_{i,t}(L^2)}{8} \qquad \text{Equation 6-17}$$

Where

$\delta_{i,t}$ = the initial deflection at midspan due to temperature gradient (in.)

$\Delta\phi_{i,t}$ = the uniform change in initial curvature due to temperature gradient (in./in.)

L = the length of the girder between supports (in.)

Because the bottom flange was initially the hottest portion of the girder, this initial temperature-induced deflection was always a negative value, meaning that the temperature gradient was causing the ends of the girder to be slightly elevated relative to midspan which also corresponds to the cracks noted in Section 3.7.2. After prestress transfer, camber readings were taken at various times as the girders were in storage at the prestressing plant and after the girders were erected and the bridge was in service. Each time that a camber measurement was taken the temperature readings across the depth at midspan of that girder were recorded. Girders that were only instrumented with one VWSG were assumed to have similar gradients as those in the same casting groups that were fully instrumented. After the girders were erected in the bridge, many of the VWSG recordings became unreliable, therefore temperature readings were again taken from girders of the same orientation. In the case that the temperature readings in the deck

were absent or unreliable, readings were used from the nearest deck VWSG to the girder under consideration. The change in deflection due to temperature gradient at the time of camber measurement, δ_t, is calculated by Equation 6-18, which is similar to Equation 6-17 above.

$$\delta_t = \frac{\Delta\phi_t(L^2)}{8} \qquad \text{Equation 6-18}$$

Where

δ_t = the deflection at midspan due to temperature gradient (in)

$\Delta\phi_t$ = the change in curvature due to temperature gradient (in./in.)

The adjusted camber for each girder at the time of each camber measurement was calculated by Equation 6-19 shown below.

$$\Delta_{adj} = \Delta_{mea} - \left(\delta_t + -\delta_{i,t}\right) \qquad \text{Equation 6-19}$$

Where

Δ_{adj} = the adjusted camber (in.)

Δ_{mea} = the unadjusted, measured camber (in)

δ_t = the deflection due to temperature gradient at the time of camber measurement (in)

$\delta_{i,t}$ = the initial deflection as calculated in Equation 6-17

The adjustments discussed above were applied to every camber measurement taken. Occasionally camber readings were taken when temperature data from the VWSGs were not recorded. In these instances, gradients from the same time of day for either the day before or the day after the camber measurement were used to provide a close approximation. Furthermore, gradients were assumed for girders that had only one VWSG in the midspan cross section by using companion girders that were fully

instrumented. There was at least one girder in each casting group that had a fully instrumented midspan, and the gradients from those girders were used for the other girders in that group.

Camber measurements were most often taken early in the morning, just after sunrise. This was done because temperature gradients across the cross section are usually the most constant at this time of day. Figure 6-5 shows some temperature gradients for Girder 54-4S. It is apparent that the temperature gradient was most severe at the time of initial prestress transfer, with the bottom bulb of the girder significantly warmer than the web and top flange. This temperature distribution was likely the main cause for the cracks observed in the girders prior to prestress transfer discussed in Chapter 3. Figure 6-6 shows a comparison of adjusted camber measurements to unadjusted measurements for SCC BT-54 girders. Almost all of the adjusted values are lower than the measured values. This is due to the initial offset calculated by Equation 6-17 and applied to every successive measurement.

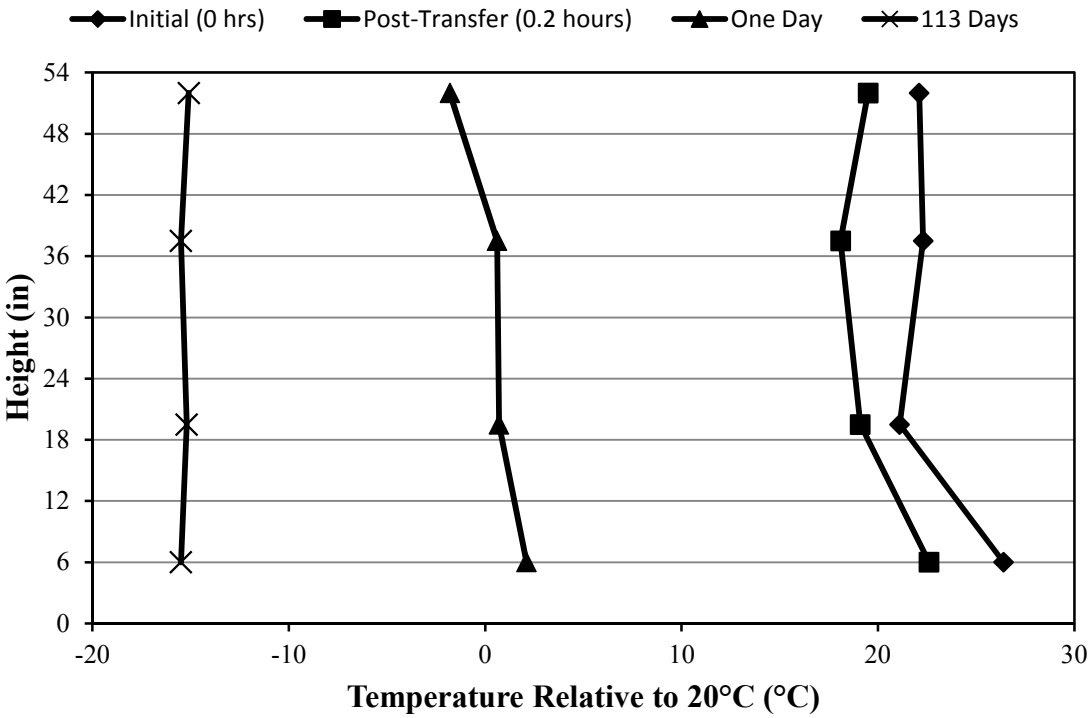

Figure 6-5: Temperature Gradients for 54-4S at Times of Camber Measurement

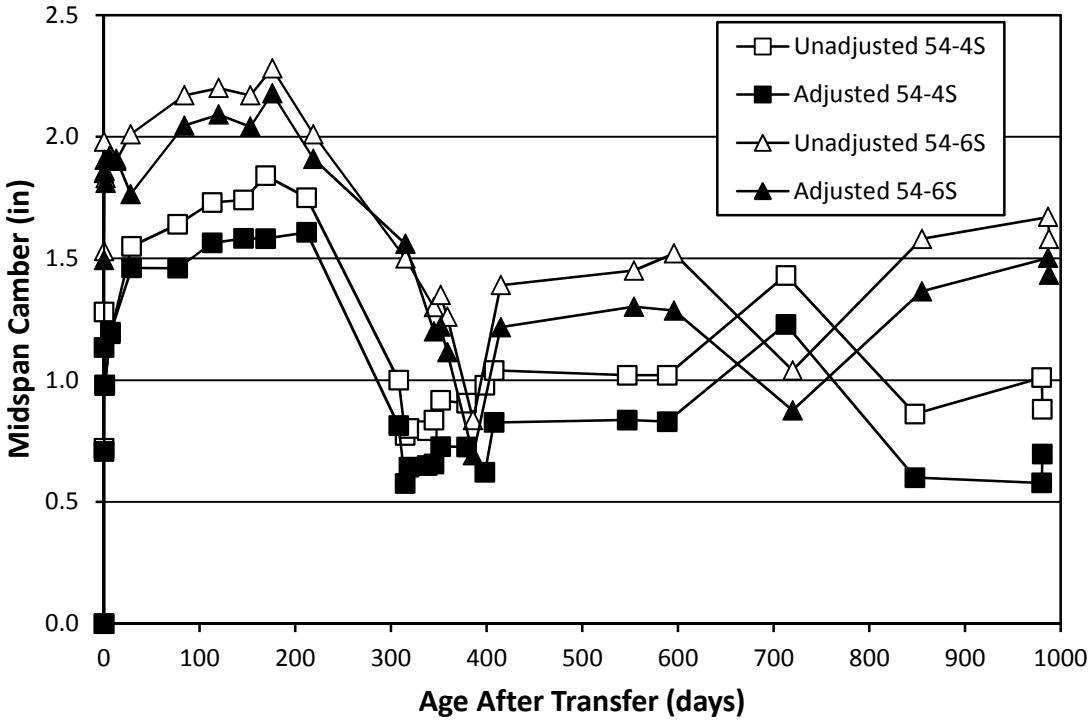

Figure 6-6: BT-54 (SCC) Cambers

6.2.2 Temperature Correction for Internal Strain

To make appropriate comparisons to predicted prestress losses, measured strain values must be adjusted so that they represent what the measured strain would have been if the girder was a constant 68°F, (20°C), throughout its cross section at the time of measurement. The correction was a two-step process. The first correction was due to the temperature of the VWSG itself, and the second correction dealt with the nonlinear temperature gradient across the cross section.

The very nature of the VWSG itself caused the need for a temperature correction to every strain reading recorded from the VWSG. The gauge measures strains by measuring the tension of a steel wire anchored at each end of the gauge. The steel wire itself is susceptible to temperature deformations. This means that even if the gauge was completely restrained against movement, a temperature change within the gauge would cause a change in the strain reading simply because the wire tension would be altered by the temperature change. The strain reading was corrected for the temperature of the gauge (relative to 20°C) by Equation 6-20 shown below.

$$\varepsilon_{rec,gt} = \varepsilon_{rec} + \left(\alpha_g T_g\right) \qquad \text{Equation 6-20}$$

Where

$\varepsilon_{rec,gt}$ = the recorded strain corrected for gauge temperature (με)

ε_{rec} = the recorded internal strain (με)

T_g = is the gauge temperature relative to 20°C

α_g = the coefficient of thermal expansion for the VWSG wire (12.2 με/°C)

After the recorded strains were corrected to account for gauge temperature, the recorded strains were corrected for the temperature gradient over the cross section of the

girder. This was done using the principles described earlier. First, a strain change at the centroid of the cross section due to thermal effects was computed by Equation 6-5 or Equation 6-7.

The strain change at any height within the cross section is the algebraic sum of the strain change at the centroid and the change in strain at that height due to the change in curvature of the section. The change in curvature of the cross section was calculated using Equation 6-1, rewritten as Equation 6-21 here.

$$\Delta\varepsilon_T = \Delta\varepsilon_{cen,t} + (y\Delta\phi_t) \qquad \text{Equation 6-21}$$

Where

$\Delta\varepsilon_T$ = the change in strain due to the temperature gradient

$\Delta\varepsilon_{cen,t}$ = the change in strain at the centroid of the cross section due to thermal gradient

$\Delta\phi_t$ = the change in curvature of the cross section due to the temperature gradient

y = the distance from the centroid of the cross section to the location of the strain reading (positive downward)

These internal strain corrections were applied to every recorded strain reading reported. Some of the girders only had one VWSG, which was located in the bottom bulb of the girder. However, changes in the curvature of the midspan cross section are required in order to correct the strain reading. Therefore, curvature values for each time step for the girders containing one gauge were estimated by using curvatures from companion girders. Each casting group contained at least one girder with a "fully-instrumented" midspan cross section. The changes in curvature resulting from the

temperature gradient measured in these girders were used to correct the strains in the other girders in the casting group that were not "fully-instrumented."

Figure 6-7 and Figure 6-8 verify the relationship between temperature profile and induced strains. Both of these figures compare the measured and predicted changes in strain gradient for specimens with and without the composite deck. The predicted values were computed using Equation 6-21, and from a fitted temperature profile discussed previously in Section 6.2. Figure 6-7 shows the measured and predicted changes in temperature and strain for girder 54-11C while the girder was still located at the storage facility on 10/16/2010 from 9:42 AM to 5:24 PM. Figure 6-8 shows the measured and predicted changes in temperature and strain for girder 72-4S after the full composite action with the deck was achieved from 10/2/2011 at 6:00 PM to 10/3/2011 at 10:50AM. The measured strain values are considered reliable due to the linearity of the measured strain profile. The close agreement between the predicted and measured strain gradients confirms the methodology presented above.

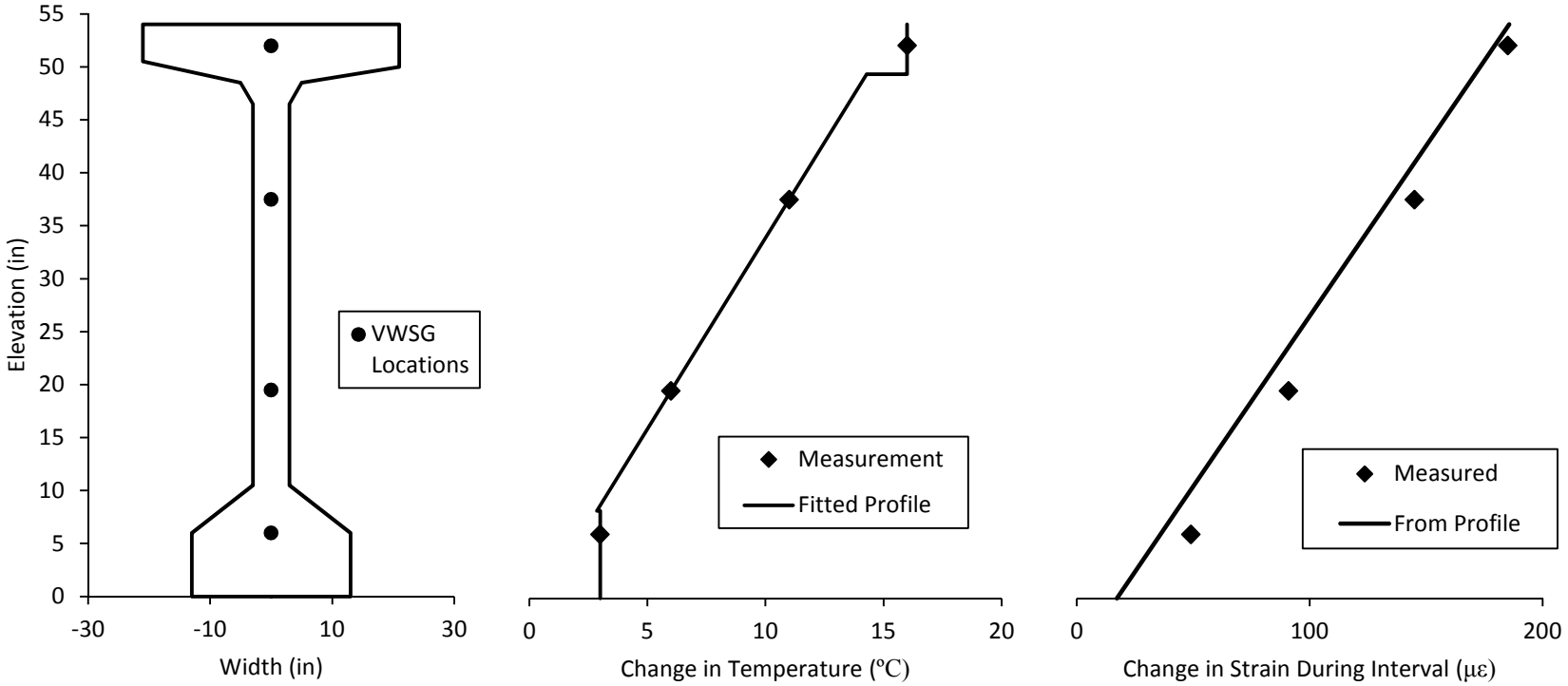

Figure 6-7: Predicted Change in Strain Due to Thermal Effects (54-11C)

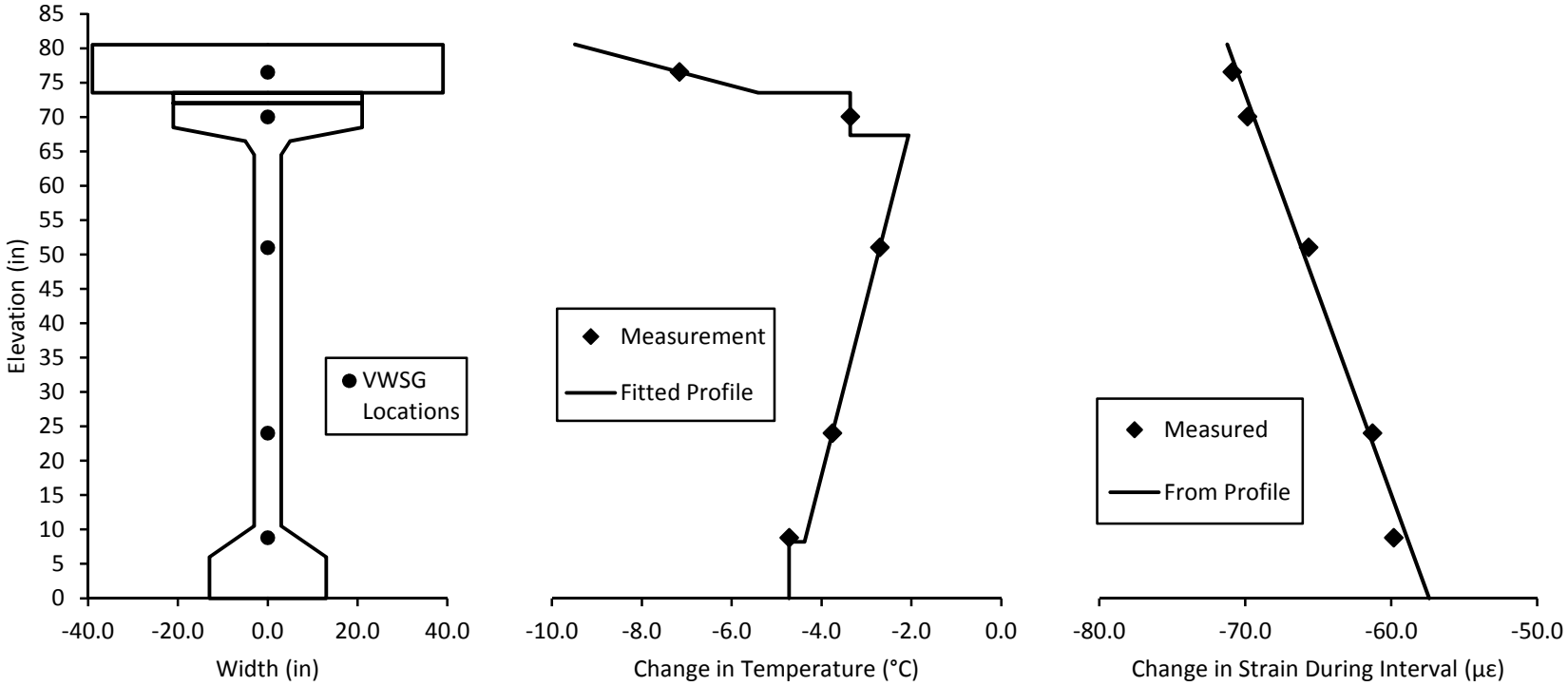

Figure 6-8: Predicted Change in Strain Due to Thermal Effects (72-4S in Bridge)

6.2.3 Determining an Effective Coefficient of Thermal Expansion

During the process of correcting measured strain and cambers for thermal effects, questions arose regarding the concrete coefficient of thermal expansion (CTE) used by Johnson (2012). Johnson assigned a CTE value of 11 με/°C for both the SCC and VC girders. This value was obtained from Section 5.4.2.2 of the AASHTO LRFD Bridge Design Manual (2010). Due to the importance the CTE has on the corrections for thermal effects, it was decided to consider refinements of the value used by Johnson (2012). The potential refinements included the possibility of using different CTE value for the SCC, VC, and VC deck concretes.

The investigation of CTE values was a two-part process. First, specimens for the SCC, VC, and VC deck concretes were tested in accordance with AASHTO T 336 (2009) in order to collect a saturated CTE, $\alpha_{t,sat}$, for the three concrete components. These lab results were taken to serve as basis of comparison to values estimated from field observation, which is described later in this section. The testing setup used in this investigation was the same used in the past investigation by Byard (2011). A full description of the testing set up can be found in Section 4.4.4 of Byard (2011). One pair each of specimens for representative SCC girder concrete and VC girder concrete, and two pairs of specimens for representative VC deck concrete were tested in accordance with AASHTO T 336 (2009). The test was conducted twice for each specimen, and the average of all the results were taken and can be seen in Table 6-1. It is important to note that all specimens were submerged for weeks before testing in order to achieve a saturated state.

Table 6-1: Averaged Saturated Coefficient of Thermal Expansion Testing Results

	$\alpha_{t,sat}$ (με/°C)
Girder SCC	9.4
Girder VC	9.0
Deck VC	7.7

The second part of the CTE investigation included determining "effective" CTE values for SCC and VC girder concretes based on field observations. The CTE values obtained from field observations are not based on a standard specification, and they are also affected by analytical simplifications discussed previously. Therefore, the CTE values obtained from field observations and implementing analytical assumptions were given the title of an "effective" CTE. In order to determine a concrete specific effective CTE, a change in measured bottom flange strains were compared with predicted bottom flange strains using varying CTE values. The girders used in this analysis were still located at the storage facility, thereby eliminating any effect that the composite deck may have on the analysis. The maximum error and standard deviation of errors for each CTE of each comparison were also computed and used to determine concrete-specific effective CTE values. Figure 6-9 through Figure 6-16 show the temperature histories along with the results of the change in measured and predicted bottom flange strains. The maximum change in strain error and standard deviation are provided as well on the following plots.

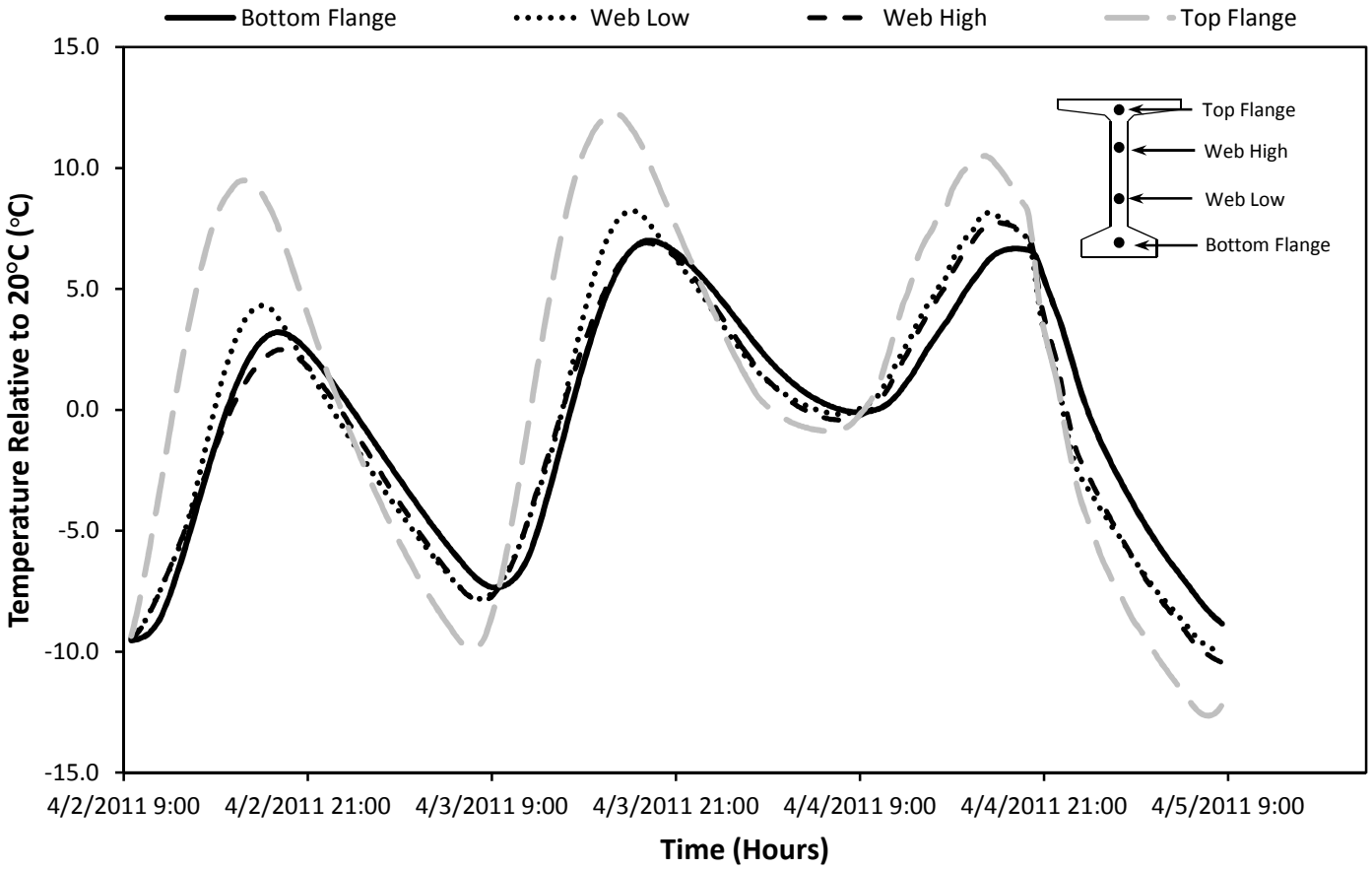

Figure 6-9: 54-4S Temperature Profile History

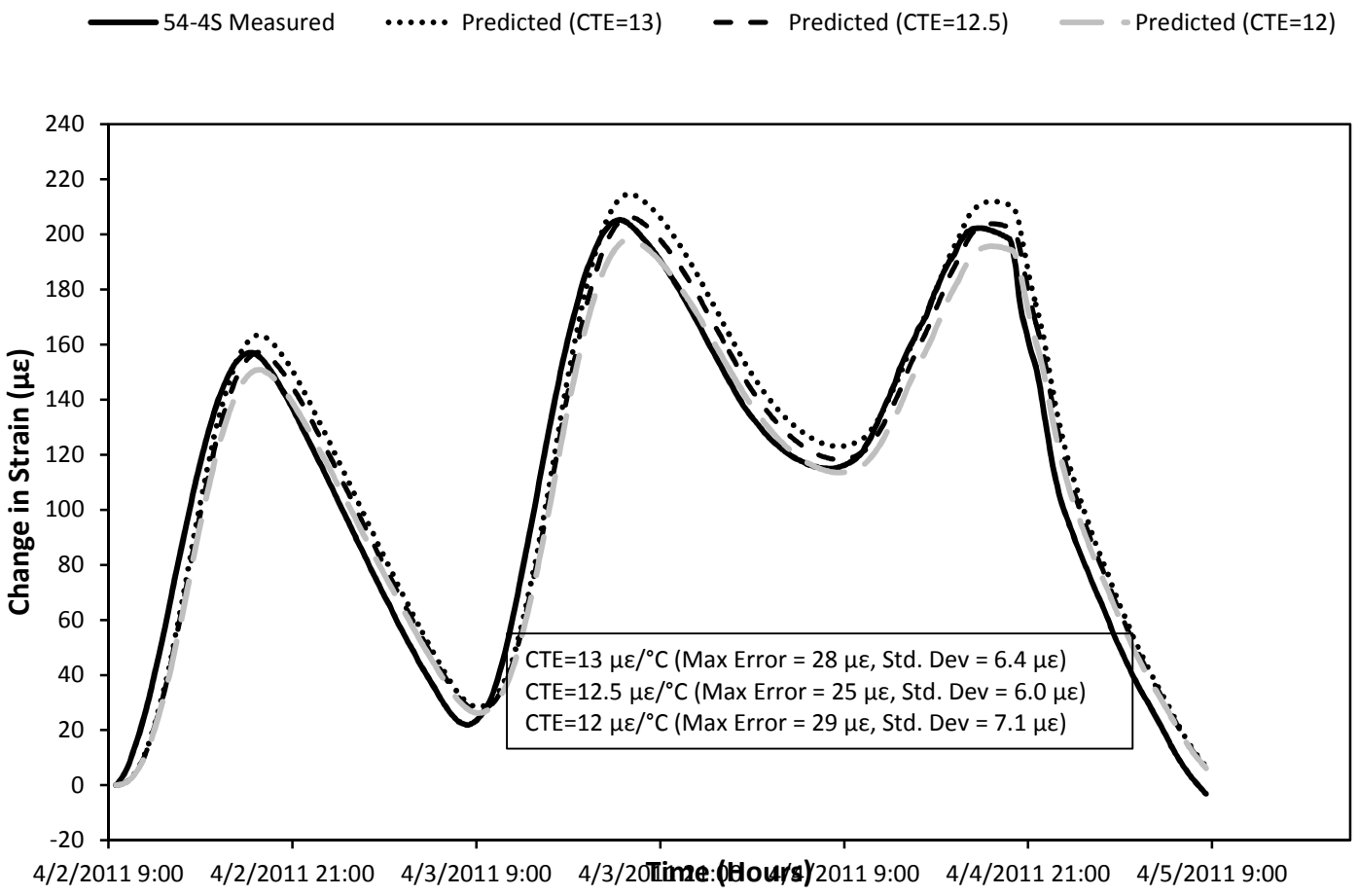

Figure 6-10: 54-4S Change in Bottom Flange Strains Due to Thermal Effects

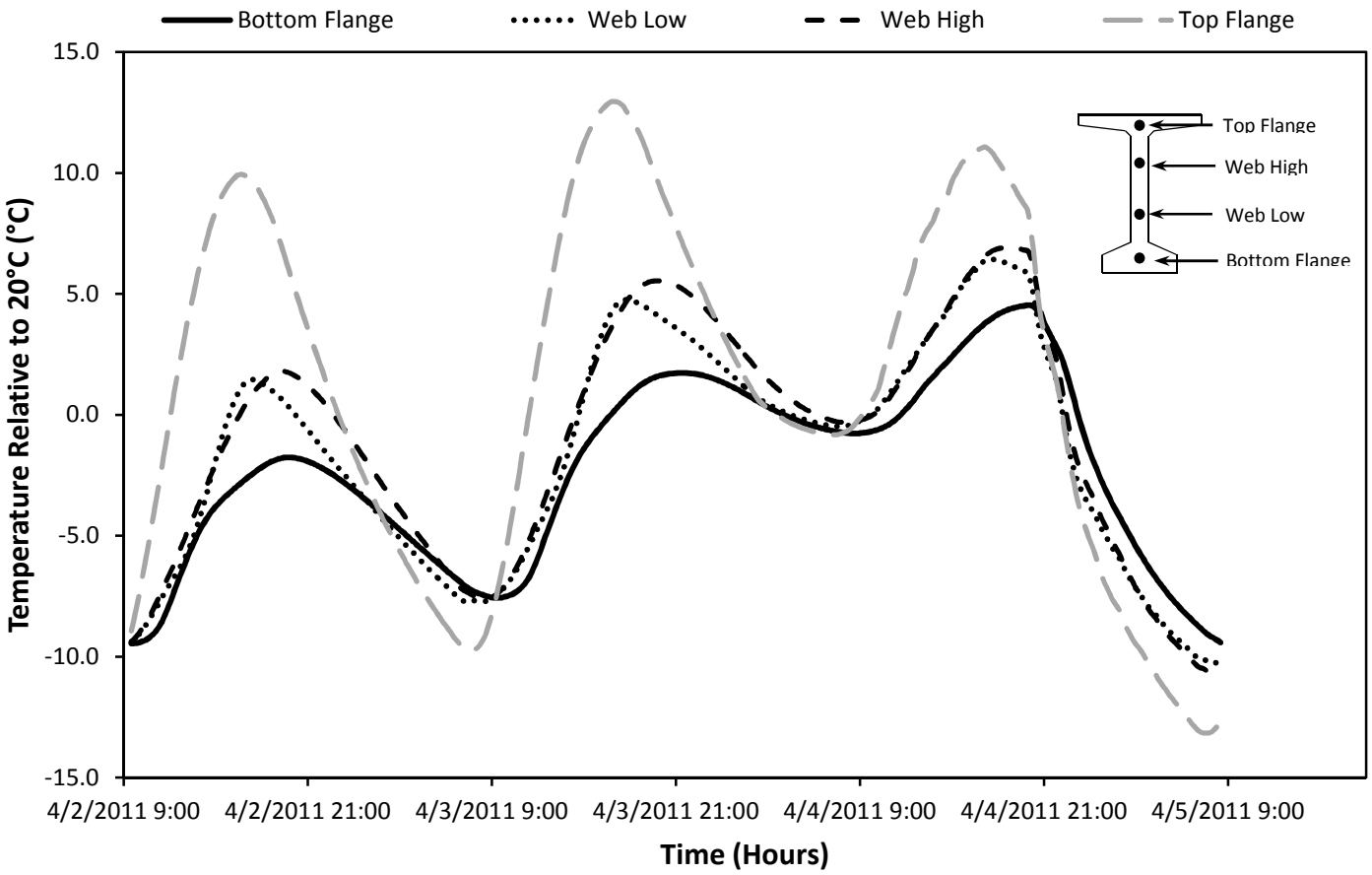

Figure 6-11: 54-11C Temperature Profile History

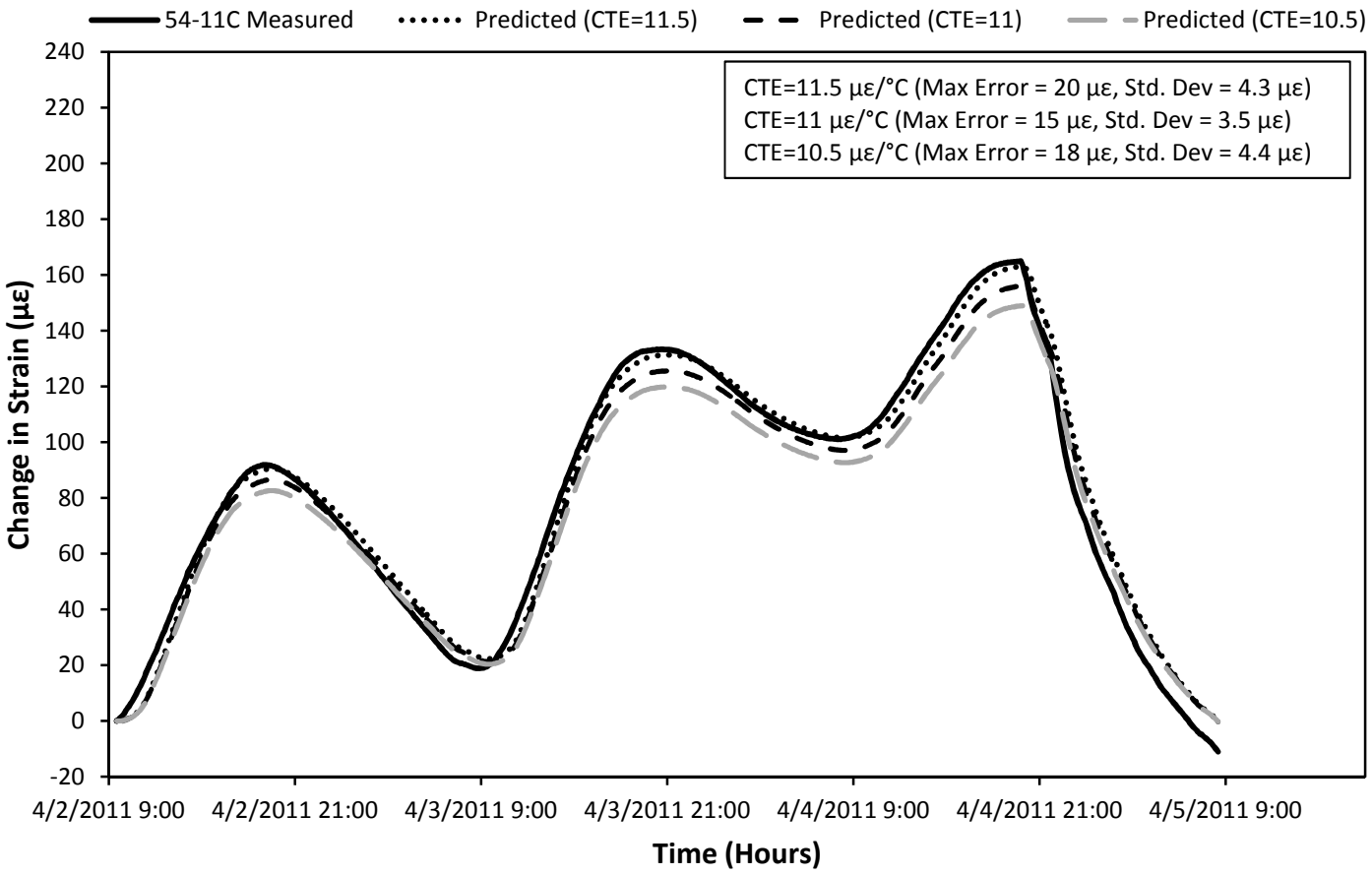

Figure 6-12: 54-11C Change in Bottom Flange Strains Due to Thermal Effects

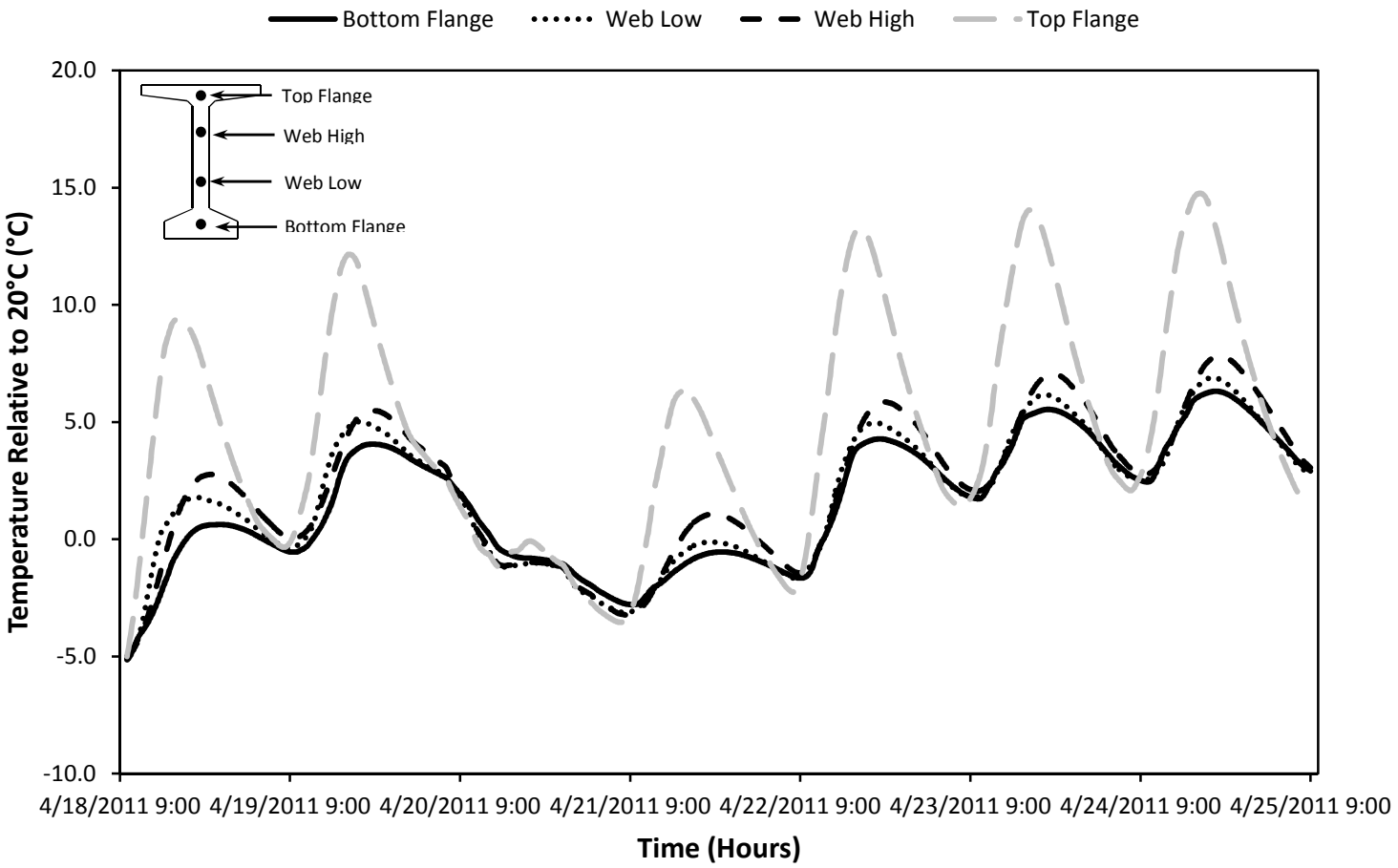

Figure 6-13: 72-6S Temperature Profile History

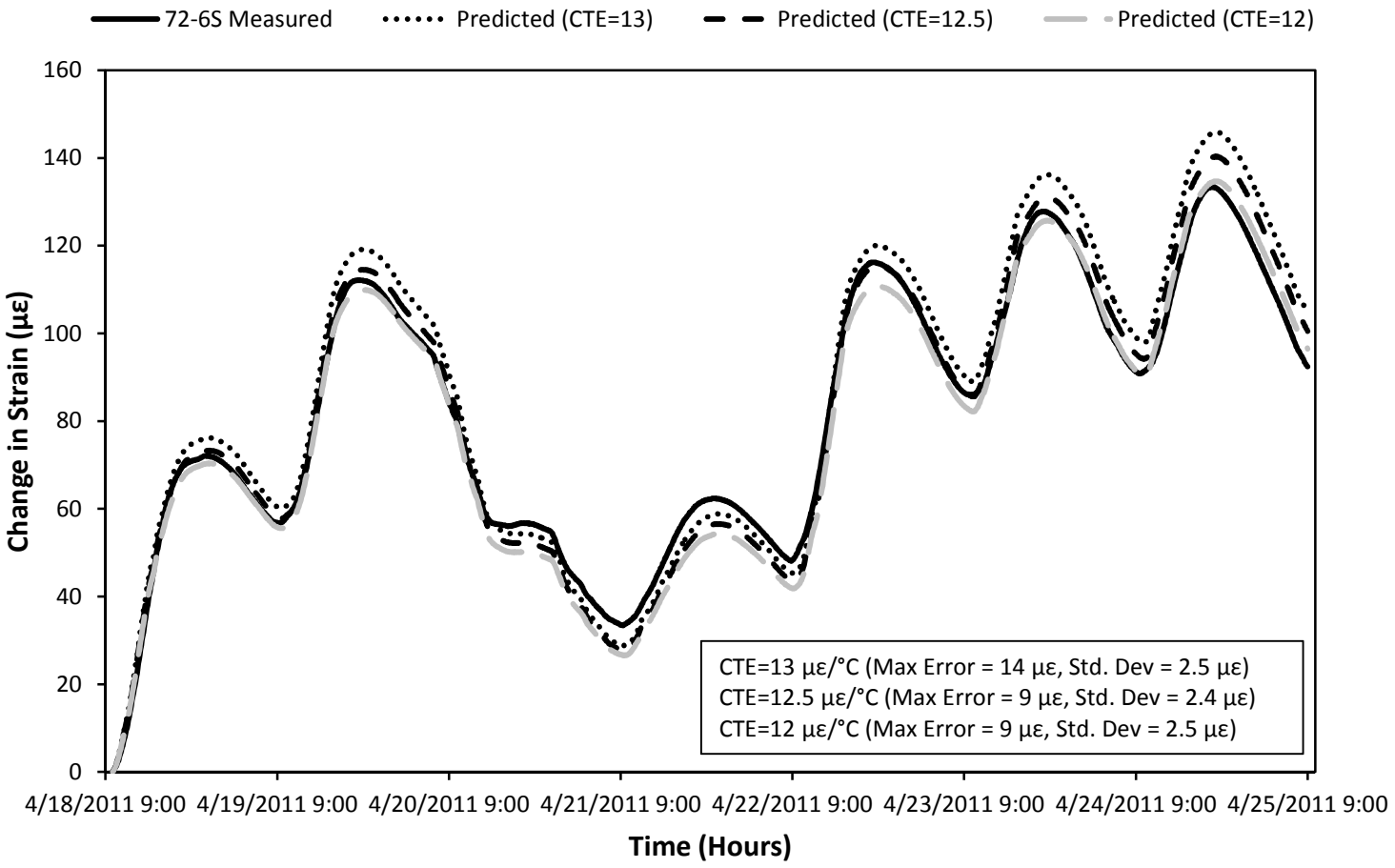

Figure 6-14: 72-6S Change in Bottom Flange Strains Due to Thermal Effects

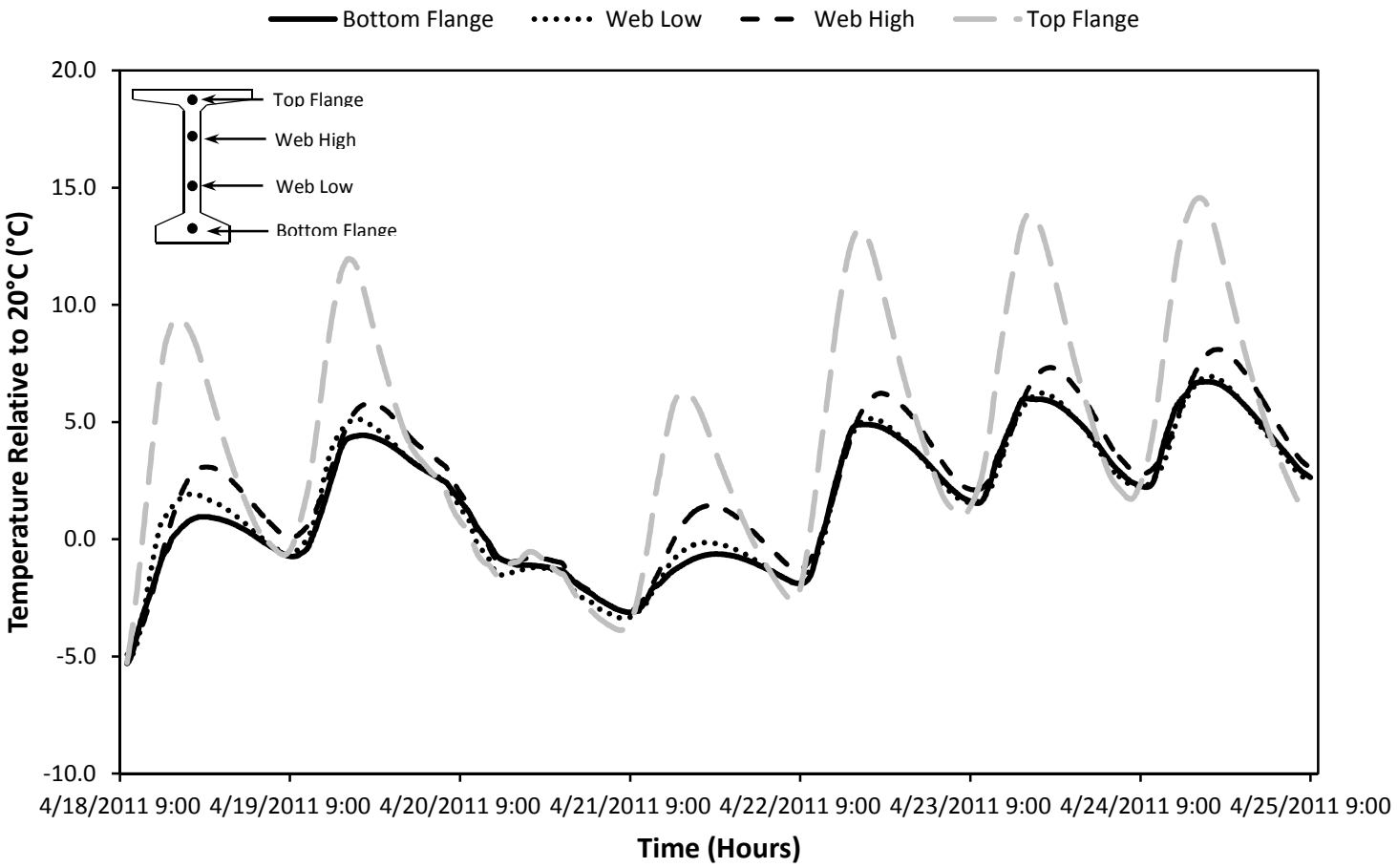

Figure 6-15: 72-11C Temperature Profile History

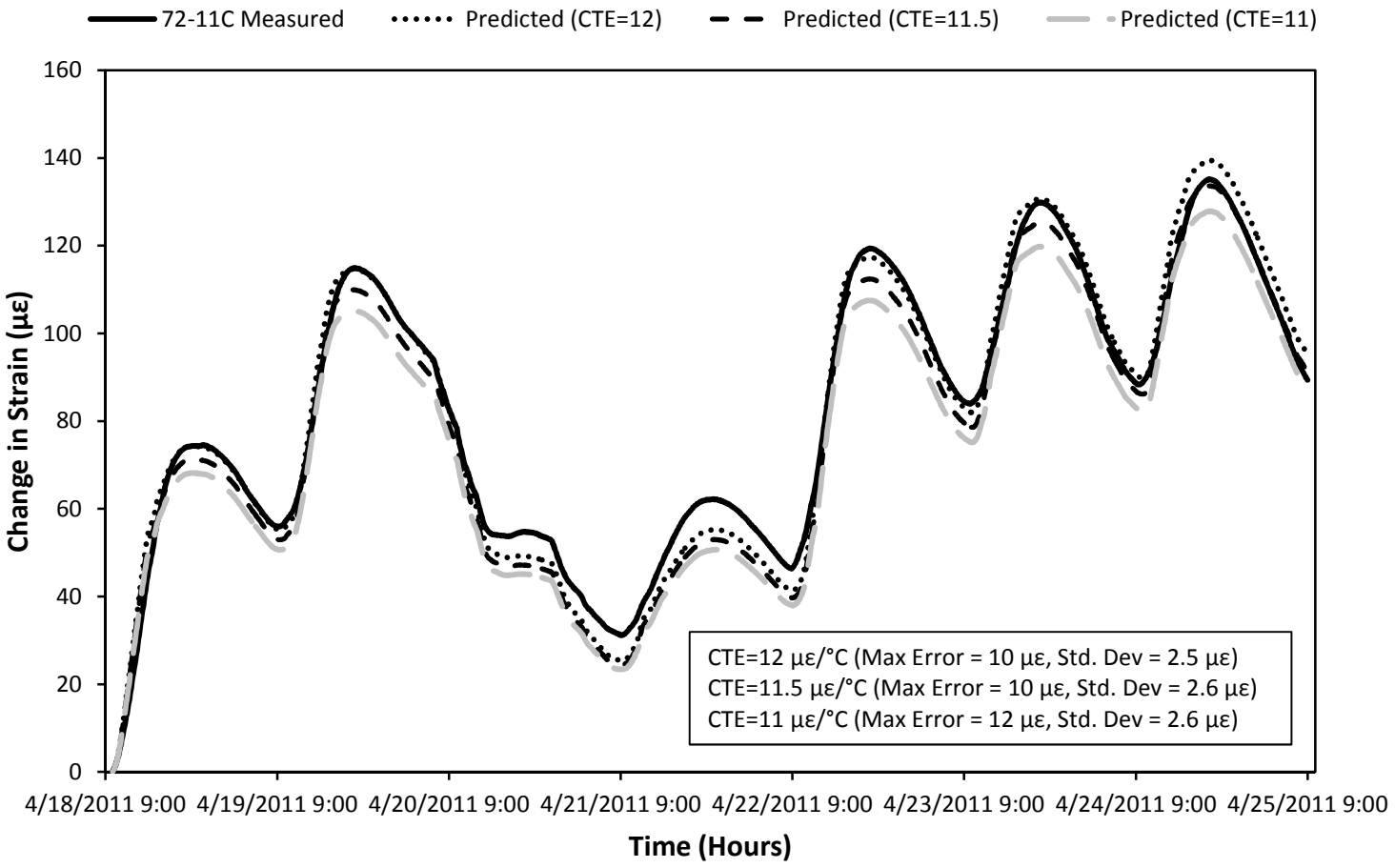

Figure 6-16: 72-11C Change in Bottom Flange Strains Due to Thermal Effects

Based on the figures, a CTE of 12.5 με/°C yielded the least maximum error and standard deviation for the SCC girders of both BT-54 and BT-72. Therefore, an effective CTE of 12.5 με/°C was assigned to all SCC girders for use in temperature corrections. The results for the VC girders were not as conclusive. For the BT-72 VC girders an effective CTE of 12 με/°C had the least maximum error and standard deviation. While the BT-54 VC girders an effective CTE of 11 με/°C had the least maximum error and standard deviation. Therefore, an effective average CTE of 11.5 με/°C was assigned to all VC girders for use in temperature corrections.

In order to justify implementing the effective CTE values in the temperature correction process, girder concrete CTE values were compared to those collected from the AASHTO T 336 (2009) tests results described earlier. One problem with directly comparing the two results is that the values collected from testing were saturated, and saturated specimens tend to have a lower CTE value than partially or oven dry specimens. ACI 209 (1992) provides an expression to predict the CTE, e_{th}, in με/°C, and can be found in Equation 6-22.

$$e_{th} = e_{mc} + 3.1 + 0.72e_a \qquad \text{Equation 6-22}$$

Where

e_{mc} = the degree of saturation component as given in Table 6-2

3.1 = the hydrated cement paste component

e_a = the average thermal coefficient of the total aggregate as given in Table 6-3 (5.5 με/°C for limestone)

Table 6-2: Suggested Values for the Degree of Saturation (ACI 209 1992)

Concrete Member Environmental Conditions	Degree of Saturation	e_{mc} 10-6/oF	e_{mc} 10-6/oC
Immersed structures, high humidity conditions.	Saturated	0	0
Mass concrete pours, thick walls, beams, columns and slabs, particularly where surface is sealed.	Between partially saturated and saturated	0.72	1.3
External slabs, walls, beams, columns, and roofs allowed to dry out or internal walls, columns slabs, not sealed (e.g. by mosaic or tiling) and where underfloor heating or central heating exists.	Partially saturated decreasing with time to the dryer conditions	0.83 to 1.11	1.5 to 2.0

Table 6-3: Average Thermal Coefficient of Expansion of Aggregate (ACI 209 1992)

Rock Group	ϵ_a 10-6/oF	ϵ_a 10-6/oC
Chert	6.6	11.8
Quartzite	5.7	10.3
Quartz	6.2	11.1
Sandstone	5.2	9.3
Marble	4.6	8.3
Siliceous limestone	4.6	8.3
Granite	3.8	6.8
Dolerite	3.8	6.8
Basalt	3.6	6.4
Limestone	3.1	5.5

If Equation 6-22 is used to predict the CTE in the saturated state, and for the condition where the actual girders can have the value e_{mc} = 2.0, then the effective CTE can be up to 28% greater than the saturated CTE (CTE_{SAT}). Neville (2000) showed that the paste fraction can be 60-70% higher at around 50-70% RH, and for these projects volumetrically weighted mixture proportions and materials, the increase would yield [1.29 to 1.34] CTE_{SAT}. In a report by Al-Ostaz (2007) the effect of relative humidity on CTE of concrete made with Alabama limestone showed an average multiplier of 1.26 at

75% RH. Therefore, from our saturated tested values found in Table 6-1, the above literature would support the implementation of the effective girder CTE values obtained, which are approximately 1.3 CTE_{SAT}.

6.3 Prestress Losses

Prestress losses were not directly measured in this research. However, prestress losses could be inferred from the strains measured using the VWSGs. The initial jacking stress was assumed to be 202.5 ksi in all of the prestressing steel with the exception of the lightly stressed top strands. Effective prestress was calculated at the level of the bottom-most gauge in each girder, which corresponded closely to the centroid of the fully prestressed steel at midspan. Assuming perfect bond and that the steel displayed a linear elastic behavior, the effective prestress, f_{pe}, after transfer was determined using Equation 6-23. It is important to note that the change in strain was taken relative to before transfer in order to determine losses over the girders lifespan and at specific events.

$$f_{pe} = f_{pbt} + \Delta\varepsilon_c E_p + \Delta f_{pR} \qquad \text{Equation 6-23}$$

Where:

f_{pbt} = Stress in prestressing strand before transfer (202.5 ksi)

$\Delta\varepsilon_c$ = Change in measured bottom flange strain relative to before transfer

E_p = Prestressing strand modulus of elasticity (28600 ksi)

Δf_{pR} = Stress change due to steel relaxation

It is important to note that any losses due to relaxation were excluded from the losses determined in this report. The stress change due to the relaxation of steel is independent of strain, so measurements taken from the strain gauges embedded in the concrete are unable to include the effects of relaxation of the prestressing strands.

Therefore, any relaxation losses in the observed measurements would need to be predicted. It was decided to subtract the AASHTO-predicted relaxation loss from the predicted losses found in this report. It is important to note that the total relaxation loss is expected to be similar for both SCC and VC girders, and would be relatively small at around 3 ksi.

6.3.1 Total Prestress Losses between SCC and VC Girders

One of the main objectives of this research was to compare the total prestress losses of girders composed with SCC to VC girders over an extended period of time. Changes in measured bottom flange strains relative to transfer were recorded and used to determine the level of stress in the prestressing strands using Equation 6-23. The prestress loss was then determined by finding the difference of the level of prestress relative to the stress in the strands before transfer. Figure 6-17 and Figure 6-18 are plots of prestress loss observed in SCC and VC girders over an extended period of time.

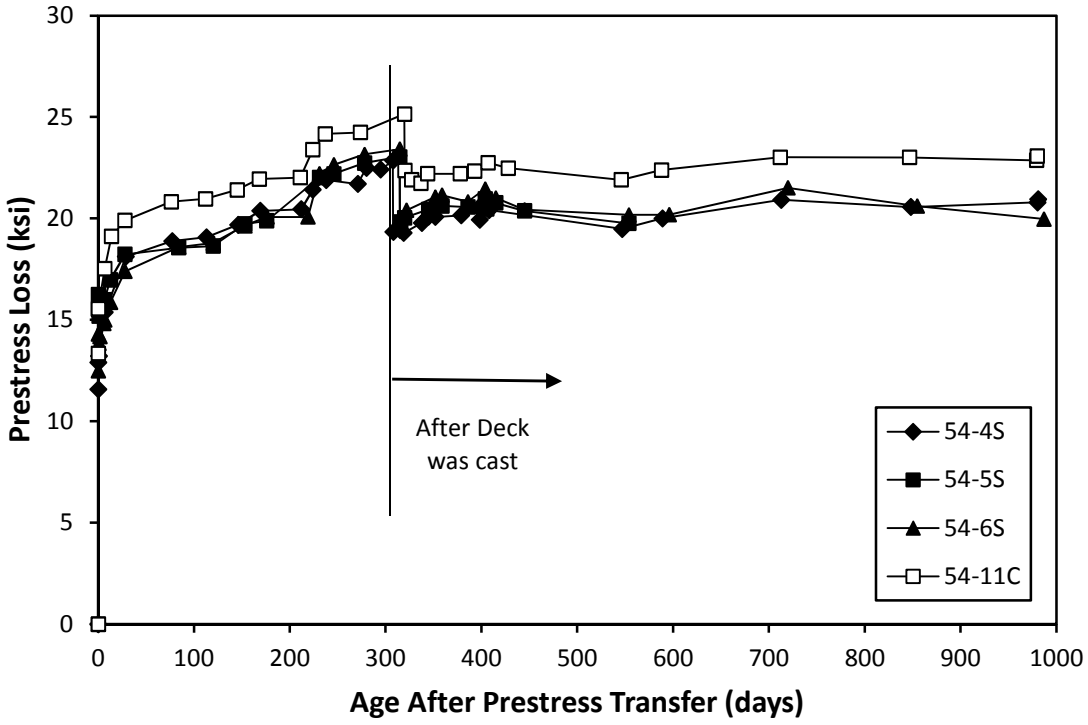

Figure 6-17: BT-54 Observed Total Prestress Loss

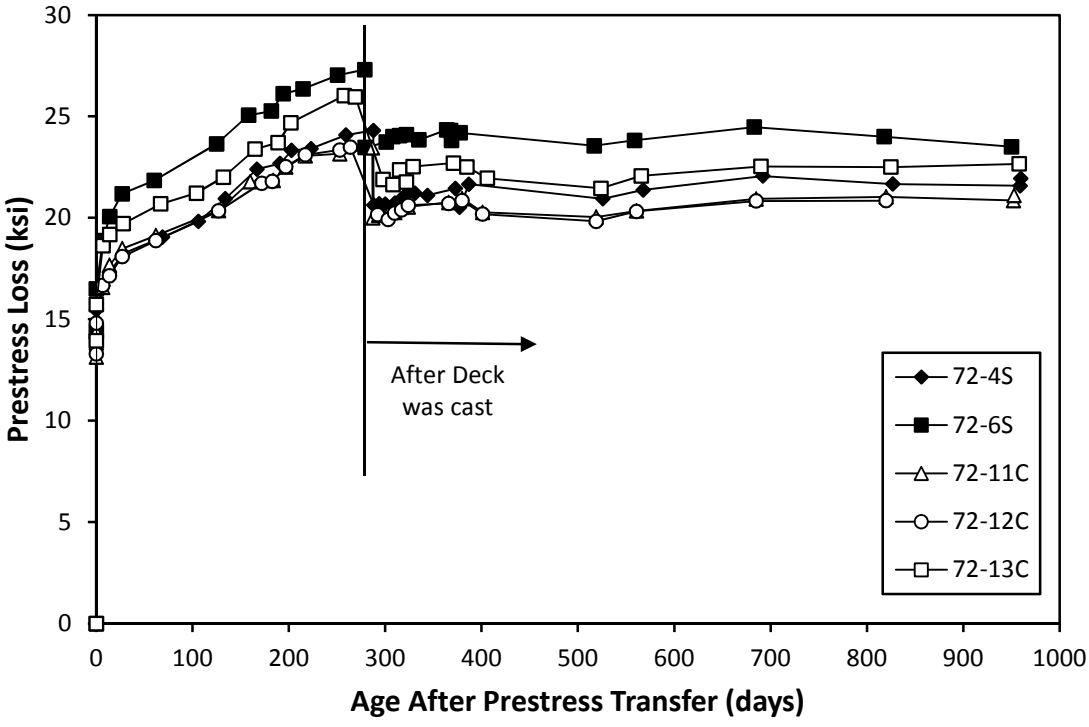

Figure 6-18: BT-72 Observed Total Prestress Loss

As seen in Figure 6-17, BT-54 girders composed with SCC had less prestress loss than the girders composed with VC. The observed prestress loss of the BT-72 girders shown in Figure 6-18 were a little less conclusive. The difference between the losses of SCC and VC girders is approximately 3 ksi or less. It is typically assumed that girders experience a long-term prestress loss of 18%-20% of the original jacking stress which equates to an approximate effective prestress of 166-162 ksi or a long-term prestress loss of 36-40 ksi. Which relates to about 8% of the total expected prestress loss. Therefore, due to the small difference relative to a typical total prestress loss, no substantial differences can be made between the total prestress loss in the SCC versus VC girders.

6.3.2 Implementation of AASHTO 2012 Method for Estimating Prestress Losses

A major portion of this investigation involved the comparison of predicted time-dependent deformations to actual measured deformations in bulb-tee girders constructed with self-consolidating concrete (SCC) and conventionally vibrated concrete (VC). The predictions were developed from the *AASHTO LRFD Bridge Design Specifications* 2012 time-dependent deformation prediction model. As mentioned in Section 2.1 the investigation by Johnson (2012) determined that prediction models displayed a higher level of accuracy when measured material properties were used in lieu of predicted material properties. Due to a higher level of accuracy measured material properties pertaining to the individual girders were used in the AASHTO 2012 prediction model. Transformed-section properties are also used in the prediction of prestress losses, where prestressing steel and deck concrete were transformed using prestressing steel-to-girder and deck-to-girder modular ratios respectively.

6.3.2.1 AASHTO 2012 Total Prestress Loss

The AASHTO 2012 prediction model separates the estimation of total prestress loss into two different categories: instantaneous and time-dependent losses. Losses due to anchorage set, friction, and elastic shortening are instantaneous, whereas losses due to creep, shrinkage, and relaxation are time-dependent (AASHTO 2012). The equation used to predict a girders' total prestress loss can be found in Equation 2-1. It is also important to note that transformed-section properties were used in the prediction of prestress losses, where prestressing steel and deck concrete were transformed using prestressing steel-to-girder and deck-to-girder modular ratios respectively. The losses due to elastic shortening and elastic gains due to the addition of the deck were determined by using the methods outlined in Section 6.3.2.2. As mentioned in Section 2.3 time-dependent losses were determined using the AASHTO 2012 Refined Estimate of Time-Dependent Losses. This is primarily due to the higher level of accuracy and the capability to estimate losses at different construction stages. Further explanation of the refined method can be found in Section 2.3 and in the following sections.

6.3.2.2 AASHTO 2012 Elastic Shortening Loss and Elastic Gains

At the time of transfer, the axial compression resulting from the applied prestressing force causes an axial shortening of the member. The strands simultaneously shorten due to their bond with the concrete, causing a prestress loss due to elastic shortening. AASHTO 2012 allows the designer to determine elastic shortening losses in a few different ways: gross-section approximation, iterative gross-section approach, and a transformed-section approach.

The transformed-section approach is straight forward, and it alleviates any iterative process. Therefore, the transformed section approach is used in this investigation. The following equations outline the transformed-section approach to determine the stresses in the concrete and prestressing steel immediately after transfer.

$$f_{cgp} = -\frac{f_{pbt}A_{ps}}{A_{tr}} - \frac{f_{pbt}A_{ps}e_{tr}y_{tr}}{I_{tr}} + \frac{My_{tr}}{I_{tr}} \qquad \text{Equation 6-24}$$

and

$$f_{pt} = f_{pbt} - n_p\left(\frac{A_{ps}}{A_{tr}} + \frac{e_{tr}^2 A_{ps}}{I_{tr}}\right)f_{pbt} + n_p\frac{Me_{tr}}{I_{tr}} \qquad \text{Equation 6-25}$$

Where

f_{cgp} = concrete stress at the center of gravity of prestressing force immediately after transfer

f_{pbt} = stress in prestressing steel immediately before transfer

f_{pt} = stress in prestressing steel immediately after transfer

A_{ps} = area of prestressed reinforcement

A_{tr} = transformed area of cross section (reinforcement area to concrete area of equivalent stiffness)

I_{tr} = moment of inertia of the transformed section

e_{tr} = eccentricity of prestress force with respect to centroid of transformed area

y_{tr} = distance from centroid of transformed section to center of gravity of prestressing force

$n_p = \frac{E_p}{E_{ci}}$ = modular ratio of prestressing reinforcement with respect to concrete at transfer

E_p = modulus of elasticity of prestressed reinforcement

E_{ci} = modulus of elasticity of concrete at time of prestress transfer

M = bending moment experienced by cross section immediately after transfer (usually due to self-weight of the girder)

Using Equation 6-24 and Equation 6-25, the elastic shortening loss, $\Delta f_{pES,}$ is the difference between f_{pt} and f_{pbt}.

$$\Delta f_{pES} = -n_p \left(\frac{A_{ps}}{A_{tr}} + \frac{e_{tr}^2 A_{ps}}{I_{tr}} \right) f_{pbt} + n_p \frac{M e_{tr}}{I_{tr}} \qquad \text{Equation 6-26}$$

or

$$\Delta f_{pES} = f_{pt} - f_{pbt} \qquad \text{Equation 6-27}$$

The first term in Equation 6-26 represents the loss from the prestress transfer process, while the second term represents the opposing effect of the self-weight moment on the cross section. The elastic gain due to the application of the web-walls, deck, and barriers were directly calculated using the second term in Equation 6-26, and are included in the sum of all instantaneous elastic gains or losses at the appropriate stage in construction.

6.3.2.3 AASHTO 2012 Refined Estimates of Time-Dependent Losses

A detailed description of the AASHTO 2012 Refined estimate of time-dependent losses can be found in Section 2.3. The estimated total time-dependent losses are broken into two parts: sum of time-dependent prestress losses between prestress transfer and

deck placement, and sum of time-dependent prestress losses after deck placement. This total time-dependent prestress loss estimate is determined by using Equation 2-2.

Losses due to concrete creep and shrinkage are two components that are consistently present within the girder no matter the construction phase. The losses due to creep are accounted for by determining a creep coefficient at any given time, and applying it to the compressive strain caused by permanent loads in order to obtain the strain due to creep. This creep coefficient is determined by Equation 2-3 and is used in the estimation process to determine prestress loss at various construction phases throughout the girders life. The change in concrete stress at centroid of prestressing strands due to long-term losses between transfer and deck placement, combined with deck weight and superimposed loads, Δf_{cd}, was determined by Equation 2-16. When determining the value of, Δf_{cd}, it was taken that only the girder resisted the weight of the deck until the deck concrete hardened, and after that point any additional superimposed dead loads were considered to be resisted by the full composite section. In this investigation it was assumed that a full composite action developed seven days after the deck was cast.

The losses due to concrete shrinkage are accounted for using Equation 2-8. Prestress losses due to shrinkage for this method is based on aggregate characteristics, concrete strength, curing method, average humidity, volume-to-surface ratio, duration of drying, and the age at the start of drying. AASHTO 2012 states that if the concrete is exposed to drying before 5 days of curing have elapsed, the shrinkage as determined in Equation 2-8 should be increased by 20 percent. The time development factor, k_{td}, used

in Equation 2-8 for determining the shrinkage strain was taken as one. This is due to fact that the time, *t*, found in Equation 2-7 approaches final time.

It is important to note that prestress losses due to the relaxation of the prestressing strands are omitted from the predicted values reported in this investigation. This is primarily due to the fact that losses due to relaxation cannot be measured with the VWSG located in the observed girders. The prestressing loss due relaxation of the prestressing strands is relatively small compared to the overall prestress losses with expected values around 1.5 ksi. Therefore, omitting the loss due to relaxation from predicted values will not have a profound effect on comparing predicted versus measured values.

A more in depth explanation of the AASHTO 2012 Refined Method for determining losses is explained in Section 2.3.

6.3.3 Measured Versus Predicted Total Prestress Losses

Another goal in this research was to compare measured prestress levels to what would be expected using AASHTO 2012 prediction methods. Measured prestressing levels were compared with predicted values at corresponding ages. Figure 6-19 and Figure 6-20 are two of such comparisons over an extended period of time. See Appendix A for the remainder of all girders compared in this study.

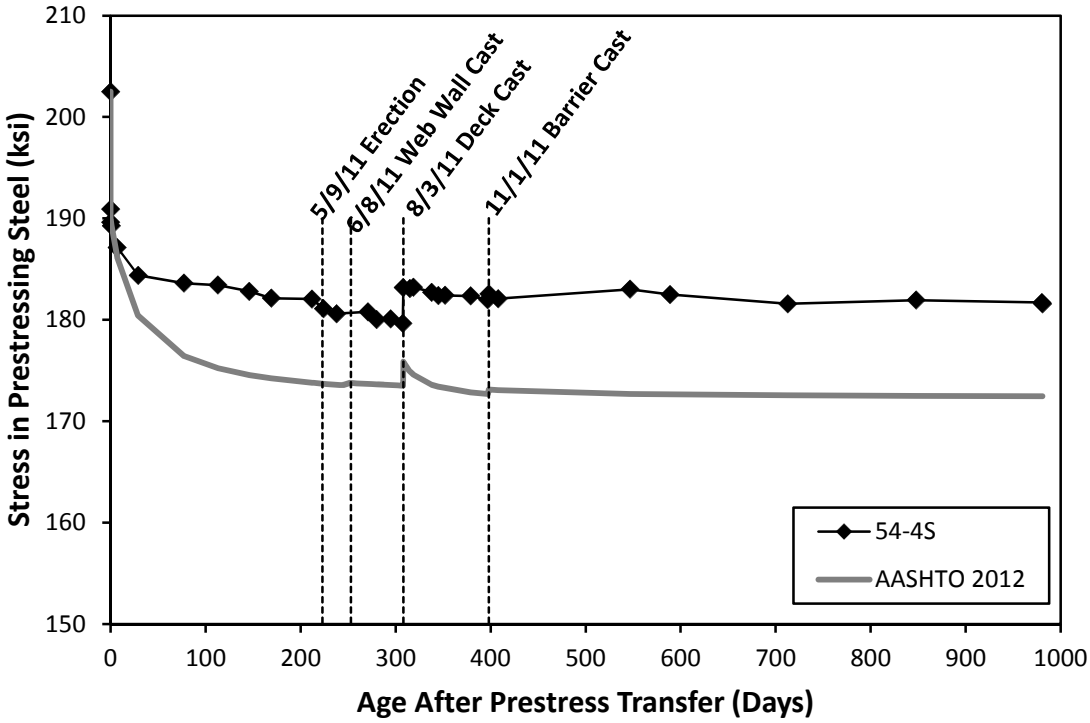

Figure 6-19: Observed and Predicted Effective Prestress (54-4S)

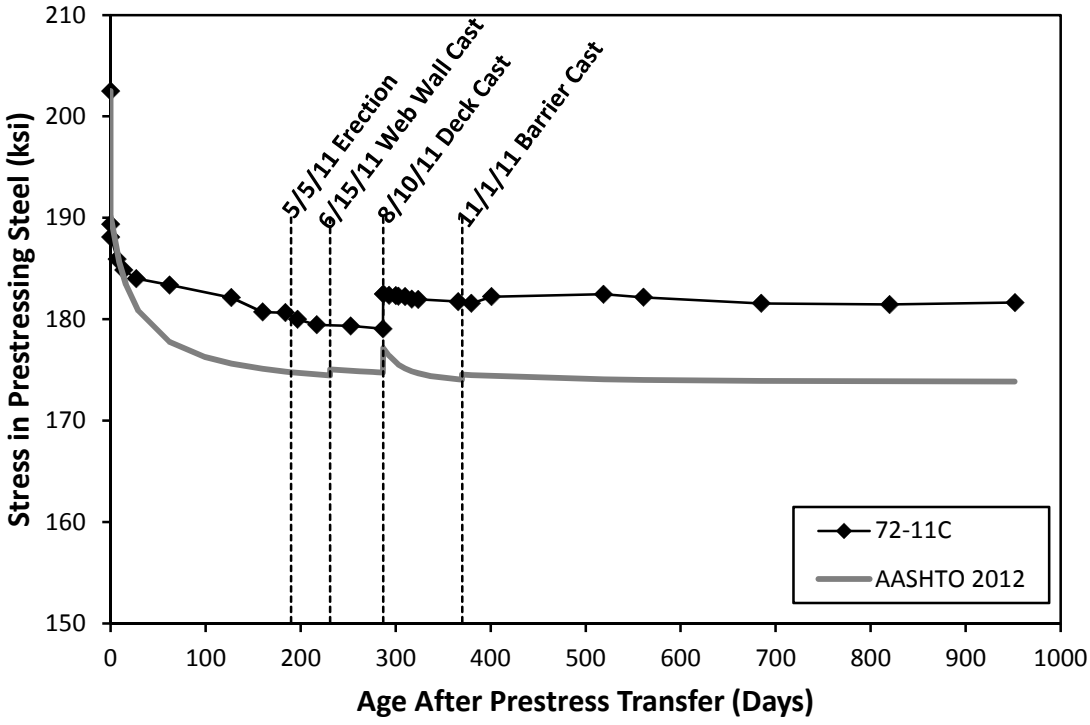

Figure 6-20: Observed and Predicted Effective Prestress (72-11C)

As seen in Figure 6-19 and Figure 6-20 there is an observed prestress gain in the prestressing steel at the time the deck was cast. The added weight of the deck causes an increase in tensile stresses in the bottom of the girders and as a result the prestressing tendons experience a sustained increase in stress. This elastic gain due to the casting of the deck is discussed further in Section 6.3.6.

It is apparent from the above figures that the AASHTO 2012 prediction methods over predicted prestress losses. Similar results were observed in the rest of the measured girders. Although the predicted prestress levels were over predicted the losses over time seemed to follow a very similar trend. This shows that the AASHTO 2012 prediction methods are not ineffective in predicting losses, but merely are off by a certain magnitude for the concretes in this study. Also, these results show that the AASHTO 2012 prediction method seemed to display the same level of accuracy for both SCC and VC concretes. Similar trends were observed in the investigation by Johnson (2012) before the girders were erected. Further discussion of predicted versus measured long-term losses can be found in Section 6.3.7.

6.3.4 Elastic Shortening Losses

Measured prestress losses due to elastic shortening were also determined and comparisons were made between the two types of concretes and predicted values. A similar comparison was made in Johnson (2012), but the comparisons were focused on comparing strains between the two types of concretes and predicted values. The predicted losses attributed to elastic shortening were determined using the transformed section approach outlined in Section 6.3.2.2. Figure 6-21 and Figure 6-22 show the measured and predicted elastic shortening losses for both BT-54 and BT-72 girders.

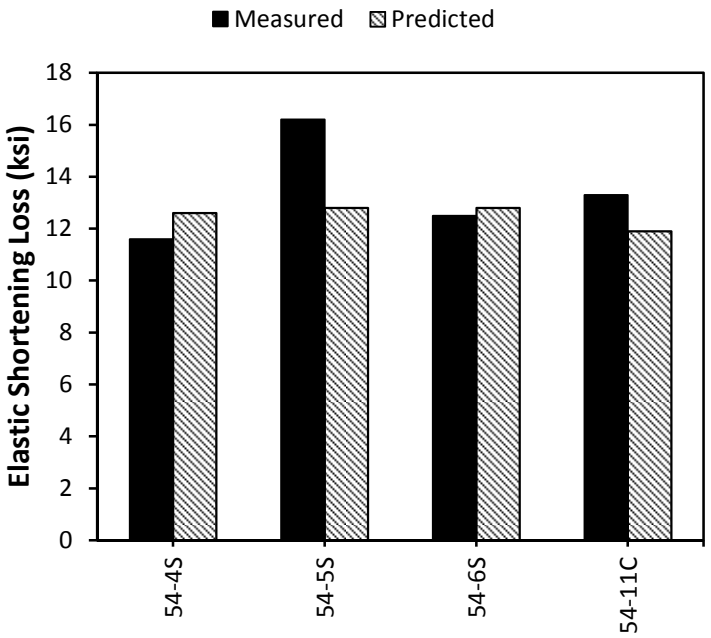

Figure 6-21: BT-54 Measured and Predicted Elastic Shortening Prestress Loss

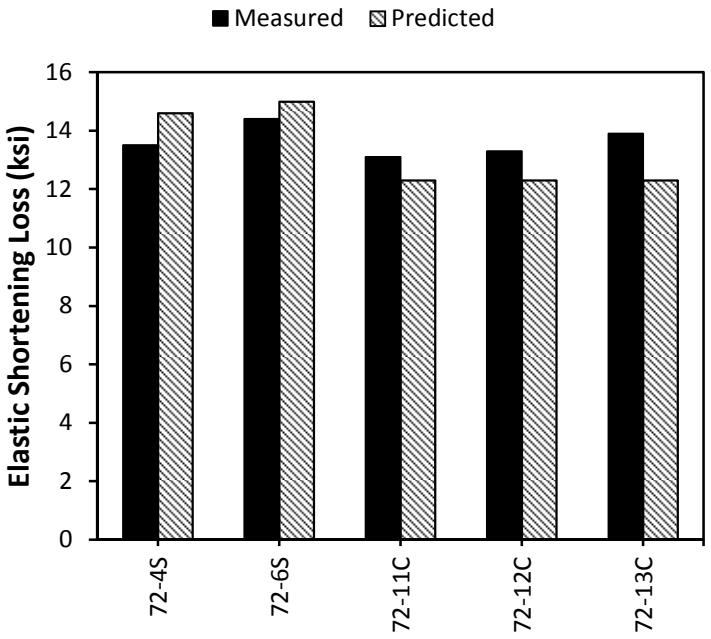

Figure 6-22: BT-72 Measured and Predicted Elastic Shortening Prestress Loss

A couple conclusions can be drawn from the results in Figure 6-21 and Figure 6-22. First, with the exception of girder 54-5S, the predicted elastic shortening loss was

over predicted for the SCC girders and under predicted for the VC girders. The large elastic shortening loss observed in 54-5S relative to the other girders in Figure 6-21 could be a reflection of an unreliable VWSG reading immediately after prestress transfer. Although the difference between the predicted values and measured values is small, it is obvious that the prediction method used to predict elastic shortening losses does not have the same level of accuracy for the two types of concrete. The predicted elastic shortening loss was determined by using the transformed-section approach outlined in Section 6.3.2.2. This approach uses both geometric and material specific properties to predict elastic shortening losses. The material specific properties were the modulus of elasticity of both the prestressing steel and concrete at the time of transfer. The modulus of elasticity was the only variable that differs between the two types of concrete. Therefore, the varying concrete modulus of elasticity's seem to be the reason why there were discrepancies in the elastic shortening losses for the two types of concrete. Second, the difference in measured elastic shortening losses for both SCC and VC girders were around 1 ksi of each other, therefore due to the small differences it can be concluded that the elastic shortening loss was similar for both SCC and VC girders.

6.3.5 Short-Term Losses

Prestress losses were also evaluated on a short term basis. Measured values were also compared to losses predicted using the AASHTO 2012 prediction methods. For this investigation short-term losses were to be considered the prestress losses occurring within the first 90 days after prestress transfer. The short-term losses reported are comprised of losses due to elastic shortening, shrinkage, and creep. Figure 6-23 and Figure 6-24 show the short term losses for both BT-54 and BT-72 girders. The presented losses were taken

at 80 days since transfer for the BT-54 and at 60 days for BT-72. In all of the observed girders the AASHTO 2012 prediction method over predicted the prestress losses occurring within 90 days after prestress transfer. In Table 6-4 and Table 6-5 are tabular values of the measured verses predicted short-term prestress losses. Included in these tables is the percent error of the predicted short-term losses as a percentage of the measured values. Although the percent errors are large for all the girders, the predicted values for the VC girders had lower percent errors. These results show that the AASHTO 2012 prediction method seems to be more accurate in predicting short-term losses for the VC girders in this investigation. The differences between the measured short-term losses between the SCC and VC concretes were minimal, 2.1 ksi for the BT-54 and 0.85 ksi for the BT-72 girders. Since these differences in measured values are small in comparison to overall short-term losses, no substantial differences between SCC and VC short-term losses can be drawn.

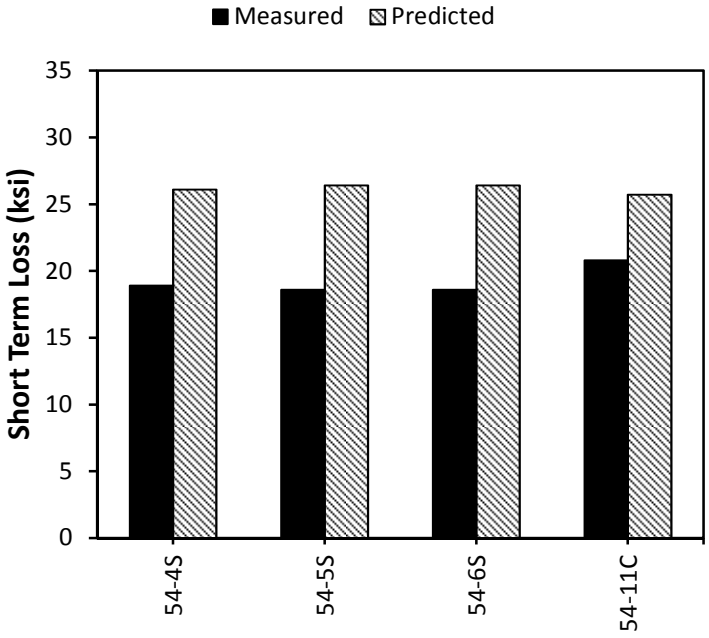

Figure 6-23: BT-54 Measured and Predicted Short-Term Prestress Losses

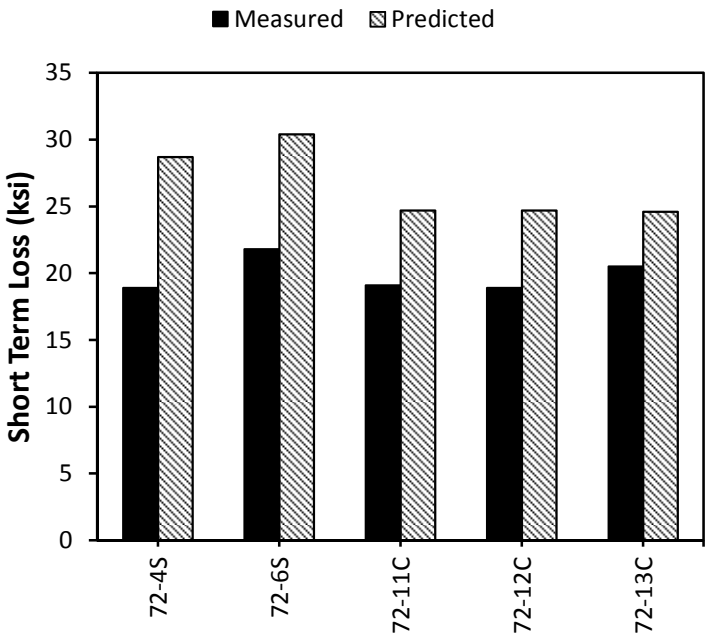

Figure 6-24: BT-72 Measured and Predicted Short-Term Prestress Losses

Table 6-4: BT-54 Short-Term Prestress Losses

Girder	Measured loss (Ksi)	Predicted Loss (Ksi)	Error (ksi)	% Error
54-4S	18.9	26.1	7.2	38.1
54-5S	18.6	26.4	7.8	41.9
54-6S	18.6	26.4	7.8	41.9
54-11C	20.8	25.7	4.9	23.6

Table 6-5: BT-72 Short-Term Prestress Losses

Girder	Measured loss (ksi)	Predicted Loss (ksi)	Error (ksi)	% Error
72-4S	18.9	28.7	9.8	51.9
72-6S	21.8	30.4	8.6	39.4
72-11C	19.1	24.7	5.6	29.3
72-12C	18.9	24.7	5.8	30.7
72-13C	20.5	24.6	4.1	20.0

6.3.6 Elastic Gains Due to Casting of the Deck

Another observed response investigated was the gain in effective prestress due to the casting of the deck. The added weight of the deck causes an increase in tensile stresses in the bottom of the girders and as a result the prestressing tendons experience a sustained increase in stress. The measured elastic gain was determined by taking strain measurements from the gauges located in the bottom flange before and after the deck was cast, and converted into an effective prestress using Equation 6-23. The elastic prestress gain due to the casting of the deck is then the difference between these two measurements. Figure 6-25 and Figure 6-26 compare measured prestress gain due to the casting of the deck to predicted values determined from the procedures outlined in Section 6.3.2.2. No trends in terms of measured prestress gains due to deck casting between the SCC and VC girders seem to be present. Table 6-6 and Table 6-7 are tabular results of the measured versus predicted results along with the percent error of the predicted values in relation to the measured effective prestress gains. With the exception of girder 54-11C the predictions seem to fall relatively close to the measured values with a percent error of less than 14%. There also seems to be no difference in the level of accuracy of the predicted values between the SCC versus VC concretes.

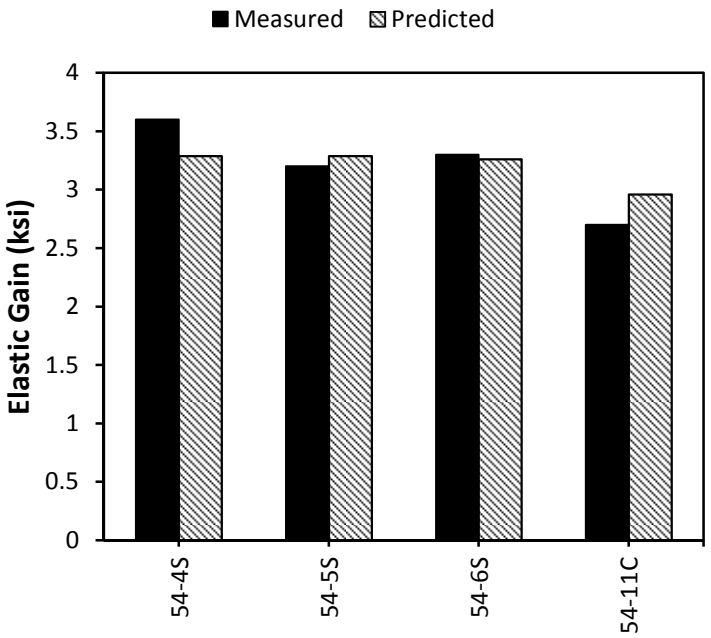

Figure 6-25: BT-54 Prestress Gain Due to Deck Casting

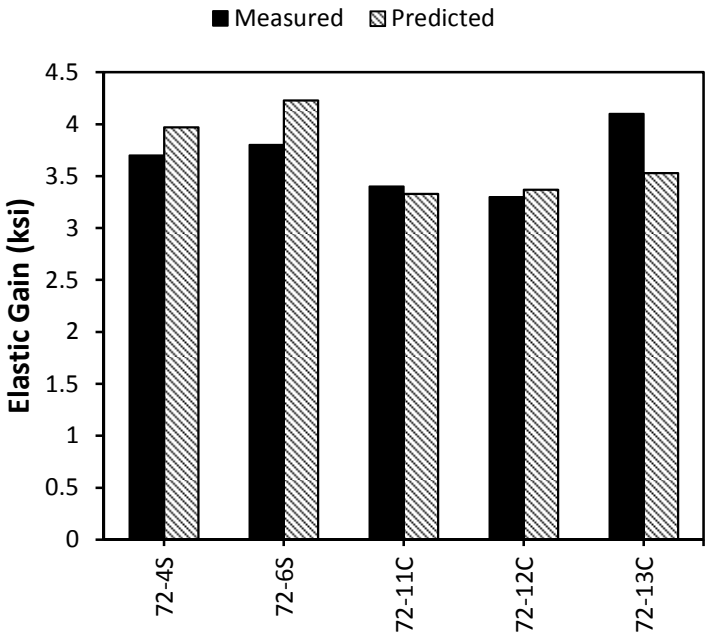

Figure 6-26: BT-72 Prestress Gain Due to Deck Casting

Table 6-6: BT-54 Prestress Gain Due to Deck Casting

Girder	Measured Gain (ksi)	Predicted Gain (ksi)	% Error
54-4S	3.60	3.29	8.6
54-5S	3.20	3.29	2.8
54-6S	3.30	3.29	0.3
54-11C	2.70	3.29	21.9

Table 6-7: BT-72 Prestress Gain Due to Deck Casting

Girder	Measured Gain (ksi)	Predicted Gain (ksi)	% Error
72-4S	3.7	4.0	7.3
72-6S	3.8	4.23	11.3
72-11C	3.4	3.33	2.1
72-12C	3.3	3.37	2.1
72-13C	4.1	3.5	13.9

6.3.7 Long-Term Losses

Prestress losses were also recorded and compared to predicted losses after the girders were in service. The last measured data available were used to establish the long-term losses of the girders and compared with predicted values at a corresponding age. Measured data was attempted to be collected all at the same age, but due to gauge malfunctions some girders losses were not able to be obtained at later ages. The values found in Table 6-8 and Table 6-9 are the measured and predicted long-term losses. The percent of total prestress loss is also presented. These values were determined by assuming all strands had 202.5 ksi tension before transfer.

According to the measured data there seem to be no major differences in the observed long-term losses between the VC and SCC girders. However, it can be concluded that the AASHTO 2012 methods over-predicted long-term prestress losses by

a significant amount. Also, the magnitude of these errors seemed to be the same for both VC and SCC girders. This tells us that the AASHTO prediction methods seem to over predict long-term prestress losses regardless of the type of concrete used.

Table 6-8: BT-54 Long-Term Prestress Losses

Girder	Age after transfer	Measured loss (ksi)	Predicted Loss (ksi)	Error (ksi)	Error as a % of f_{pbt}
54-4S	981	20.9	30.0	9.1	4.5
54-5S	554	19.8	29.4	9.6	4.7
54-6S	987	20.0	29.7	9.7	4.8
54-11C	980	23.1	31.2	8.1	4.0

Table 6-9: BT-72 Long-Term Prestress Losses

Girder	Age after transfer	Measured loss (ksi)	Predicted Loss (ksi)	Error (ksi)	Error as a % of f_{pbt}
72-4S	960	21.9	33.1	11.2	5.5
72-6S	950	23.5	35.8	12.3	6.1
72-11C	953	21.1	28.6	7.5	3.7
72-12C	820	20.8	28.6	7.8	3.9
72-13C	958	22.7	28.5	5.8	2.9

6.4 Cambers

Midspan cambers were collected using the processes outlined in Chapter 4 and recorded from before prestress transfer until the girders were in service. Measurements were adjusted for nonlinear temperature gradients using the procedures outlined in Section 6.2.1. These recorded measurements are reported relative to a baseline measurement taken just prior to prestress transfer. One of the goals of this study was to compare the camber of girders made with SCC to those made with VC. Figure 6-27 and Figure 6-28 show the camber measurements of both BT-54 and BT-72 girders for the

entirety of this study along with accompanying ranges of important events. It is important to note that the measurements after the deck was cast began to show significant variation. This variation is probably contributed by error introduced in camber readings by the implementation of the underside surveying method outlined in Section 4.3, and the value of camber measurements in girders that are mechanically joined by diaphragms and a deck is unclear. Only four interior-girders camber are reported because the exterior girders are differently restrained and are subjected to slightly different deck loads.

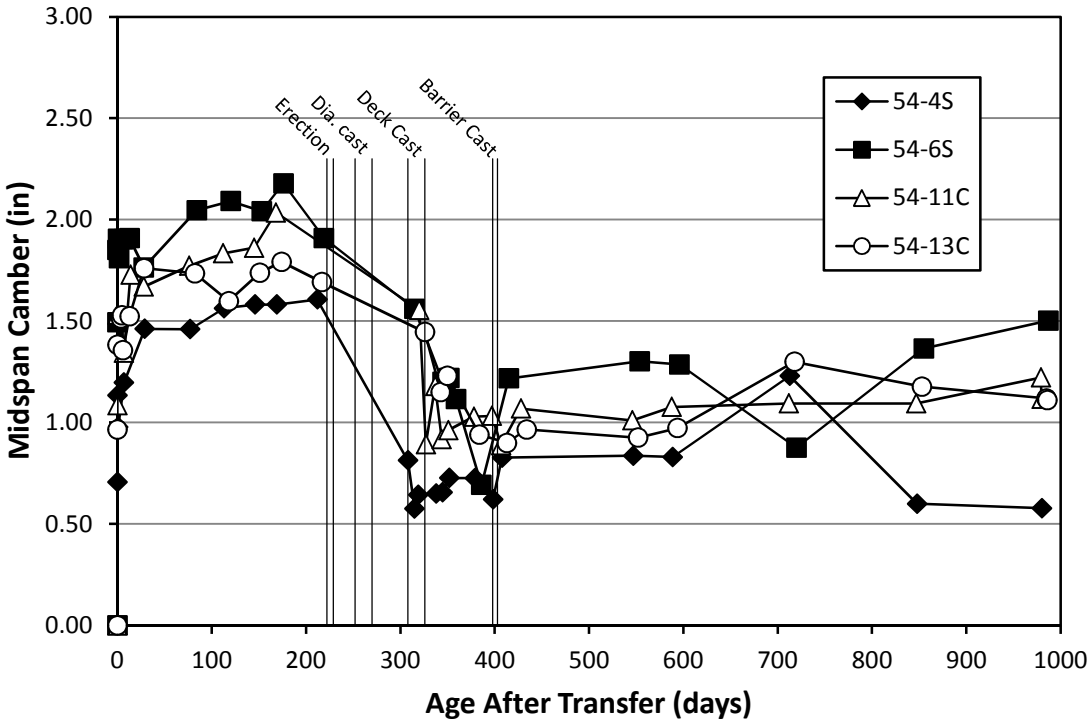

Figure 6-27: BT-54 Midspan Cambers

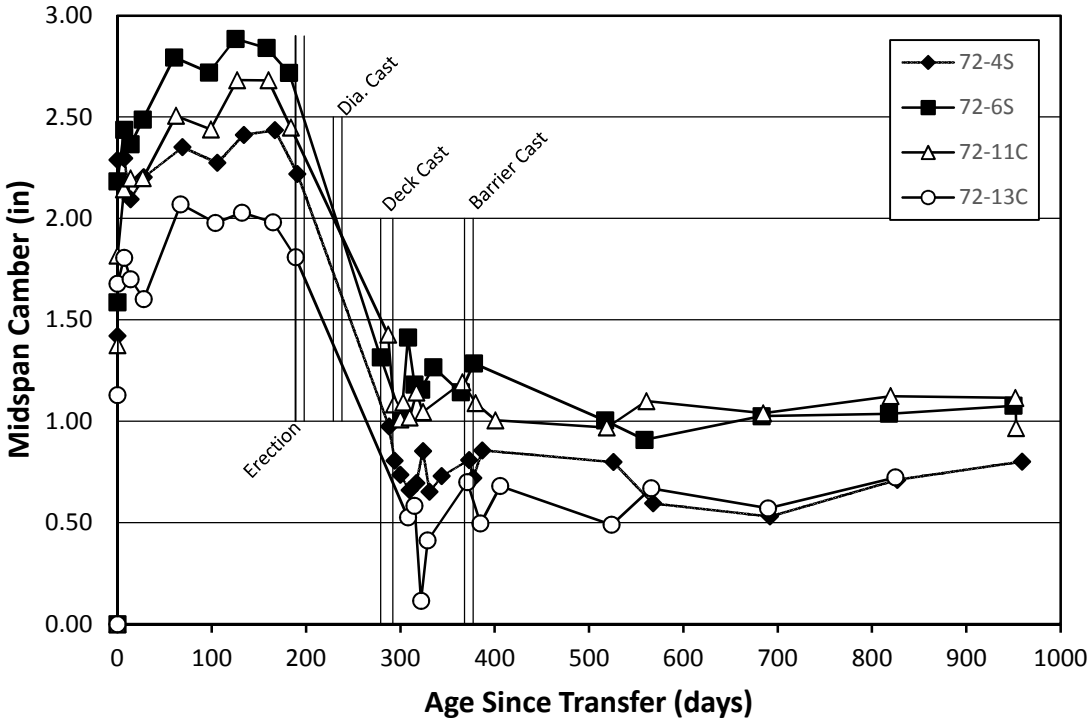

Figure 6-28: BT-72 Midspan Cambers

Camber measurements from before the girders were erected are more reliable. Camber measurements up until the girders were erected are compared with predicted values in the investigation by Johnson (2012). His results showed that SCC girders tended to have somewhat higher measured and predicted cambers than the VC girders. This is due to the fact that the stiffness of the SCC girders is most often lower than the VC girders. Johnson also concluded that direct comparison of these cambers is somewhat useful, but the varying material properties (specifically the varying stiffness) among casting groups makes direct comparison of measured values more difficult.

The investigation by Keske (2014) also included a camber analysis for the girders located at this bridge. His camber investigation focused on the changes in camber due to the addition of the deck. Camber measurements were taken before and within a few days after the deck was cast in order to alleviate any time-dependent change in camber. His

results showed that the measured post addition cambers seem to be comparable for the SCC and VC girders.

This investigation aimed at comparing the camber for SCC and VC girders after the girders have developed full composite action with the deck. High variability in measurements after the girders experienced full composite action with the deck causes a direct comparison camber trends of SCC versus VC to be very difficult. Therefore, it can be concluded that once the girders experience full composite action with the deck, independent camber measurements of the girders becomes inconclusive.

Chapter 7 Summary and Conclusions

7.1 Summary

The use of SCC for precast prestressed concrete girders is becoming widely popular throughout Alabama and the precast, prestressed industry. While the interest in implementing SCC as a standard for precast prestressed bridge girders grows, research on SCC full scale girder applications is lacking. In order to ensure safe and economical designs, time-dependent deformation responses need to be accurately predicted for all stages of construction. Engineers need to have solid evidence that prediction methods accurately predict prestress losses for both SCC and VC concrete bridge girders. Engineers also need validation that the short and long term performance of SCC girders meet or exceed those comprised of conventional VC girders.

Determining time-dependent deformations for prestressed bridge girders is very difficult. The AASHTO LRFD Bridge Design Specification provides users with methods to determine prestress losses for prestressed bridge girders at various construction stages. One of the main objectives of this study was to compare predicted prestress losses versus measured losses in full scale prestressed bridge girders at varying stages of the construction process. The AASHTO 2012 Refined Method for estimating prestress losses was implemented in predicting prestress losses for full-scale in-service prestress bridge girders. Measured concrete material properties from the 28 bulb-tee girders were used in the prediction model. The 28 bulb-tee girders were manufactured for use in a replacement bridge on State Route 22 over Hillabee Creek in Tallapoosa County,

Alabama. Half of the bridge girders were made with SCC, while the other half were constructed using VC. The remaining components of the bridge: composite deck, webwalls, and barriers were manufactured with VC. Internal strain and temperature readings for the girders and deck were collected using VWSGs located at specific locations throughout the cross sections.

Another main focus of this investigation was to compare the performance between the SCC and VC full scale bridge girders at varying stages of construction. Prestress losses and elastic gains were compared between the SCC and VC girders from the time of prestress transfer until the girders were in service and exposed to traffic for an extended period of time. Camber measurements were also made at regular intervals throughout the entire construction process and comparisons were made between the two types of girders.

7.2 Conclusions

The following conclusions were made regarding the use of SCC versus VC in the prestressed bridge girders observed in this investigation:

- The BT-54 SCC girders seemed to have less overall prestress loss than the VC BT-54 girders, but differences in the BT-72 girders were a little less conclusive. Overall the difference between long-term prestress losses between SCC and VC concretes is about 3 ksi or approximately 8% of the total expected prestress loss. Therefore, due to this small difference no conclusive differences can be made between long-term prestress losses in SCC versus VC concretes.

- Measured elastic shortening losses were similar for both SCC and VC girders.
- Measured short-term losses, or first 90 days after prestress transfer, were similar for both SCC and VC girders.
- Elastic gains due to the casting of the deck were similar between the SCC and VC girders.
- No conclusions can be drawn for camber after composite action between the girders and the deck was achieved. This is primarily due to possible error in camber measurements, the unity between girders due to the fact that they are mechanically joined by the webwalls and composite deck, and the different restraints imposed on the exterior girders which impose varying loads.

The following conclusions were made regarding accuracy of the AASHTO 2012 Refined Method of estimating prestress losses:

- Predicted losses were over predicted throughout the entire construction process for both SCC and VC girders included in this study. Although the losses were over predicted, they followed a similar trend to measured losses and were merely off by a certain order of magnitude.
- In general the elastic shortening prestress losses were over predicted for the SCC girders and under predicted for the VC girders included in this study.
- The AASHTO 2012 prestress loss prediction method over predicted the short-term losses for all of the observed girders. Although they were all

over predicted, the predicted short-term prestress losses seemed to be more accurate for the VC girders included in this study.

- Predicted elastic gains due to addition of the deck seem to be relatively accurate for both SCC and VC girders included in this study.
- The long-term prestress losses were over predicted for both SCC and VC concrete girders after the bridge was in service by a significant amount. There were no differences in the level of accuracy for both SCC and VC girders, which shows that the long-term losses were over predicted regardless of the type of concrete used.

References

AASHTO T-336. 2009. *Standard Method of Test for Coefficient of Thermal Expansion of Hydraulic Cement Concrete.* Washington, D.C: American Association of State Highway and Transportation Officials.

AASHTO. 2010. *AASHTO LRFD Bridge Design Specifications: Customary U.S. Units.* Washington, D.C: American Association of State Highway and Transportation Officials.

AASHTO. 2012. *AASHTO LRFD Bridge Design Specifications: Customary U.S. Units.* Washington, D.C: American Association of State Highway and Transportation Officials.

ACI 209. 1992. Prediction of Creep, Shrinkage, and Temperature Effects in Concrete Structures (ACI 209R-92). (Reapproved 1997). Farmington Hills, MI: American Concrete Institute.

ACI 209. 2008. Guide for Modeling and Calculating Shrinkage and Creep in Hardened Concrete (ACI 209.2R-08). Farmington Hills, MI: American Concrete Institute.

ACI 214. 2002. Evaluation of Strength Test Results of Concrete (ACI 214R-02). Farmington Hills, MI: American Concrete Institute.

ACI 237. 2007. Self-Consolidating Concrete (ACI 237R-07). Farmington Hills, MI: American Concrete Institute.

ACI 318. 2011. Building Code Requirements for Structural Concrete (ACI 318-11) and Commentary. Farmington Hills, MI: American Concrete Institute.

ACI 363. 1992. State-of-the-Art Report on High-Strength Concrete (ACI 363R-92). Farmington Hills, MI: American Concrete Institute.

Alabama Department of Transportation. 2010a. Procedure ALDOT-367: Production and Inspection of Precast Non-Prestressed and Prestressed Concrete. *ALDOT Testing Manual.* Montgomery, AL: Alabama Department of Transportation.

Alabama Department of Transportation. 2010b. Section 513: Prestressed Concrete Bridge Members. *ALDOT Testing Manual*. Montgomery, AL: Alabama Department of Transportation.

Alabama Department of Transportation. 2012. Bridge Standard Drawing I-131. *ALDOT Standard and Special Drawings for Highway Construction*. Montgomery, AL: Alabama Department of Transportation.

Al-Omaishi, N. 2001. Prestress Losses in High Strength Pretensioned Concrete Bridge Girders. Dissertation, University of Nebraska-Lincoln.

Al-Omaishi, N., M.K. Tadros, and S.J. Seguirant. 2009. Elasticity Modulus, Shrinkage, and Creep of High-Strength Concrete as Adopted by AASHTO. *PCI Journal* 54 (4): 44–63.

Al-Ostaz, A. 2007. *Effect of Moisture Content on the Coefficient of Thermal Expansion of Concrete*. Report FHWA/MS-DOT-RD-07-187. Oxford, MS: University of Mississippi.

ASTM C39. 2010. Standard Test Method for Compressive Strength of Cylindrical Concrete Specimens. *ASTM International*. West Conshohocken, PA.

ASTM C469. 2010. Standard Test Method for Static Modulus of Elasticity and Poisson's Ratio of Concrete in Compression. *ASTM International*. West Conshohocken,PA.

ASTM C496. 2011. Standard Test Method for Splitting Tensile Strength of Cylindrical Concrete Specimens. *ASTM International*. West Conshohocken, PA.

Baran, E., C. French, and C. Shield. 2003. *Effects of Vertical Pre-Release Cracks on Prestressed Bridge Girders*. University of Minnesota Report MN/RC 2003-33. Minneapolis, MN: University of Minnesota.

Barr, P.J., B.M. Kukay, and M.W. Halling. 2008. Comparison of Prestress Losses for a Prestress Concrete Bridge Made with High-Performance Concrete. *Journal of Bridge Engineering*, ASCE. (September/October): 468–475.

Boehm, K.M., R.W. Barnes, and A.K. Schindler. 2010. *Performance of Self-Consolidating Concrete in Prestressed Girders*. Auburn, AL: Auburn University Highway Research Center.

Collins, M.P. and D. Mitchell. 1991. Prestressed Concrete Structures. Englewood Cliffs, N.J.: Prentice Hall.

Dunham, E.L. 2011. Transfer Length in Bulb-Tee Girders Constructed with Self-Consolidating Concrete. M.S. Thesis, Auburn University.

Ellis, M.A. 2012. Time-Dependent Deformations of Concrete for Precast/Prestressed Bridge Components. M.S. Thesis, Auburn University.

Emanuel, J.H. and J.L. Hulsey. 1977. Prediction of the Thermal Coefficient of Expansion of Concrete. *ACI Journal* 74 (4): 149–155.

Erkmen, B., C.K. Shield, and C.E. French. 2008. *Self-Compacting Concrete (SCC) for Prestressed Bridge Girders*. MnDOT Report 2008-51. Minneapolis, MN: University of Minnesota.

fib. 2010. Creep and Shrinkage. In *fib Model Code for Concrete Structures 2010.* Lausanne, Switzerland: International Federation for Structural Concrete (*fib*).

FHWA. 2011. Coefficient of Thermal Expansion in Concrete Pavement Design. *ACPT TechBrief* FHWA-HIF-09-015.Springfield, VA: ACPT.

Geokon. 2010. Model 4200/4204/4210 Vibrating Wire Strain Gauge Instruction Manual. Rev. N, 8/10.

Gross, Shawn P. and Ned H. Burns. *Field Performance of Prestressed High Performance Concrete Highway Bridges in Texas*. Federal Highway Administration Report No. FHWA/TX-05/9-580/589-2. February 2000.

Hamilton, H.R., T. Labonte, and M.H. Ansley. 2005. *Self-Consolidating Concrete (SCC) Structural Evaluation*. University of Florida Report BD545, RPWO#21. Gainesville, FL: University of Florida.

Hinkle, Stephen D. 2006. Investigation of Time-Dependent Deflection in Long Span,High Strength, Prestressed Concrete Bridge Beams. M.S. Thesis, Virginia Polytechnic Institute and State University.

Horta, A. 2005. Evaluation of Self-Consolidating Concrete for Bridge Structure Applications. M.S. thesis, Georgia Institute of Technology.

Huo, X.S., N. Al-Omaishi, and M.K. Tadros. 2001. *Creep, Shrinkage, Modulus of Elasticity of High-Performance Concrete*. ACI Materials Journal 98, no. 6: 440-449.

Johnson, B.R. 2012. Time-Dependent Deformations in Precast, Prestressed Bridge Girders. M.S. Thesis, Auburn University.

Kavanaugh, B. 2008. Creep Behavior of Self-Consolidating Concrete. M.S. thesis, Auburn University.

Keske, S.D., R.W. Barnes, A.K. Schindler, E.L. Dunham, M.A. Ellis, B.R. Johnson, and W.O. Bullock. 2013a. SCC Precast, Prestressed Girders in the Hillabee Creek Bridge. In *Proceedings of the 5th North American Conference on the Design and Use of Self-Consolidating Concrete*. Chicago, May 12–15, 2013. Center for Advanced Cement-Based Materials, Chicago.

Keske, S.D., R.W. Barnes, A.K. Schindler, E.L. Dunham, B.R. Johnson, and M.A. Ellis. 2015a. *Self-Consolidating Concrete for Prestressed Applications—Phase I: Girder Fabrication and Pre-Erection Performance.* Research Report 930-738. Auburn, AL: Auburn University Highway Research Center.

Keske, S.D., R.W. Barnes, A.K. Schindler, B.R. Johnson, M.A. Ellis, D.E. Miller, and T.L. Neal. 2015b. *Self-Consolidating Concrete for Prestressed Applications—Phase II: Bridge Construction and In-Place Performance.* Research Report 930-799. Auburn, AL: Auburn University Highway Research Center.

Labonte, T. and H.R. Hamilton III. 2005. *Self-Consolidating Concrete (SCC) Structural Investigation*. Florida Department of Transportation Report No. BD545, RPWO No. 21.

Mokhtarzadeh, A. and C. French. 2000. Time-Dependent Properties of High-Strength Concrete with Consideration for Precast Applications. *ACI Materials Journal* 97, no. 3: 263-271.

Levy, K.R., R.W. Barnes, and A.K. Schindler. 2010. Time-Dependent Deformations of Pretensioned, Self-Consolidating Concrete. In *Think Globally, Build Locally: Proceedings of the Third International fib Congress and Exhibition in Washington*, D.C. 29 May-2 June 2010, Chicago: Precast/Prestressed Concrete Institute.

Naito, C., G. Brunn, G. Parent, and T. Tate. 2005. *Comparative Performance of High Early Strength and Self-Consolidating Concrete for Use in Precast Bridge Beam Construction: Final Report*. ATLSS Report 05-03. Lehigh, PA: Advanced Technology for Large Structural Systems.

Neville, A.M. 1996. *Properties of Concrete*, Fourth Edition. New York: John Wiley & Sons, Inc.

PCI (Precast/Prestressed Concrete Institute). 2004. *Interim Guidelines for the Use of Self-ConsolidatingConcrete in Precast/Prestressed Concrete Institute Member Plants*, 1st ed. Chicago: Precast/Prestressed Concrete Institute.

Sakyi-Bekoe, K.O. 2008. Assessment of the Coefficient of Thermal Expansion of Alabama Concrete. M.S. Thesis, Auburn University.

Schindler, A.K., R.W. Barnes, J.B. Roberts, and S. Rodriguez. 2007. Properties of Self-ConsolidatingConcrete for Prestressed Members. *ACI Materials Journal* 104 (1): 53–61.

Schrantz, C.E. 2012. Development of a User-Guided Program for Predicting Time Dependent Deformations in Prestressed Bridge Girders. M.S. Thesis, Auburn University.

Stallings, J.M., R.W. Barnes, and S. Eskildsen. 2003. Camber and Prestress Losses in Alabama HPC Bridge Girders. *PCI Journal* 48 (5): 90–104.

Tadros, M.K., N. Al-Omaishi, S.J. Seguirant, and J.T. Gallt. 2003. *NCHRP Report 496: Prestress Losses in Pretensioned High-Strength Concrete Bridge Girders*., National Cooperative Highway Research Program (NCHRP). Washington, DC: Transportation Research Board.

Trent, J.D. 2007. Transfer Length, Development Length, Flexural Strength, and Prestress Loss Evaluation in Pretensioned Self-Consolidating Concrete Members. M.S. thesis, Virginia Polytechnic Institute and State University.

Zia, P., R.A. Nunez, and L.A. Mata. 2005. *Implementation of Self-Consolidating Concrete for Prestressed Concrete Girders*. Raleigh, NC: North Carolina Department of Transportation.

Ziehl, P.H., D.C. Rizos, J.M. Caicedo, F. Barrios, R.B. Howard, and A.S. Colmorgan. 2009. *Investigation of the Performance and Benefits of Lightweight SCC Prestressed Concrete Bridge Girders and SCC Materials*. Report No. FHWA-SC09-02. Columbia, South Carolina: University of South Carolina.\

Appendix A Measured Versus Predicted Total Prestress Losses

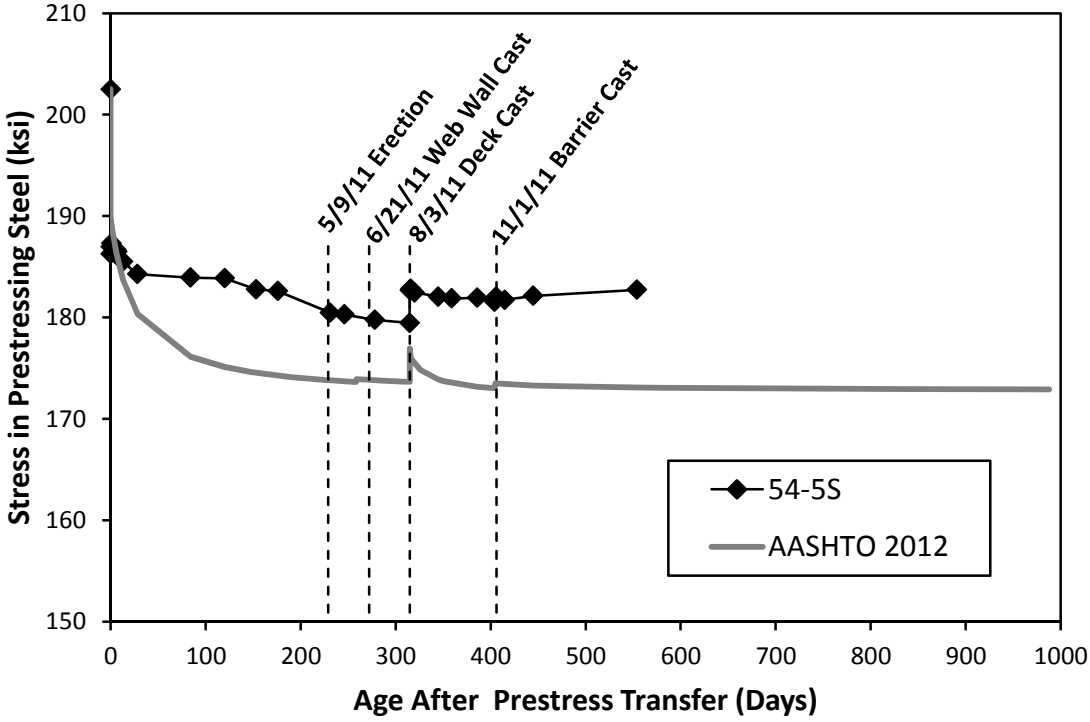

Figure A-1: Observed and Predicted Effective Prestress (54-5S)

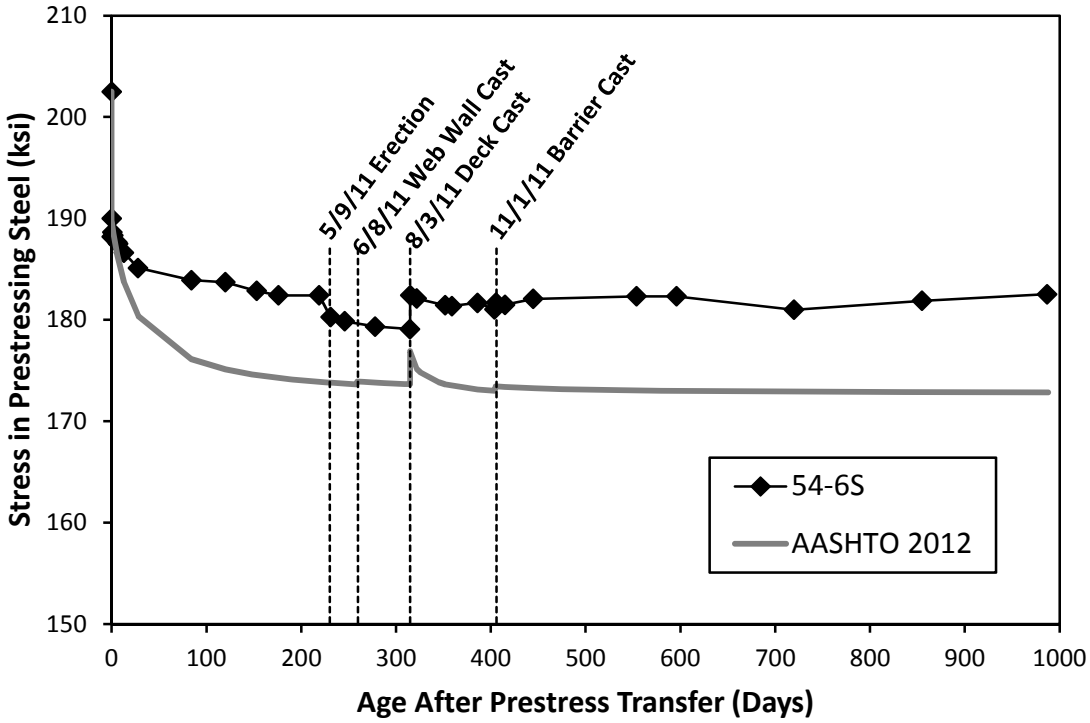

Figure A-2: Observed and Predicted Effective Prestress (54-6S)

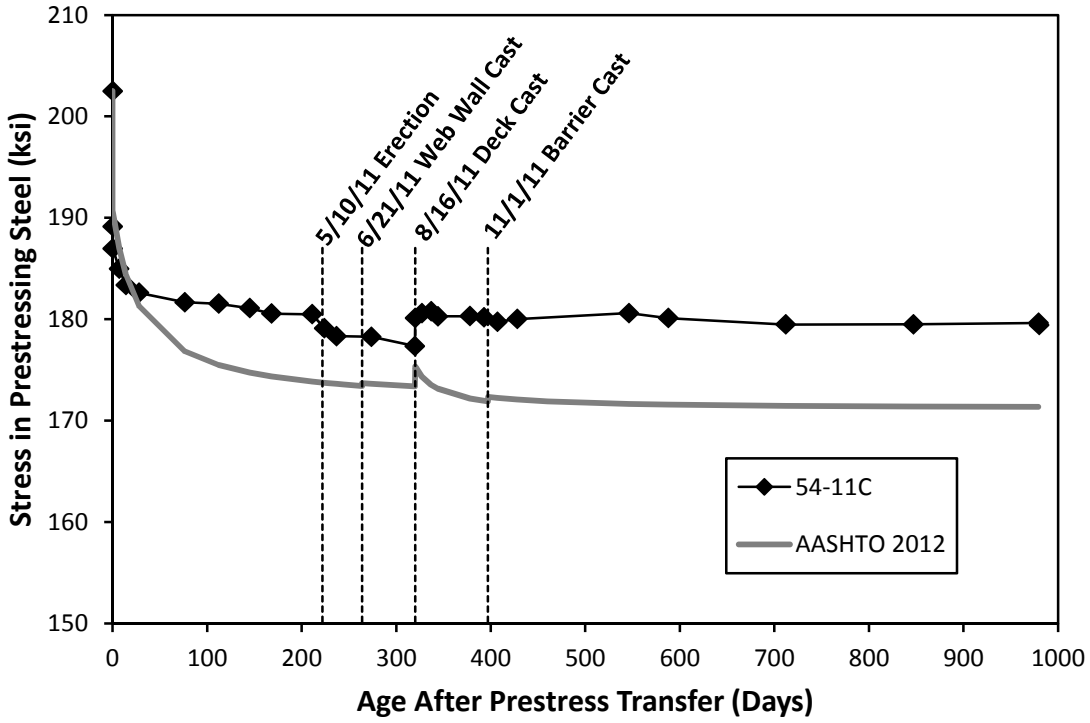

Figure A-3: Observed and Predicted Effective Prestress (54-11C)

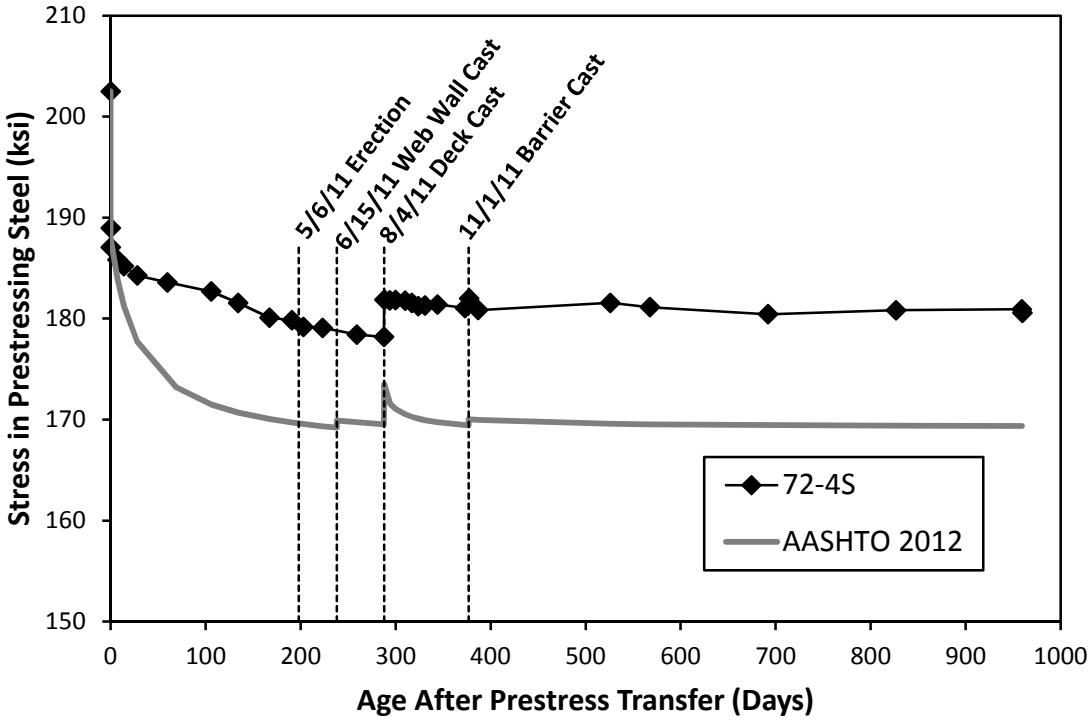

Figure A-4: Observed and Predicted Effective Prestress (72-4S)

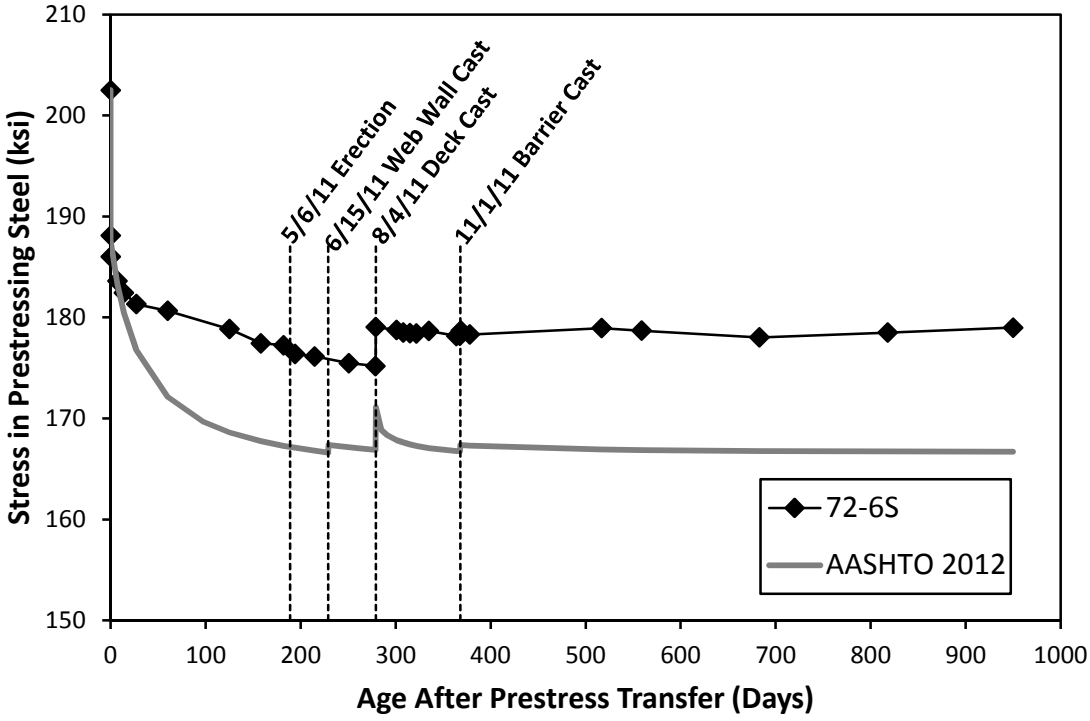

Figure A-5: Observed and Predicted Effective Prestress (72-6S)

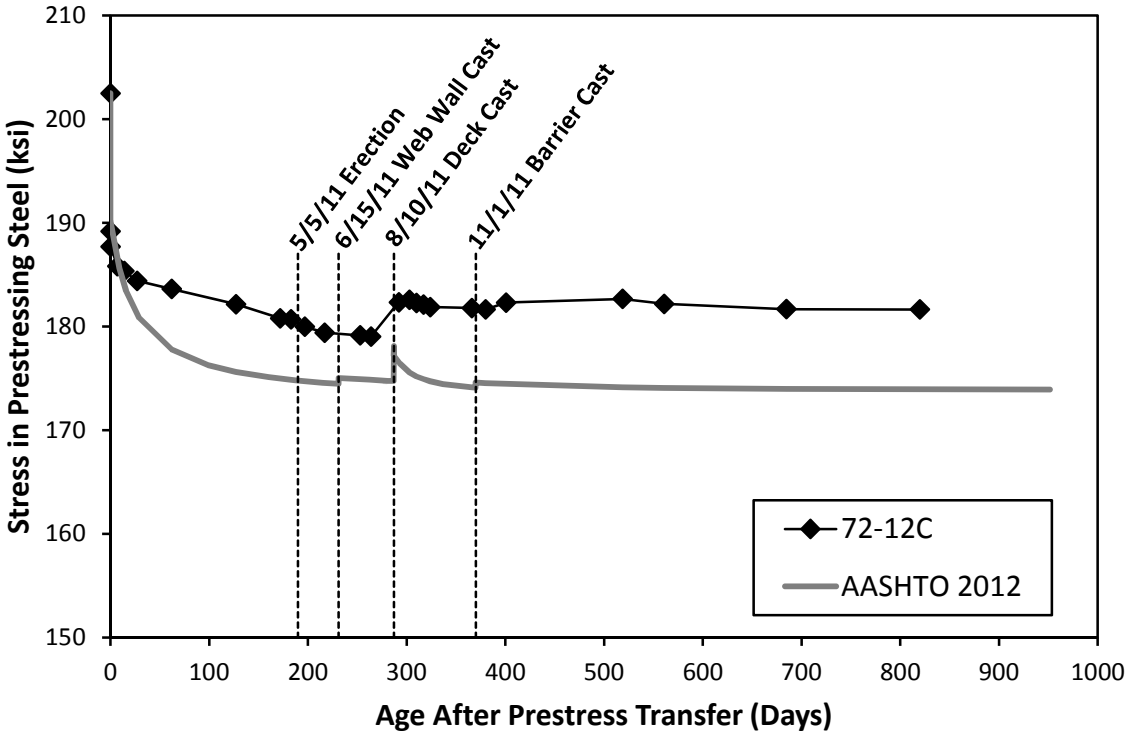

Figure A-6: Observed and Predicted Effective Prestress (72-12C)

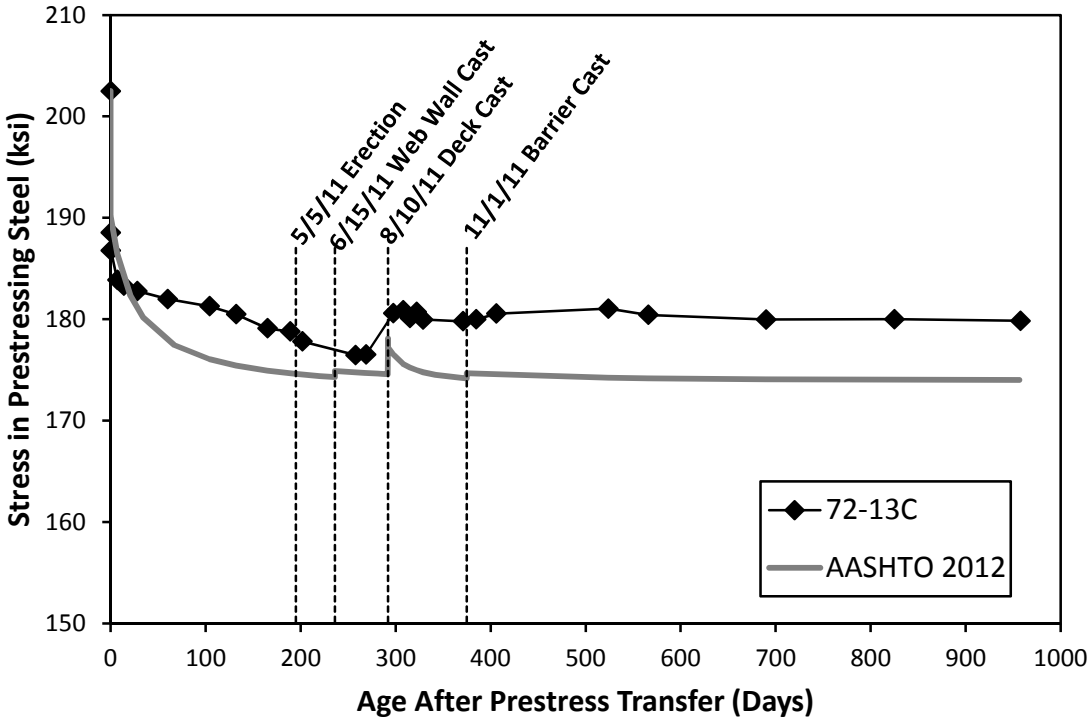

Figure A-7: Observed and Predicted Effective Prestress (72-13C)